Adaptive torrefaction of stem biomass in a horizontal moving bed with normalized direct measurement of quality characteristics

A Dissertation Submitted to the College of Graduate and Postdoctoral Studies in Partial Fulfillment of the Requirement for the Degree of Doctorate of Philosophy in the Department of Chemical and Biological Engineering

University of Saskatchewan

Saskatoon

By

William Allan Campbell P.Eng.

Permission to use

In presenting this thesis/dissertation in partial fulfillment of the requirements for a Postgraduate degree from the University of Saskatchewan, I agree that the Libraries of this University may make it freely available for inspection. I further agree that permission for copying of this thesis/dissertation in any manner, in whole or in part, for scholarly purposes may be granted by the professor or professors who supervised my thesis/dissertation work or, in their absence, by the Head of the Department or the Dean of the College in which my thesis work was done. It is understood that any copying or publication or use of this thesis/dissertation or parts thereof for financial gain shall not be allowed without my written permission. It is also understood that due recognition shall be given to me and to the University of Saskatchewan in any scholarly use which may be made of any material in my thesis/dissertation.

Requests for permission to copy or to make other uses of materials in this thesis/dissertation in whole or part should be addressed to:

Head of the Department of Chemical and Biological Engineering
57 Campus Drive
University of Saskatchewan
Saskatoon, Saskatchewan S7N 5A9
Canada

OR

Dean
College of Graduate and Postdoctoral Studies
University of Saskatchewan
116 Thorvaldson Building, 110 Science Place
Saskatoon, Saskatchewan S7N 5C9
Canada

Disclaimer

References in this thesis/dissertation to any specific commercial products, process, or service by trade name, trademark, manufacturer, or otherwise, does not constitute or imply its endorsement, recommendation, or favoring by the University of Saskatchewan. The views and opinions of the author expressed herein do not state or reflect those of the University of Saskatchewan, and shall not be used for advertising or product endorsement purposes.

Abstract

Torrefaction is a method for thermally treating biomass such that its physical and chemical properties are changed to resemble low-rank coal. Torrefied biomass is brittle, homogeneous, resistant to moisture and decay, and has greater energy density than raw biomass, yet retains 90 % or more of its original energy content. These properties facilitate co-firing with coal or full replacement of coal in existing power generation systems.

This research project was initiated to investigate the torrefaction process and develop more advanced methods for the process, control, and measurement in order to improve its economic viability and expand its use as a precise chemical process. This project began with the design and assembly of a pilot plant, based on a reactor design that adhered to the constraints of the torrefaction process. In conjunction with process development, new methods were examined and validated for assessing torrefaction severity using change in solid carbon concentration, as well as using near-infrared diffuse spectroscopy to directly measure differences in char torrefaction severity.

A gas-solid contactor was designed that combined a screw conveyor reactor with elements of moving bed and fluidized bed systems. A pilot plant was constructed based on this "horizontal moving bed" process. This pilot plant was then evaluated and characterized using several types of stem biomass that had been converted to flowable granules using a prototype biomass segmenting unit developed for the project.

Characterization experiments with the pilot plant were conducted using coppiced willow, wheat straw, and other feedstocks. The results illustrated that the horizontal moving bed pilot plant could achieve greater severity of torrefaction and shorter residence time as compared to similar pilot plants, was more flexible in terms of feedstock, and had reliable and repeatable control of temperature and residence time.

An investigation into how carbon content relates to torrefaction severity compared more than 100 torrefaction experiments including in-house experiments and results from a literature review. The result was a polynomial correlation relating the torrefaction mass yield (Y_m) to change in carbon concentration (ΔC), or; ($Y_m = 4.29\Delta C^2 - 3.66\Delta C + 0.98$). This correlation fits larger-scale torrefaction experimental values with a coefficient of determination of 0.935. Using the full set of the same data, a linear correlation was developed relating the loss in mass of carbon to the total mass loss for torrefaction experiments; this correlation illustrates that after the first 3.4 % of mass loss, carbon is consistently lost at a rate of 37 % of the total mass loss.

Wheat straw was torrefied in 15 batch and continuous experiments and was then subject to elemental and diffuse reflectance analysis. A linear correlation was developed that related the average change in absorbance

(ΔABS) in the short-wave infrared band from 960 nm to 1060 nm to the change in carbon concentration (ΔC) between raw and torrefied wheat straw. The $\Delta C = 0.231\Delta ABS - 0.0036$ fit the experimental values with a coefficient of determination of 0.95.

This torrefaction research project has demonstrated a very promising new process method, as well as methods for measuring and controlling chemical composition with much greater precision than was previously possible. These accomplishments as well as the potential for developing these technologies further are a significant contribution to the field of torrefaction research and development.

Acknowledgements

I would first and foremost like to thank my wife and partner, Joanna Smith for her support and encouragement during the past eight years that I spent working on this project. My thanks extend also to my parents and Joanna's parents who have all contributed to making my life such that I could carry out this research.

Dr. Richard Evitts and Dr. Aaron Phoenix stepped in at a very early stage in this work to become my research supervisors and the principals of this large project. Their continuous support of this work has ensured that we did not lose sight of our goals, or lose momentum in achieving the funding needed or in completing the research and manuscripts that followed. The ideas upon which this research was based were first shared with Regan Gerspacher, who offered his own perspective, criticism, and assistance with design, assembly, and operation of the lab equipment during the entire process. Dr. Kurt Woytiuk was my main partner in this research, and completed his doctorate in conjunction with me, on the same research project. Kurt always provided key perspective on this research and contributed greatly to my knowledge of many techniques and processes.

I would also like to acknowledge the assistance of Amy Coller, who helped with lab work, literature reviews, and in proofreading and providing feedback on this dissertation.

I would like to state my appreciation to Tim Zulkoski with SaskPower Corp, which was the first organization to fund and support this project. Dr. Joy Agnew with PAMI had a strong belief in this work as well, and assisted us with critical funding through the Applied Bioenergy Centre (ABC), and construction of the pilot plant through PAMI's office in Humboldt, SK. I would also like to state my appreciation to the Government of Saskatchewan Ministry of Agriculture ADF fund (20120072), as well as the National Sciences and Engineering Research Council collaborative research and development grant (442436-12) for funding this research.

Table of Contents

List of Tables

List of Figures

Nomenclature

Abbreviations

ABS	absorbance (with respect to electromagnetic energy)
AR	as received basis
CTU	continuous torrefaction unit (pilot plant)
daf	dry, ash-free basis
db	dry basis
F.C.	fixed carbon
HHV	higher heating value (MJ/kg)
LHV	lower heating value (MJ/kg)
MC	moisture content (% w/w)
MTOE	million tonnes of oil equivalent
NIR	near-infrared (electromagnetic spectrum)
NIRS	near-infrrared spectroscopy
SWIR	short-wave infrared (electromagnetic spectrum)
TGA	thermogravimetric analysis
VIS	visible (spectrum)
V.M.	volatile matter

Symbols

ΔC	change in carbon concentration (%)
ΔMc	change in mass of carbon per 100 g of feedstock (grams/g)
ΔMt	change in total mass per 100 g of feedstock (grams/g)
F	motor operating frequency (Hertz/Hz)
F_B	base motor frequency (Hertz/Hz)
GR	conveyor gearbox ratio (unitless)
L	heated conveyor length (m)
M_i	initial mass (grams/kilograms g/kg)
M_f	final mass (grams/kilograms g/kg)
M_m	milled mass (grams/kilograms g/kg)
MW_e	megawatts of electricity (MW)
MW_{th}	megawatts of heat or chemical heat energy (MW)
P	screw conveyor pitch (mm)

P_g grinding power (Watts)

P_{nl} no-load mill power (Watts)

Q_{input} mass flowrate (kg/hr)

R reflectance (%)

R_{char} reflectance of char (%)

R_{raw} reflectance of raw biomass (%)

S_F base motor rotational rate (RPM)

T_{tor} torrefaction peak temperature (°C)

$t_{grinding}$ grinding time interval (seconds / s)

t_{tor} torrefaction residence time (minutes / min)

Y_m torrefaction mass yield (% w/w)

Y_e torrefaction energy yield (% e/w)

Greek Symbols

Δ (delta) representing change

ϕ (phi) sphericity - unitless

1.0 Introduction

This work was inspired by the quest for energy. Energy sustains every living thing and the biosphere that we live in on earth. This includes heat from the sun to keep our environment warm enough for life to thrive, and light to drive photosynthesis that stores the chemical energy we all rely on in the food that sustains us. Humans also rely on the harnessing of energy to maintain our level of civilization and technology. This has been the case since we first started a fire to keep warm and cook our food. Now we harness energy for use in a multitude of ways, from industrial-scale farming, to massive logistical networks to move products and commodities around, as well as air and land travel, and the many energy uses we have in home and office that we take for granted.

In essence, our shared future relies on our ability to extract, store, and efficiently use chemical and electrical energy. Maintaining our energy needs currently relies to a significant degree on stockpiles of fossil-based fuels, which fuel the majority of our energy needs in the areas of transport, heating, and electricity generation. One must acknowledge the convenience and durability of the forms of these fuels, as well as their high level of flexibility to be put to whatever type of use we require.

At the same time, our civilization has the knowledge and foresight to see both that the supply of fossil fuels is finite, and that their continued use is altering the composition of our atmosphere in detrimental ways. However, altering the course of resource use is extremely challenging at this point, given the scale of fossil fuel extraction and use worldwide, which has peaked at 470×10^9 GJ of energy used in 2015[1]. This usage included 7.02 billion tonnes of coal, 50 billion hectolitres of oil (31.9 billion barrels), and 3500 billion cubic meters of natural gas (Table 1.1).

Table 1.1: World Energy Use by Type – 2015
(from source)[2]

	Oil	Nat. Gas	Coal	Nuclear	Hydro	Renew.	Total
MTOE	4341	3146	3784	582	883	366	13105
GJ	181×10^9	131×10^9	158×10^9	470×10^9			
	HL	M3	Tonnes				
	50.4×10^9	3.5×10^{12}	7.02×10^9				

To begin to replace this vast quantity of energy and chemical resources requires that all available alternative sources be investigated and exploited in attempt to mitigate the continued use of the fossil fuels. This includes utilizing solar and wind energy to their maximum extent, investigating third generation biofuels such as algae-based oils, and beginning to take full advantage of available biomass and it's potential as low-impact energy crops.

In addition to developing renewable energy production, there is also an effort underway to replace fossil fuels directly so that current infrastructure can continue to be used. In this work, coal was examined for direct replacement. Coal is a highly durable and widely available fuel has been used for hundreds of years, and the technology to extract as much energy as possible from it is being continually perfected.

The research presented in this thesis was focused on the process of torrefaction, which is used to alter the physical and chemical properties of biomass such that it can be used as a coal replacement. This project was influenced by the local reliance on coal for electricity production. The provinces of Saskatchewan and Alberta rely on coal for 44 %[3] and 47 %[4] of electricity production, respectively (2016 values). The other influence on this work was the scale of agricultural production and magnitude of arable land in Saskatchewan. The gross yield of wheat and canola in Saskatchewan for 2017 was 12.9 and 11.2 million tonnes, respectively. The scale of production for these crops in Saskatchewan is such that the energy value of the residual biomass could make a significant impact on electricity production if used for fuel.

In addition, van Rees *et al*. had been conducting a research project for several years examining short rotation coppiced willow as a potential energy crop[5–8]. Amichev *et al*. suggested that there were more than 2 million hectares of marginal or non-productive land in Saskatchewan that could be used to grow willow for use as an energy feedstock[5]. Willow had also been planted in coppices throughout the province for research purposes and thus a significant quantity was available for examination as feedstock[8]. With the varieties of available biomass, it was determined that torrefaction would be the appropriate process to modify the plants for energy use. Thus, a project was proposed to develop torrefaction for use with locally available biomass including willow, wheat straw, and others. To properly investigate the torrefaction process with these biomass varieties, a pilot plant would be required and therefore this was to be the first step of the research project.

1.1 Structure of this dissertation

This dissertation is structured in six main chapters following this introduction. Chapter 2 introduces the topics covered and provides background information on biomass, fuels, and torrefaction. The final section of Chapter 2 (2.5) outlines the overall hypothesis and objectives of the research project. Chapter 3 provides a description of the theory behind the pilot plant that was built, as well as the design, assembly, and testing of that plant. The following three chapters, 4-6, each represent manuscripts that have been prepared and submitted for publication which answer the three individual objectives outlined in section 2.5. Finally, Chapter 7 summarizes the research and discusses how the research resolved the hypothesis and objectives.

2.0 Literature review

This chapter introduces and provides depth of detail on the various subjects covered in this dissertation. This research project was an examination of the thermal treatment process known as torrefaction, which is used to alter the physical and chemical properties of biomass. This work included more than 80 bench and pilot scale experiments, detailed reactor and process design, pilot plant construction and commissioning, and an in-depth investigation into the chemical and physical properties of several species of biomass and torrefied products.

The relevant properties of biomass are described, including the macromolecular structure, composition, bulk properties, and behaviour as a fuel. Focus is placed on what differentiates biomass from other fuels and feedstocks. The properties of fossil fuels are also discussed, with particular attention to the properties of coal. Coal is the material that torrefaction chars are intended to replace, so its properties are highly relevant in assessing the torrefaction process.

Pyrolysis is the broad classification of processes that torrefaction falls within. A general description of pyrolysis and the variations of this process are provided. The torrefaction process is described in more detail, including the different biomass characteristics that it affects, and how the process is typically implemented and optimized. Some background is also provided on the history, research and development, and commercial implementation of this process. The different reactors and processes used for torrefaction are then described, as well as their specific benefits and limitations. Finally, the knowledge gaps in this field are described, taking the viewpoint of a process engineer who must design a torrefaction reactor and plant from scratch, and determine how to measure the process and product parameters to control that plant.

2.1 Physical and chemical properties of energy feedstocks

2.1.1 Structure of lignocellulosic biomass

The word biomass can be defined as either the "total living matter in a habitat", or as a classification of "organic plant and animal matter" that can be used as fuel or other raw material[9]. It is the second definition that is most pertinent to engineers and scientists interested in augmenting biomass for human energy use. Biomass that is usually considered a suitable feedstock for chemical or energy production is referred to as lignocellulosic biomass. This classification refers to solid material derived from non-food plant matter that makes up the structural elements of plants, such as stems, bark, leaves, seed hulls, and

shells, and excludes sugars, starch, protein, and fats[10]. The term lignocellulosic refers to the fact that the majority of the dry mass of this material is comprised of three classes of macromolecules: lignin, cellulose, and hemicellulose. Most lignocellulosic biomass is also considered renewable, which means that the organisms that produced the material can regrow or be replanted to rapidly replace the harvested material. Renewability is important both in terms of maintaining carbon-neutrality as well as establishing a reliable source of feedstock for continued use.

In examining how lignocellulosic biomass can be used as fuel or chemical feedstock, several inherent properties are observed which limit these uses. These properties include tenacity, hygroscopicity, susceptibility to decay, heating value, and density. The structure of lignocellulosic biomass is fundamental to understanding these properties.

Referring to Figure 2.1, cellulose, lignin, and hemicellulose structures fit together to form plant cell walls. Cellulose is the largest of these three macromolecules, with individual structures comprised of up to hundreds of thousands of D-glucose units[10] arranged in straight chains. These chains form 'microfibrils' or bundles of cellulose strands that stretch along the inside of the cell walls, forming their main structural elements.

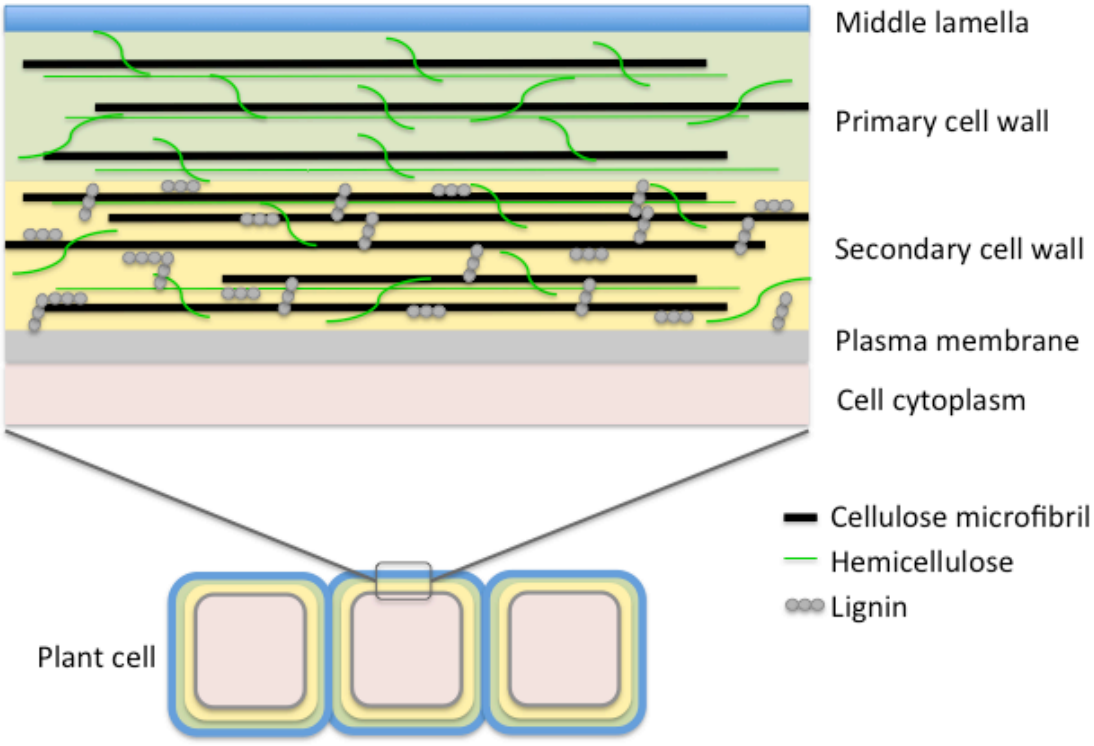

Figure 2.1: Illustration of a plant cell wall macro-molecular structure. (Adapted)[11]

Like cellulose, hemicelluloses are comprised of sugar monomers, although their chains are much shorter, containing hundreds of sugar units as opposed to hundreds of thousands. Unlike cellulose, which is comprised of straight chains of D-glucose monomers, hemicelluloses are inhomogeneous and amorphous structures that can be comprised of several different types of polysaccharides. Polysaccharides present in hemicellulose can include xylan, mannan, arabinan, glucan, and galactan; the relative presence of these will depend on cell function and plant type[10,12,13]. Hemicelluloses link the cellulose microfibrils, providing rigidity and enzymatic resistance to the cell wall[12].

Lignin, another macromolecule found in cell walls, is inhomogeneous and comprised of phenolic and aromatic structures[12]. Lignin is located in the secondary and tertiary cell walls, which form only after the cell has stopped growing. Lignin provides rigidity and strength to mature plant cells, allowing for plant stems that can support large vertical structures. Lignin is also relatively hydrophobic and is concentrated in higher amounts in 'xylem' structures, which act as the plant vasculature to transport water and nutrients from the roots up to the highest parts of the plant[14]. In terms of elemental composition, cellulose and hemicellulose contain slightly more oxygen than carbon, around 50 % oxygen (w/w) by some accounts and 43 % carbon (w/w)[10]. Lignin, on the other hand, contains over 55 % carbon, and less than 35 % oxygen[10].

2.1.2 Tenacity of fuels

Cellulose, hemicellulose, and lignin are essential components of multicellular plants. Part of the difficulty in using plant biomass as a commercial feedstock, however, is the strength that results from the combination and interconnection of these macromolecules. The result of this strength is greater difficulty in breaking this type of biomass down, as it is found to be tenacious and require significant energy input. Biomass derived from large and very sturdy plant matter such as tree wood, shells, and pits will have thicker and more rigid secondary cell walls, requiring more energy input for mechanical processing as compared to other types of biomass. Woody biomass in particular requires more than 200 kWh/tonne to achieve a sieve size of 1.5 mm[15], while for grasses (wheat straw, barley straw, switchgrass) the required range is 20-60 kWh/tonne[16,17]. By comparison, the milling energy requirement for coal ranges from 7-36 kWh/tonne to achieve the same particle sieve size[17]. Coal has a much lower energy requirement for grinding, as most coal is quite brittle compared to raw biomass due to differences in molecular structure. For woody biomass, this energy requirement can mean that more than 10 % of the energy content of the feedstock may be consumed in grinding that feedstock to use it as fuel for electricity generation.

2.1.3 Hygroscopicity of biomass

The structures illustrated in Figure 2.1 demonstrate several other key properties of biomass. The cell cytoplasm is mostly water and comprises most of the plant volume. As a result, newly harvested biomass will often contain greater than 50 % moisture (w/w). Biomass in this state is also highly hygroscopic, meaning that it will gain and lose moisture from the air and ground quite easily.

Hydroxy or O-H groups present throughout lignocellulosic structures are thought to be the structural element which makes raw biomass highly hygroscopic[10]. These O-H structures act as hydrogen bond donors due to the electronegativity of oxygen[18]. Since carbon has relatively low electronegativity, C-H bonds do not act as hydrogen bond donors unless the carbon atom itself is bound to an electronegative atom such as chlorine (Cl)[19]. The presence of oxygen in these O-H structures thus makes biomass susceptible to shifts in moisture content as a result of rainfall, snow, and humidity when stored outdoors.

In order to dry biomass and maintain low moisture content, it has to be stored in such a way as to prevent exposure to new moisture from the air and ground. In terms of using biomass as fuel, the moisture content is the main factor in determining its gross heating value. The presence of water in the fuel not only adds unusable mass to what must be processed and transported, but will also absorb some of the energy from the fuel that is burned as the water evaporates.

2.1.4 Susceptibility to decay

Moisture content is a significant contributor to increased fungal and bacterial activity in biomass stockpiles. This can lead to self-heating, reduction in energy content, and can result in a reduction in physical quality through particle disintegration and mould formation[20]. Fungi in particular are capable of metabolizing the cellulose, hemicellulose, and lignin found in wood and other biomass[21]. Elimination of either moisture or these cell structures thus has the effect of reducing this microbial activity and degradation of the biomass.

2.1.5 Heating value and elemental composition

For all hydrocarbon-based fuels including biomass and fossil fuels, their energy can be expressed in terms of heating or calorific value. This heating value assumes complete combustion with oxygen of all components of the fuel under standard conditions and is expressed as energy per unit mass of fuel. The unit typically used to express heating value is MJ/kg. The gross or higher heating value (HHV) is defined as the total energy released through combustion of all components of the fuel where the product

gases are returned to the pre-combustion temperature. The lower heating or calorific value (LHV) subtracts the heat of vaporization of water from that total and is a more realistic representation of the amount of energy that is recoverable. The heating value of a fuel can be measured directly, or estimated using a correlation such as that by Channiwala and Parikh[22] (Equation 2.1).

$$\mathbf{HHV = 34.91C + 117.83H + 10.05S - 10.34O - 1.51N - 2.11A} \quad (2.1)$$

Correlations for heating value can be based on elemental composition as in Equation 2.1 which uses the relative mass content of carbon (C), hydrogen (H), sulfur (S), nitrogen (N), oxygen (O) and ash (A), or based on proximate data (volatile matter and fixed carbon), and there are many different approaches available[23]. The correlations using elemental composition are based on the fact that most hydrocarbon fuels contain carbon, hydrogen, sulfur, and nitrogen and that each of these elements have an associated amount of energy that will be released by oxidation. For solid fuels, most of the chemical energy potential is associated with the carbon content as it is almost always the most prevalent source of combustion energy, followed by hydrogen. Non-combustible components include oxygen, any water present, as well as ash. Fuels with significant amounts of these non-combustible components will have reduced heating value compared to fuels with less. The oxygen content of raw lignocellulosic biomass for example almost always exceeds 40 %, while for coal this is typically less than 20 %.

Elemental composition and heating value for several biomass types as well as lignite coal are outlined in Table 2.1.

Table 2.1: Properties of Lignocellulosic biomass and Lignite Coal.
(from source)[24,25]

Material	C	H	N	S	O	Cl	Ash	HHV	Bulk Density	Energy Density
	%	%	%	%	%	%	%	MJ/kg	kg/m^3	GJ/m^3
Wheat straw	43.4	6.0	0.8	0.1	44.5	0.05	7.7	18	20	0.36
Corn stover	43.7	5.1	0.5	0.1	44.6	0.14	5.1	19	50	0.95
Soybean hulls	43.2	6.2	1.8	0.2	44.3	0.30	4.3	18	170	3.06
Willow	50.1	5.8	0.5	0.1	41.4	0.01	2.1	19	220[26]	4.18
Oat hulls	46.7	6.1	6.1	0.1	41.1	0.10	5.1	19	240	4.56
Lignite coal	58.8	4.2	0.9	0.5	13.6	0.00	22.0	22	700	15.4

Biomass will typically have carbon content of 50 % or less, and hydrogen content between 5-6 %, and will usually have a higher heating value less than 20 MJ/kg. Biomass or coal types with high ash content will also have reduced calorific value. When fuel moisture is included, this will further reduce the calorific value, as free water included in the total fuel mass is not only non-combustible but also absorbs heat from the combustible elements in order to vaporize. Moisture content is not only an issue for biomass; subbituminous coal can contain 20-30% moisture content and lignite up to 45% moisture[27], and these fuels are most often burned without drying[28].

2.1.6 Ash content and composition of fuels

The ash or mineral content and composition are significant factors in how biomass can be used as fuel. Agricultural residues such as wheat straw, corn stover, shells, and hulls can contain ash in significant quantities that will accumulate in a combustion chamber or flue ducting when burned. While coal can contain significant quantities of ash as well, power plants have been well adapted to the particular composition and properties of coal ash. Most types of coal ash contain varying percentages of CaO (lime), SiO_2 (silicon dioxide), Fe_2O_3 and Al_2O_3 (fly ash), and MgO. Fly ash containing at least 20 % CaO (lime) is often extracted and sold as a cementitious additive for concrete production[29]. Agricultural residues, however, can have significant amounts of the alkaline minerals potassium oxide (K_2O) and sodium oxide (Na_2O). The presence of these minerals can have a twofold deleterious effect when used as fuel. These minerals can lower the ash melting temperature inside a boiler which increases slag formation, and when combined with chlorides that are also present in some agricultural residues can result in corrosion and fouling in flue gas systems[30]. A power plant burning coal and producing fly ash that is sold as a cement additive would thus face a significant economic burden when shifting to biomass containing these alkaline minerals: loss of the fly ash revenue stream and increase in maintenance costs from the increase in slagging, fouling, and corrosion. Changing the type of fuel that is used in a generation station thus must be approached with knowledge of all downstream impacts and costs. In some cases this may limit, but not preclude, the amount of biomass that can be co-fired with coal to still produce a sufficient quality fly ash for cement use[31], or may require changes to how the fly ash is used as a cement additive or to the standards that regulate its composition.

2.1.7 Fuel density

Another property associated with biomass is its low density due to its cellular structure. Once biomass has been well dried, the cellular structures that were filled with cytoplasm sit empty, and as such at least 50 % of the dry biomass is filled with air. For some varieties this is even greater: wheat straw essentially

consists of hollow tubes with a wall thickness that can be as little as 1/8 of its diameter. Grasses like wheat straw and other varieties can also be difficult to render into a bulk form that will pack or transport well. As a result, raw biomass will nearly always have lower bulk density than fossil fuels (Table 2.1); for grasses and straw the bulk density can be less than 5 % of that of coal. The combination of the lower heating values typical of biomass and its low bulk density means the energy density of biomass can be as little as 2.5 % on a volumetric basis as compared to coal. The implications of this in terms of transport and storage are significant when considering conversion of coal power plants to co-firing or 100 % biomass. Since agricultural biomass is not produced in a centralized fashion, transport to upgrading or power facilities is a significant logistical barrier.

2.1.8 Industrial use of raw biomass for fuel

Biomass is a major energy source for several sectors. Industries such as lumber production and pulp and paper have made significant investments in utilizing residual biomass streams from their operations for producing heat and power on-site and there are many examples of pulp and paper plants in Canada that have such generation capability[32]. Some jurisdictions have also implemented heat and energy recovery from municipal solid waste that is partly comprised of biomass, although that material has its own challenges. Wood pellets are also a major fuel source for residential and commercial heating in many parts of central and northern Europe.

Some power plants have also been converted from burning fossil fuels to biomass, though such conversions have significant cost. In Canada, Ontario Power Generation has converted two power stations to using 100 % biomass, where they had previously used lignite coal. The Atikokan 220 MW_e power station was converted from burning coal to 100 % firing of 'white pellet' biomass. White pellets are produced from raw biomass, typically from residues associated with the timber and pulp and paper industries. This conversion, which required new fuel storage and handling, new burners, feedwater systems, and ash handling systems reportedly cost $170 million (CAD). The Thunder Bay 160 MW_e Unit #3 power station was converted to burning advanced biomass or 'black pellet' biomass, having similar characteristics to the lignite that was burned previously, with the conversion costing $5 million (CAD). This was a much lower cost conversion, as the advanced biomass could be stored outdoors, and only required relatively minor changes to the milling and material handling systems already in place.

Co-firing of raw biomass with coal is also something that has been investigated, but in general the co-firing ratio of raw biomass is relatively low. Co-firing raw biomass with coal is generally limited to 5-10

% (w/w) due to limitations in grinding, feeding properties, boiler combustion zone, and differences in flue gas volume[10].

Biomass to energy operations are generally limited to situations where biomass growth is highly concentrated, relatively low cost, the only fuel source available, and/or where feed-in tariffs or carbon taxes are implemented or above-mean costs are absorbed. In scenarios where these conditions do not apply, it is difficult to rationalize on a direct cost comparison basis the use of biomass over readily available fossil fuels such as coal or natural gas.

2.1.9 Fossil fuels: comparison and relation to biomass

Fossil fuels are remarkable in their stability, homogeneity, and concentration. Modern power and chemical processing infrastructure have been purpose-built around these features. For coal, the higher the 'rank' of coal, the more homogeneous it will be in terms of structure and composition. Referring to Figure 2.2, ranks of coal, peat, biomass, and several liquid fuels are indicated along with their relative composition of carbon, hydrogen, and oxygen; this type of representation is referred to as a van Krevelen diagram. This diagram illustrates how these different materials have successively less oxygen and hydrogen as the 'rank' increases, which gives higher degrees of homogeneity to these different ranks. The relative positions of fuel oil and gasoline are illustrated in Figure 2.2; these materials are distanced from most ranks of coal due to their lack of oxygen and higher ratio of hydrogen to carbon.

Methane is the main component of natural gas with a range of 87-97{33} (mole %), and would occupy a position at 4,0 on the van Krevelen diagram (not shown). The constituents of petroleum and natural gas are referred to as 'hydrocarbons', as they contain carbon, hydrogen, and little else as is clearly indicated in this diagram.

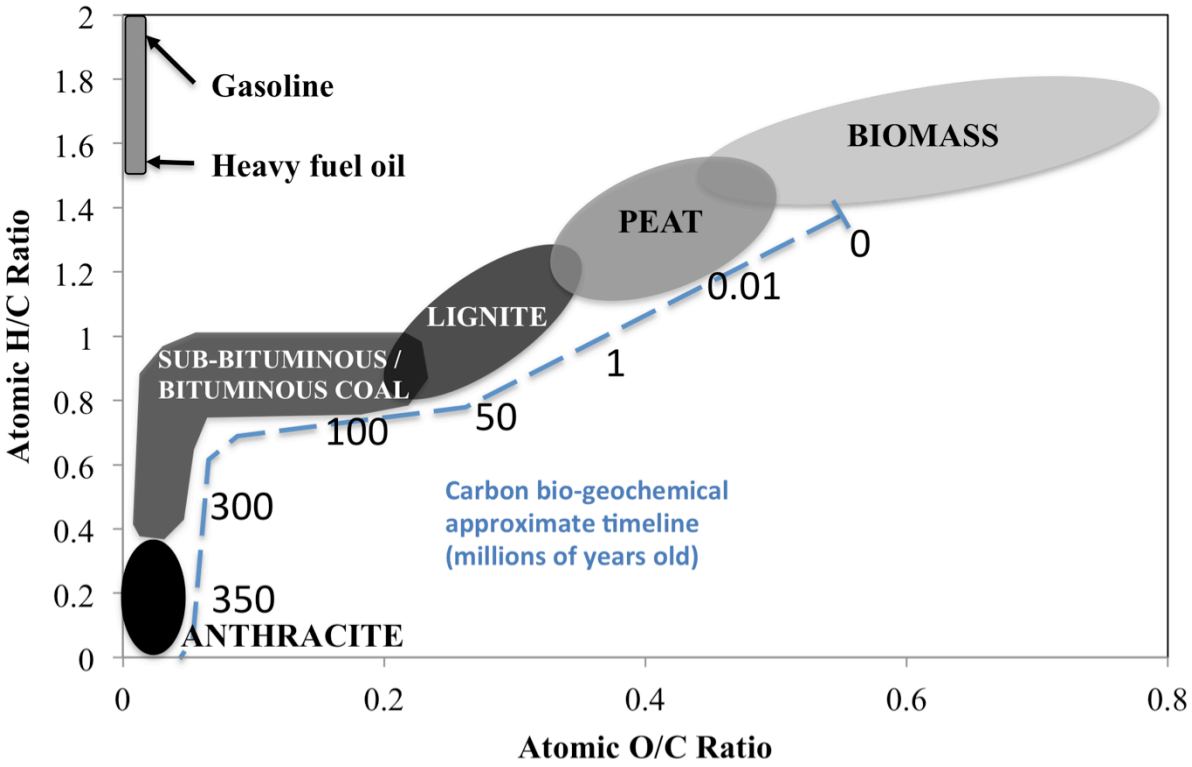

Figure 2.2: Van Krevelen diagram, illustrating fossil fuel formation timeline. (Adapted).[34–36]

All fossil fuels started as plant matter that have had their chemical and physical properties gradually altered by their environmental conditions and the passage of time. Coal is the product of plant matter in ancient marshes undergoing anaerobic decay over thousands of years to form peat. As this peat is buried under successive layers of material, the geochemical phase of change begins and continues over hundreds of thousands of years. In this phase, the peat undergoes a clear change from organic material to something more similar to mineral matter. At the point where this material resembles low rank lignite/brown coal, a million or more years has passed. Figure 2.2 illustrates the different ranks of coal as well as the bio-geochemical timeline of their formation from biomass and peat. As this low rank coal continues to age it will further change in composition, properties, and rank. Lignite/brown coal is on average 50-60 million years old; bituminous coal is 300 million years old, and anthracite at least 350 million years old. As the age of coal increases, not only does the heating value increase, but the homogeneity increases as well.

This homogeneity refers specifically to the elemental composition and molecular structures found in these materials; coal in particular is defined by its amorphous, non-polar homogeneous structure. The timeline in which biomass is converted to anthracite is one where the matter is subject to increasing

temperature and pressure. As this process goes on volatile matter is released, mainly consisting of oxygen and hydrogen, leaving behind carbon and ash, which become more concentrated as time passes. Table 2.2 illustrates some of the chemical properties of fossil fuels and biomass types.

For solid fuels, geologic processes gradually reduce the amount of gas, volatile matter, and oxygen present in the fuel. The molecular complexity is also reduced, referring to Figure 2.3. Biomass initially has a highly organized and complex structure at both the molecular and macro levels. The effect of time and pressure is to reduce this complexity in form and composition; as oxygen and hydrogen are stripped away, the remaining structures become non-polar and highly stable. The propensity for hydrogen bonding and moisture absorption is reduced. With adequate time, biomass is reduced to highly concentrated carbon in the form of anthracite.

Table 2.2 illustrates how the fixed carbon (FC) and volatile matter (VM) are different for biomass and various ranks and classifications of coal.

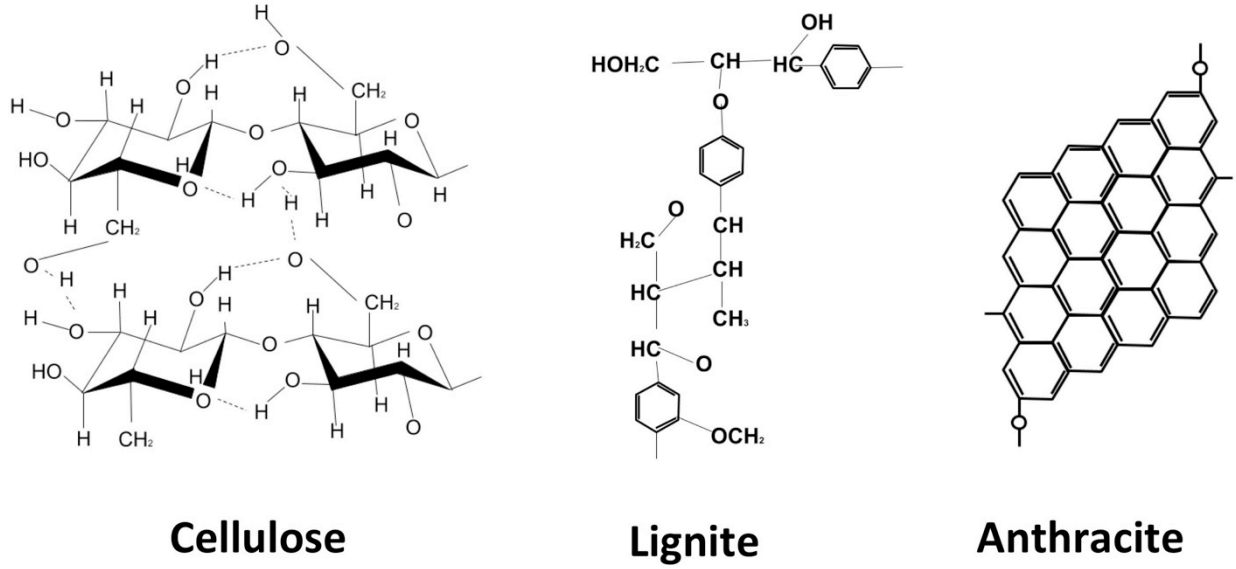

Figure 2.3: Sample molecular structures of cellulose, lignite and anthracite (Adapted)[37]

Table 2.2: Elemental and proximate composition of biomass and fossil fuel types

Material	C	H	N	S	O	Ash	F.C.	V.M.	HHV
	%	%	%	%	%	%	%	%	MJ/kg
Coppiced Willow[24]	50.1	5.8	0.5	0.1	41.4	2.1	10.6	87.3	20.2
Wheat Straw[25]	43.4	6.0	0.8	0.1	44.5	7.7	16.5	75.9	18.9
Lignite Coal[25]	58.8	4.2	0.9	0.5	13.6	22			20.0
Lignite-Subbit.*[38]	48.9	4.0	0.9	2.1	15.1	26.5	33.2	37.8	16.8
Subbit.-Bitum.*[38]	67.1	4.5	1.0	0.7	9.5	16.7	48.8	34.0	22.8
Bitum.-Anthracitic*[38]	75.1	3.5	1.0	1.4	4.0	15.0	67.7	17	24.7
Crude oil	86.4	12.4	-	-	1.2	-	-	-	42.7[39]
Natural gas	75	25	-	-	-	-	-	-	47[39]

* Average values from sampling of 40 coal sources, classified by into 3 groups by carbon content[38].

These two factors are used to describe the combustion properties of different fuels; volatile matter is released as gas/vapour during heating and will combust very rapidly in gas phase, while fixed carbon remains solid and combusts more slowly in solid phase. Likewise, as coal increases in age and depth, volatile matter is released naturally through increased heat and pressure, increasing the concentration of fixed carbon in the coal, and changing its combustion behaviour.

Anthracite, crude oil, and natural gas are the most energy rich fuels, and are defined by their high concentration of carbon and/or hydrogen, lack of oxygen, as well as their consistency and homogeneity. It is the desire for homogeneous fuel from biomass that brings one to thermal treatment processes such as pyrolysis, with the intent of simulating the geological process that forms fossil fuels.

2.2 Pyrolysis

Pyrolysis is the general term for any process where solid biomass is heated in the absence of oxygen, causing structural degradation and phase changes to the material. The pre-stages of pyrolysis start with dehydration and begin when temperature exceeds 100 °C. After the biomass is completely dry and the temperature exceeds 200 °C, molecular bonds will begin to break and volatile matter consisting of reaction water, gases, and organic condensable vapours will be liberated from the material, leaving behind a solid char residue. The final temperature for a pyrolysis process can range from 200 °C to 1000 °C and will determine the extents or severity of the changes to the solid char and the composition of the gases and condensed liquids produced.

Several parameters in addition to temperature will change the effect of pyrolysis on biomass, including the residence time, pressure, heating rate, and biomass particle size. The method used for pyrolysis is therefore dependent upon the intended end use of the products and the type of feedstock available.

2.2.1 History of pyrolysis

Humans have used a form of pyrolysis for thousands of years to convert wood into charcoal. Charcoal is a highly carbonaceous, low-smoke fuel that can be burned at much higher temperatures than wood, as high as 2700 °C. These properties made charcoal quite suitable for indoor cooking, as well as for the refining of metals from ore and production of metal alloys. Most early metal refining utilized charcoal, including early refining of copper, tin, zinc, and iron. Extensive use of charcoal for metallurgy is theorized to have led to substantial deforestation in central Europe, as well as the development of managed forest coppicing in the same region in order to produce a continuous supply of wood for this purpose. Production of charcoal throughout history was of such importance that individuals, known as colliers, were dedicated to this profession.

Until coal deposits were discovered and exploited, wood and charcoal were the principal fuels used for domestic and industrial purposes. Charcoal and wood are still widely used for heating and cooking in developing countries, particularly in Africa and South America. These are regions where either significant coal deposits were never found, or where the inhabitants must rely on local and renewable energy sources due to economic conditions and differences in energy and utility infrastructure.

2.2.2 Types of pyrolysis processes

In the modern era, knowledge and understanding of pyrolysis has been greatly expanded. The processes and chemical reactions that occur during pyrolysis have been characterized, as well as the effect of heating rate and residence time on the products produced.

Pyrolysis has been of interest for research as it can be used to reduce raw biomass into three product streams that roughly correspond to coal, oil, and natural gas.

Biomass pyrolysis produces final products that are solid, liquid, and gaseous. The solid product is known as char or biochar, the liquid is referred to as bio-oil, and the gas phase as pyrolysis gas. The composition and properties of biochar will greatly depend on its yield: lower char yield will be associated with char having higher calorific value, carbon content, and fixed carbon content. For bio-oil,

however, composition is relatively independent of yield and typically consists of a minimum 20% water content, relatively high oxygen content, and the remainder consisting of complex hydrocarbons[40]. One major difference between bio-oil and fossil (crude) oil is that crude oil has almost no water or oxygen content. As a result, bio-oil will have one-third to one-half the heating value of crude oil. The yield of bio-oil is highly dependent upon how rapidly the volatile stream is cooled prior to collection, which limits any secondary reactions between the condensable products in that stream.

Modern pyrolysis processes have been classified into four regimes: mild, slow, fast, and flash. The general constraints and requirements of these regimes are outlined in Table 2.3. Flash and fast pyrolysis processes are geared towards producing high yields of bio-oil, where slow pyrolysis produces a relatively even ratio of solid, liquid, and gaseous products, and mild pyrolysis is for producing solid product.

Flash pyrolysis requires feedstocks of less than 200 μm particle size, and temperatures of 800-1000 °C. Flash pyrolysis has the highest potential bio oil yield as well, up to 75 % (w/w), while solid and gas yields are 12-13 % (w/w). The process vapour must be quenched very rapidly to achieve the liquid yield stated. Fast pyrolysis is quite similar to flash pyrolysis: biomass is heated in only seconds to 450-650 °C, is associated with small feedstock size of less than 2 mm, very short vapour residence time, and rapid cooling of the vapour to prevent secondary reactions from occurring. The result is very high liquid yields of up to 70 %.

Table 2.3: Pyrolysis Regimes

	ARCHAIC (Charcoal)	MILD[41,42] (Torrefaction)	SLOW[40]	FAST[40,43]	FLASH[44,45]
TEMPERATURE (°C)	~ 400	200-300	300-800	450-650	800-1000
SOLID RES. TIME (sec)	> 10^5	300-3000	300-10000	< 2	< 1
PARTICLE SIZE	< 500 mm	< 25 mm		< 2 mm	< 200 μm
SOLID YIELD	< 20 %	> 75 %	> 35 %	> 20 %	12-13 %
LIQUID YIELD	N/A	< 20 %	< 30 %	< 70 %	~ 75 %
GAS YIELD	N/A	< 10 %	35 %	> 15 %	12-13 %

The liquid pyrolysis product is referred to as bio-oil and has some advantages over solid biomass. Though it contains a significant water and oxygen content, storage and transport for bio-oil is easier than for solid feedstocks due to its liquid form and relative stability.

Slow pyrolysis is quite different from flash or fast processes; slow pyrolysis is less constrained in terms of feedstock particle size, maximum temperature can range widely from 300 °C to 800 °C and residence time from 1-2 hours. For slow pyrolysis, the liquid yield is much lower at around 30 %, while gas and solid yields are each around 35 %.

2.3 Torrefaction: mild pyrolysis

Mild pyrolysis, or 'torrefaction', is different from other pyrolysis regimes in that its focus is on the yield and properties of the solid char product. Torrefaction is used for producing a brittle, hydrophobic solid char product that has 75-85 % yield of the starting dry mass and 85-95 % of the feedstock chemical energy[40,41,46–48]. The specific properties of the liquid and gas phases are less important to a torrefaction process, as they are normally used as make-up fuel to heat the process. Figure 2.4 illustrates a typical process flow diagram for torrefaction.

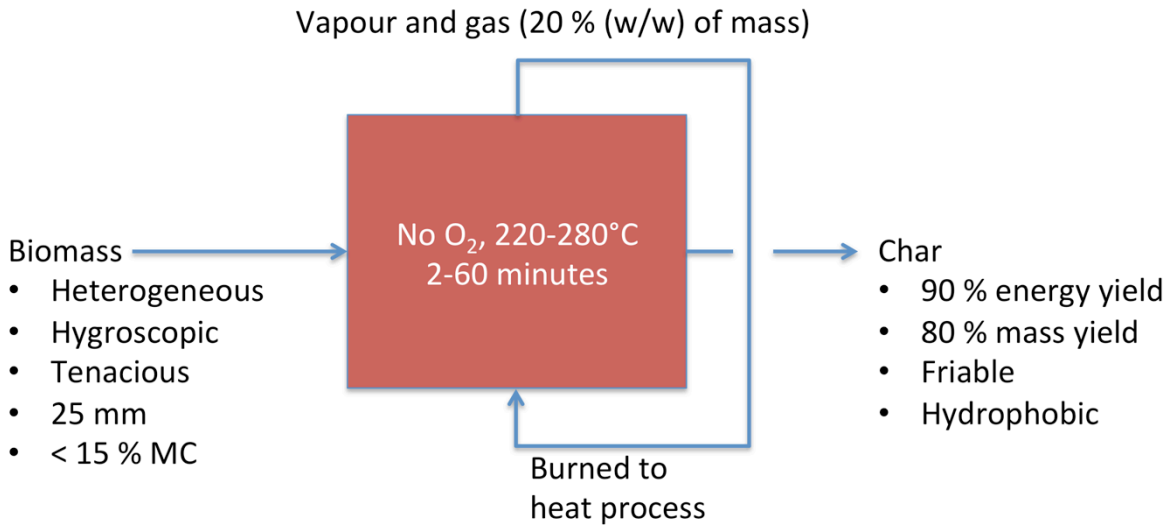

Figure 2.4: Illustration of mass and energy flows in a conventional torrefaction process (Adapted)[41]

2.3.1 Torrefaction process constraints

Torrefaction processes typically operate in a temperature range of 200-300 °C [41,47,49,50], while the torrefaction process time can range from seconds to hours, depending on biomass particle size, density, and heating rate[10,34,41]. Biomass feedstock should be not greater than 25 mm in size in any dimension and should be as dry as possible, though up to 15 % moisture content is typically considered acceptable[41].

2.3.2 Structural effect

Torrefaction changes the structure and composition of solid biomass. Of the three main plant polymers, hemicellulose begins to break down at the lowest temperature. Figure 2.5 illustrates the temperature range of torrefaction, and how hemicellulose undergoes depolymerisation, devolatilization, and carbonization reactions to a much greater extent than cellulose or lignin[41]. While raw biomass may contain more than 15 % hemicellulose, torrefaction at temperatures exceeding 275 °C will reduce detectable hemicelluloses to less than 5 %[51]. As a result of these reactions, hemicelluloses are converted to a separate stream of volatile matter relatively rich in oxygen and hydrogen[41,51,52]. Lignin and cellulose also are devolatilized in the temperature range of torrefaction, but to a lesser extent. The hydrogen and oxygen content of the solid matter is thus lowered[53], which also reduces its hydrogen bonding capacity and related hygroscopicity.

While most hemicellulose will be disintegrated at 300 °C, cellulose and lignin require higher temperatures to be eliminated in the same way: 325-400 °C and 300-550 °C, respectively[45]. Torrefaction primarily targets hemicellulose, reducing its concentration significantly, while falling short of the temperatures required to impact the cellulose or lignin content significantly.

The directly observable effects of torrefaction include a significant change in the solid feedstock color, from light to dark brown and then black, an overall more homogenous appearance and character, an increase in brittleness, and an increased resistance to microbial decay[54–56]. The extent of these changes relates directly to the process temperature and residence time; for a given torrefaction process and biomass, increasing either of these parameters will increase the severity of torrefaction observed in the char product[57].

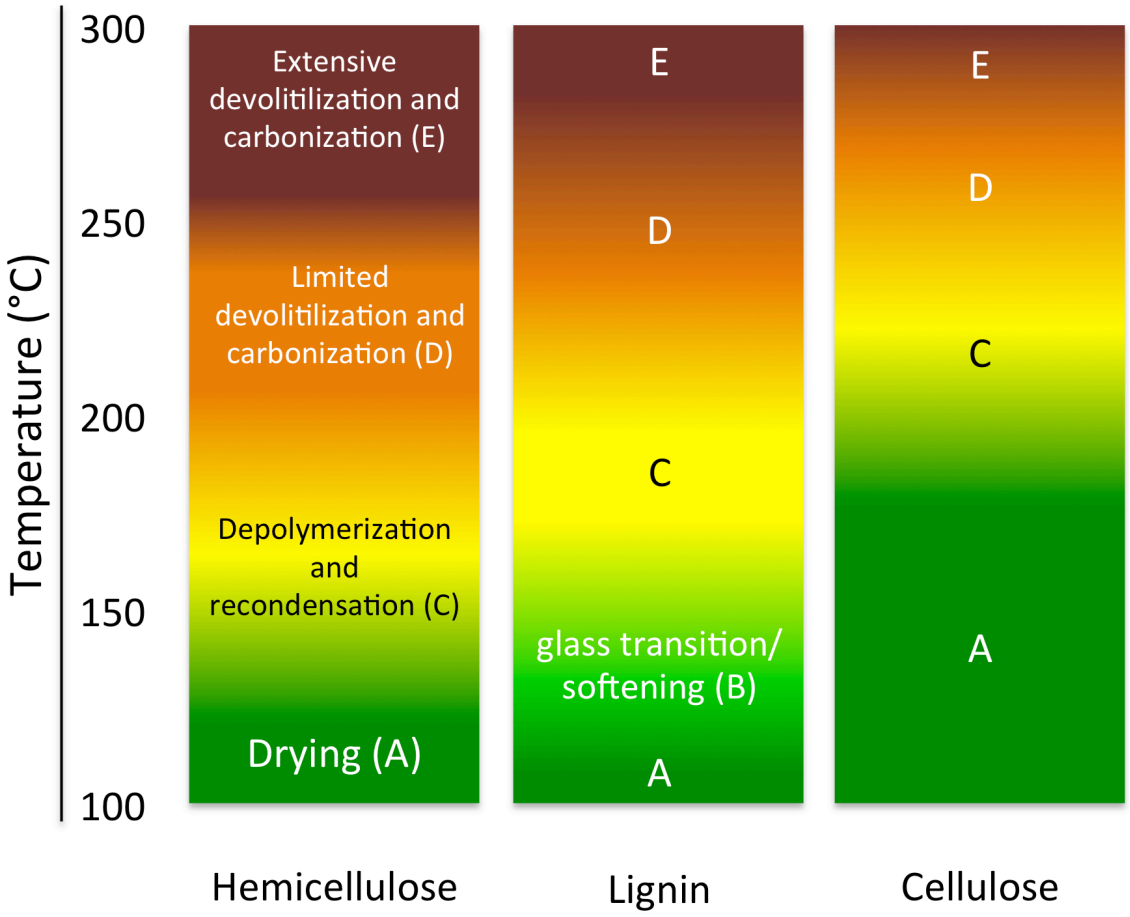

Figure 2.5: Temperature sensitive reactions of torrefaction for biomass macromolecules. (Adapted)[41]

Referring again to a van Krevelen diagram in Figure 2.6, the arrow representing typical torrefaction process data from van der Stelt *et al.* [34] can now be understood as parallel to the geological process by which biomass is converted to coal. Torrefaction in effect advances the age of our solid biomass by several million years and imparts some of the properties that would be found in coal of that age.

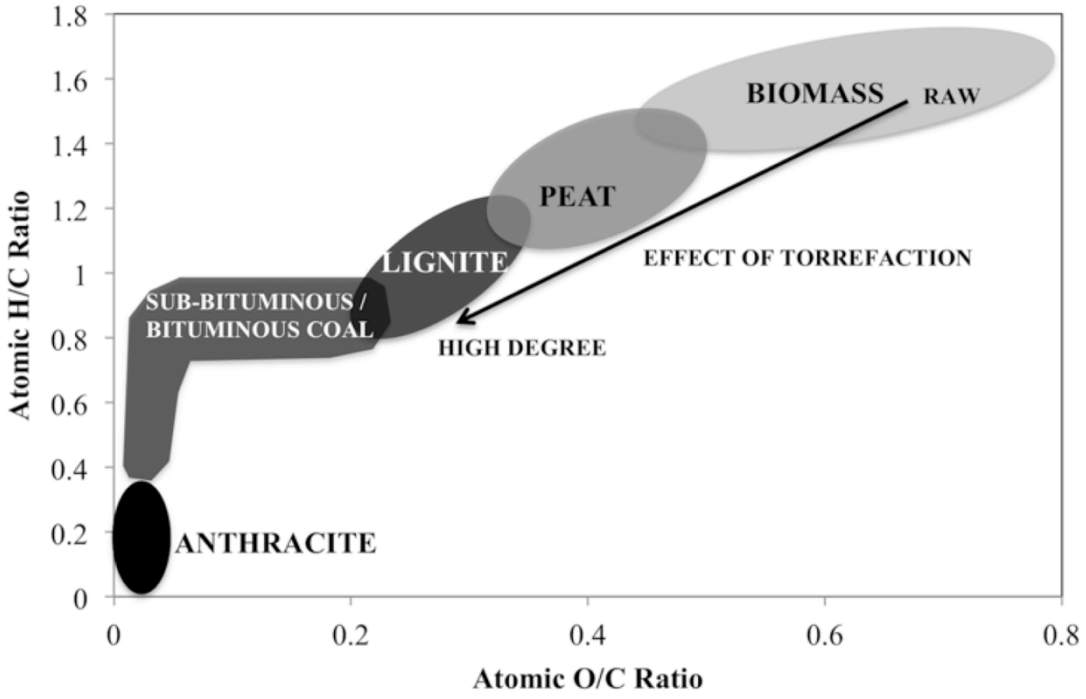

Figure 2.6: Van Krevelen diagram illustrating torrefaction pathway.
(Adapted)[34]

A secondary effect of reducing the volatile matter concentration in biomass is the reduction in the hydrogen bonding capacity of the molecular structure and thus a reduction in hygroscopicity, as well as reduction in the capacity for microbial decomposition[10,41,50,58]. This means that torrefied biomass may be stored and stockpiled for longer periods with far reduced potential for loss through decay. A secondary, but important, constraint of the process is that the volatile matter ejected from the biomass can contain sufficient chemical energy to provide greater than half of the total heating load for the process itself, if that energy can be efficiently extracted through combustion. If too much or too little energy is available in the gas stream, this can have a significant negative effect on the economic viability of the overall process.

Torrefaction of biomass causes significant changes to its structure and properties discussed in section 2.1. Hemicellulose content is reduced significantly, lowering tenacity as well as the oxygen content. The reduction in oxygen content lowers the hydrogen bonding capacity which reduces the hygroscopicity as well. Reduced hygroscopicity is associated with increased resistance to decay and degradation. Reduction in oxygen content also increases the net heating value. Reduced tenacity allows fine milling, and along with increase in heating value means the energy density is dramatically increased. In total, the

effect of torrefaction is to rapidly change the properties of biomass to be more like that of very dry, low rank coal such as lignite.

As a result of these change, the uses of torrefied biomass are considered to be twofold: it can be used to partially or fully replace coal in power generation applications, requiring minimal infrastructure and process changes while also reducing net CO_2 emissions [56,59,60]. Co-firing ratios of 1:1 are considered to be quite realistic, and conversion of coal boilers to 100 % torrefied biomass is reportedly technically straighforward. Torrefaction char has also been shown to be superior to raw biomass as feedstock for gasification, producing fewer tars and overall higher quality syngas[51,61].

2.3.3 Stages of torrefaction and key parameters

For a given process method, torrefaction severity is directly related to two process parameters: time and temperature. Figure 2.7 illustrates how the time and temperature parameters are interpreted for torrefaction. The torrefaction residence time (t_{tor}) is defined as the total time that the biomass holds a temperature above 200 °C. The torrefaction temperature (T_{tor}) is the peak temperature value that the biomass reaches within the duration of the residence time. These parameters are mainly relevant when comparing results for a single process and form of biomass.

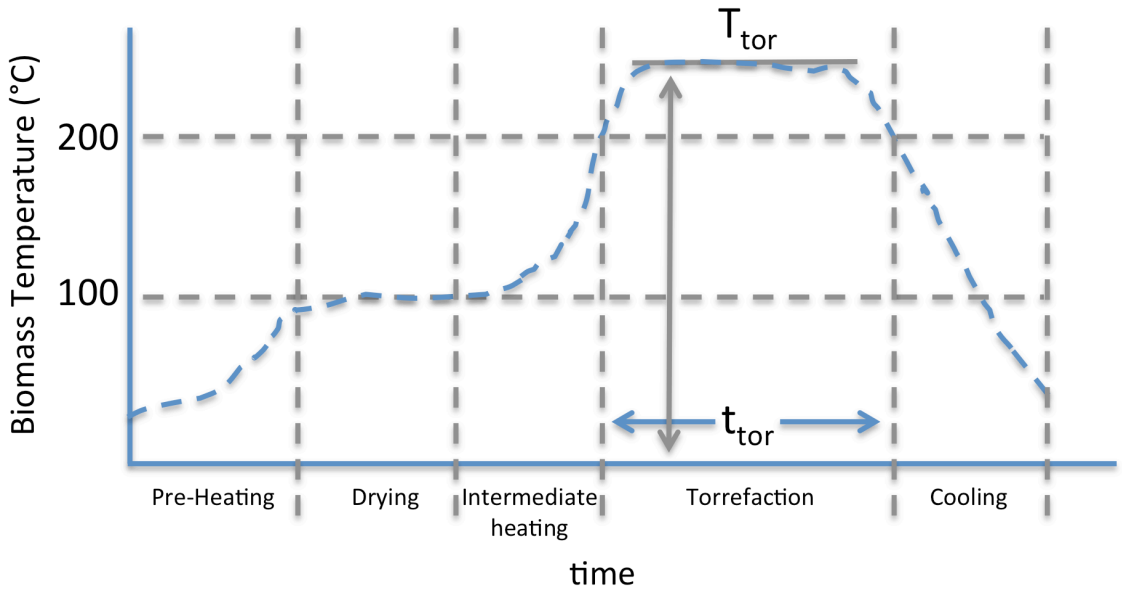

Figure 2.7: Temperature and time stages of torrefaction.
T_{tor} represents the torrefaction 'peak' temperature parameter, while t_{tor} is the torrefaction residence time. (Adapted)[41]

2.3.4 Mass flow in a torrefaction processes

Torrefaction is a process of destruction, breaking solid matter down into gas and condensable liquid. Since torrefaction mainly disintegrates and devolatilizes hemicellulose, which is rich with hydroxy groups, the volatile matter that is produced is relatively rich in oxygen, with lesser amounts of hydrogen and carbon[10,40]. Consequently, the gas stream is relatively low in energy, while the energy density of the solid increases.

As an example, Le Thanh *et al.* examined the torrefaction gas stream for dry ash wood (a hardwood) torrefied to 77 % char mass yield, and found the gas fraction to consist of CO_2 (16.1 %), CO (3.9 %), reaction water (33.5 %), acetic acid (11.7 %), methanol (3.0 %), and other organic condensable compounds (31.7 %) consisting of approximately 200 different species[52]. Wheat straw torrefied to 81% char yield, had a gaseous product consisting of CO_2 (21.6 %), CO (7.9 %), reaction water (34.7 %), acetic acid (10.0 %), methanol (1.6 %), and other organics (24.2 %). A graphical representation of this mass balance is shown in Figure 2.8.

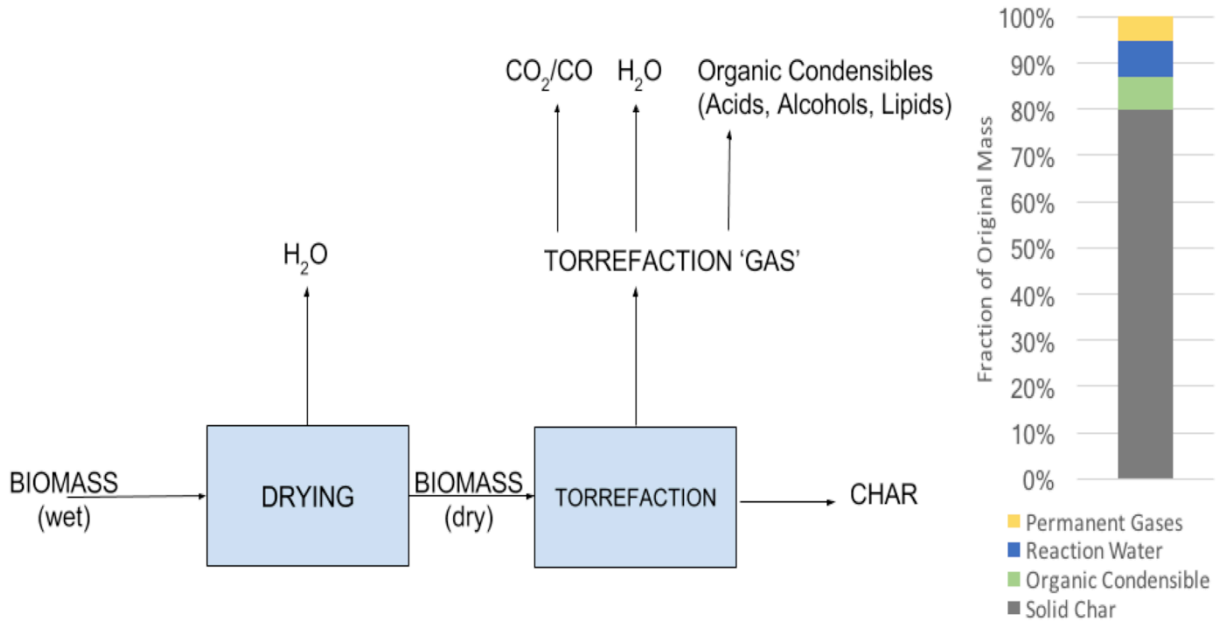

Figure 2.8 Graphical Mass Flow Diagram of Torrefaction Process

2.3.5 Energy flow of torrefaction process

Torrefaction is not constrained to being carried out at a particular pressure, but is typically conducted near atmospheric pressure for the purposes of energy efficiency. Once torrefaction temperatures are achieved, the reactions that occur are only mildly endothermic, thus the energy demand is a small fraction of the energy needed to achieve the required temperature[41]. The primary energy input to the

process is therefore consumed in drying and heating the raw material. The heat energy required for drying can exceed all other energy inputs to the system, particularly for wet biomass, therefore passive drying in ambient conditions should be used as much as possible in order to avoid unnecessary energy input towards active drying.

Given that the energy requirement of dry biomass torrefaction is mainly the increase in temperature to the 200-300 °C range, and subsequently cooling the biomass back to ambient temperature, heat recovery systems can make a substantial impact on total energy input. Further, when possible, raw biomass should be used as make-up heating fuel when required, in addition to the chemical energy of the torrefaction gas. The exception to this would be where waste heat is already available from other processes, which could be used for pre-heating or drying the biomass for the torrefaction process. Optimized systems for producing torrefaction chars will typically rely on torrefaction gas to provide between 60 to 90 % of the heat load for the entire process[10,41,58]. An example of this type of thermal optimization is illustrated in Figure 2.9, adapted from Bergman *et al.*[41].

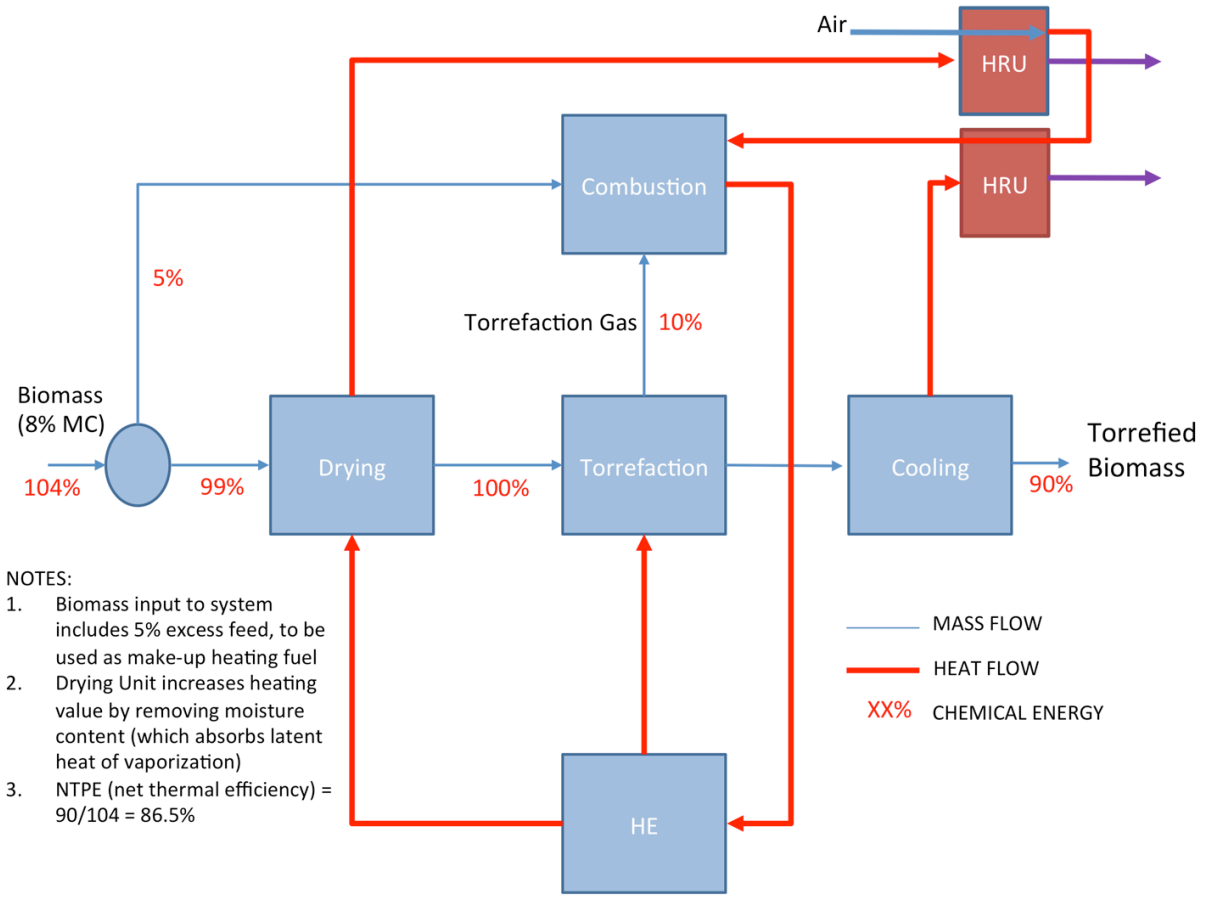

Figure 2.9: Example Energy Flow Diagram of a Torrefaction Process. (Adapted)[41]

The example in Figure 2.9 has a 90 % solid chemical energy yield for the torrefaction unit, which would correspond to a mass yield of 80-85 %. In this range, most biomass would be sufficiently brittle and hydrophobic, and have the required properties for co-firing, gasification, or storage. In this example, the torrefaction gas has sufficient chemical energy for 2/3 of the heat load, with the remaining 1/3 supplied by a stream of raw biomass splitting off from the beginning of the process. The reference point for this example process is the chemical energy flow into the torrefaction process (100 %), as this provides a useful comparison for the energy yield of the torrefaction unit (90 %), as well as clear illustration of the fuel energy gained through drying (1 %), and the amount of excess fuel needed for makeup heat (5 %). Heat recovery from the hot biomass exiting the torrefaction unit, and from the drying and torrefaction gas streams supply remaining heat load, and their implementation essentially determine how much additional biomass fuel is needed for make-up heat load. The net thermal process efficiency (ratio of thermal-chemical energy exiting the process to total input of heat/chemical energy) in this scenario is 86.5 %, while the potential economical range for torrefaction has been reported from a bit lower than 80 % (Van der Stelt *et al.* 2011) up to 90 %[41]. This efficiency will depend greatly on the moisture content of incoming biomass as well as the amount of heat recovery possible, and the practicality of fully utilizing the chemical energy content of the gas stream. It is reportedly possible to operate a torrefaction unit at the autothermal point (where the chemical energy of the gas can provide all the required heat) but it is generally considered to be more cost-efficient to use raw biomass for make-up heat fuel than to sacrifice the char energy yield, which is the desired product from this process and thus has higher economic value. This autothermal point for a torrefaction process is reportedly between 85 and 89 % char energy yield[41], thus any process operating at a higher char energy yield than that range will require make-up heat/fuel.

The non-thermal energy demand must be considered as well, which would consist of electricity for operating conveyors, fan/blower motors, and control systems. This (non-thermal) parasitic energy demand can be highly variable depending on the process type, but should be minimized as much as possible by correctly sizing mechanical systems[57].

2.3.6 Defining and measuring the severity of torrefaction

A number of measurable properties can be used to express the severity or extent of torrefaction that has occurred. Torrefaction severity is almost always defined in terms of how the solid product differs from the original feedstock, as it is the degree of this change that expresses the process severity.

The solid mass yield (Y_m), which is the ratio of final product (M_f) to initial feedstock mass (M_i), is the most common and easily measured property, and is a distinguishing factor for torrefaction from other types of pyrolysis. The mass yield for torrefaction is normally expressed on a dry feed basis (db), as in Equation 2.2, but can also be expressed on a dry, ash-free basis (daf) as in Equation 2.3.

$$Y_m(db) = \frac{M_f(db)}{M_i(db)} \quad (2.2)$$

$$Y_m(daf) = \frac{M_f(db) - M_{Ash}}{M_i(db) - M_{Ash}} \quad (2.3)$$

Other measurable properties that change in response to torrefaction are the energy density (per unit mass) and the relative milling energy of the char as compared to the raw biomass.

The severity of torrefaction can also be expressed by the solid energy yield (Y_e), which is the ratio of the total chemical energy in the solid product to that in the feedstock (Equation 2.4). This is an important parameter for a torrefaction process, as a slightly low energy yield in the char product can make the overall process non-economical[41]. The energy yield can be calculated from the mass yield, and the ratio of final heating value per unit mass (HHV_f) to initial heating value per unit mass (HHV_i)

$$Y_e(db) = \frac{M_f(db)}{M_i(db)} * \frac{HHV_f(db)}{HHV_i(db)} \quad (2.4)$$

In addition to the stated severity measures (mass and energy yield, energy value ratio, milling energy), which are bulk quantitative parameters, the severity of torrefaction can also be viewed through the lens of composition. Three compositional domains are particularly relevant to how torrefaction changes biomass: macromolecular, proximate, and elemental. Figure 2.10 illustrates how the composition in these three domains changes with respect to four torrefaction mass yields for coppiced willow.

In the macromolecular domain, the effect of the torrefaction process is to structurally weaken the biomass by volatilizing hemicellulose. Hemicellulose undergoes thermal decomposition at a lower temperature than cellulose or lignin, embrittling the structure without losing a significant portion of the energy value[41,46]. Figure 2.10 illustrates how hemicellulose content diminishes in significant steps with mass yield. As the torrefaction mass yield changes from 0.95 to 0.896, the hemicellulose content drops from 17.4 % to 12.3 %, and as mass yield drops from 0.896 to 0.798 the hemicellulose content drops further to 3.9 %.

Proximate analysis of solid fuel categorizes its contents into moisture, ash, volatile matter, and fixed carbon[40] in order to well describe the behaviour of fuel both during and after combustion. Moisture (water) will vaporize at temperatures above 100 °C, which counts against the calorific value, while volatile matter will also vaporize with increasing temperature but contribute positively to heating value as it contains some fraction of carbon. Fixed carbon is the fraction of carbon that remains after the moisture and volatile matter have been extracted, and it has the lowest rate of conversion/combustion.

With respect to elemental composition, the loss of oxygen mass is greatest during torrefaction while carbon loss is the least next to ash content[62]. As a result, the carbon content as a fraction of final mass will increase as the torrefaction conditions are intensified. The energy density will thus increase, since carbon is the main contributor to biomass calorific value, while oxygen has zero or negative contribution to the combustion value. The chemical energy remaining in the char will generally be around 90 % of the starting quantity while the mass will be around 80 % of the original[41,50].

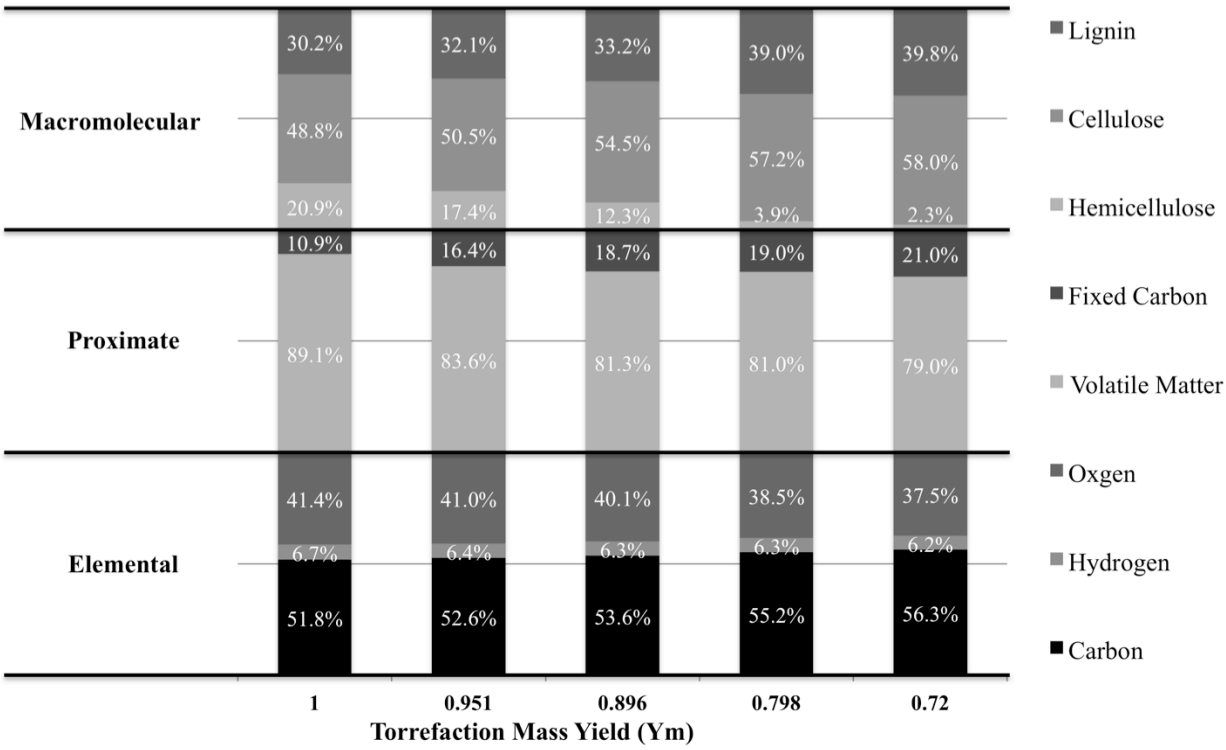

Figure 2.10: Effect of torrefaction extents on composition in three physical domains.
Values indicated are residual composition fractions.
(Data from [51,62])

Ash does not combust at all, and remains in solid form after combustion is complete, but may remain stationary (bottom ash) or carried into the air as small, suspended particles (fly ash). Torrefaction

essentially vaporizes water and volatile matter, as well as carbonizing some fraction of the volatile matter (converting it to fixed carbon). The gradual effect of torrefaction on these chemical domains is illustrated in Figure 2.10, where it is well illustrated that in torrefaction reaching a mass yield of 0.72 (well torrefied) the hemicellulose is greatly diminished, and the volatile matter and oxygen are both significantly reduced.

2.3.7 Commercial and Pilot Scale Torrefaction

The earliest reported research into torrefaction was reportedly carried out in France in the 1930's and thus the term was coined in that language, torréfaction being the French word for roasting[41]. Researchers at the Ecole des Mines in Saint-Etienne (FR) resumed this research in torrefaction again in the 1980's and the first commercial demonstration plant was built in Laval-de-Cère (FR). Pechiney S.A., an aluminum refining, recycling, and commercial product company, built the plant in order to examine if torrefaction char could economically replace metallurgical coke produced from coal. The demonstration plant operated for several years but ultimately the production cost was deemed too high. This was likely due to two factors. Firstly, the torrefaction reactor was heated indirectly using a thermal-liquid jacket, resulting in long residence times and poor throughput. Secondly, the process was reportedly optimized for specific fixed carbon content rather than energy balance. This likely resulted in char mass yield below 75 % which is generally indicated as being non-economical.

Interest in biomass enhancement technology was again rekindled around 2000 in response to concerns over anthropogenic global warming from greenhouse gas emissions. Torrefaction was immediately of interest for its potential to produce a renewable and carbon neutral replacement for low-rank coal. The use of coal for electricity, concrete, and metallurgical production is a source of more than 40 % of all CO_2 emissions, and is the single most significant source of all greenhouse gas emissions[63]. Efforts to curtail emissions from coal or replace coal directly would therefore have significant potential to reduce these emissions.

Many of the first torrefaction systems implemented what is referred to as indirect heating, essentially a conductive thermal reactor like that used in the Pechiney process, where heating is induced by conduction and radiation rather than forced convection. These systems typically utilize either a screw conveyor or drum reactor, with an envelope that draws heat conductively from another source: electricity, steam, or other heating fluid. This type of process has low efficiency and scalability but uses mature technology and off-the-shelf equipment. The longer times required here are the result of higher

thermal resistance and therefore lower heating rates. Developers of indirect heated systems include Agritech's Torr-Tech 5.0 (US), and systems by Solvay, and Arigna Fuels[10,64], which typically require torrefaction residence times in the order of 30 minutes to 1 hour because of their lower heating rate. Developers have generally found that indirect-heated technologies with poor throughput do not scale in a cost-effective manner. The major varieties and developers of torrefaction technologies are listed in Table 2.4, along with their relative advantages and disadvantages.

Table 2.4: Comparison of conventional/dry torrefaction technologies

(Adapted from [10,64])

Reactor Type	Developers	Advantages	Disadvantages
Rotary Drum	Torr-Coal (NL), Bioendev (SE), BIO3D	Proven, low P drop, direct & indirect heating	Low heat rate, difficult temp. control, large, hard to scale
Screw Conveyor	BTG, Biolake, Agri-tech Producers (US), Bioendev, Solvay (US)	Plug flow possible, proven tech,	Indirect heating only, low heat rate, hard to scale
Multiple Hearth	Wyssmont(US), CMI-NESA, Terra Green (USA)	Proven, good scale up, good control	Low heat rate, limited capacity, large Size
Moving Bed	ECN (DK), Thermya/Areva(FR), Buhler, Torftech, LMK	Density, high heat rate, simplicity	High pressure drop, difficult temp. control
Belt Conveyor	Stamproy, NewEarth	Proven, good scale up, low P drop, high heating rate	Large size, complexity, difficult temp control
Fluidized/Circulating bed	Airex (CA), River Basin (US)	High heat rate, scalable	Particle size constraint, fluidizing gas needed, attrition, no plug flow

The most efficient and rapid commercial plants, use 'direct' or convective heating methods, including vertical/compact moving beds (ECN/Andritz, Torrec, LMK Energy), multiple tray systems (Wyssmont (USA), Terra Green (USA)), as well as some drum reactors (Torr-coal, Andritz), and cyclonic systems (Airex (Canada)). The key benefit with direct heated systems is the higher heat transfer rate and thus the shorter turnover of material and higher throughput[10]. With the higher heat transfer rate of these systems comes corresponding challenges such as poor and limited temperature control, high pressure, requirement for small particle sizes, and complexity.

Beyond direct and indirect torrefaction methods, other reactor designs have been developed that can produce a very similar product. These include microwave torrefaction, hydrothermal carbonization, and steam explosion. While these methods have their own applications, they do not compare well to 'dry' torrefaction because the reaction kinetics, efficiencies, reactor designs, and products are quite different. Microwave torrefaction achieves heating of biomass through use of microwave radiation generated using electricity. While promising, this method requires significant electrical power to operate, and cannot make use of the torrefaction gas stream or other biomass for heating[10]. Hydrothermal torrefaction is mainly used to treat very wet biomass or biomass in the form of a slurry, requires a reactor that can be pressurized, and requires de-watering of the products. Steam explosion involves heating biomass to 170-230 °C with steam under pressure from 1 to 3.5 MPa, followed by explosive decompression which causes rupture of the macromolecular-structures. This is a mature technology, but due to the operating requirements and safety constraints pertaining to pressure vessels, has significant capital cost compared to systems operating at or near atmospheric pressure.

Dry torrefaction, has been viewed as a process with relatively low capital and operating cost, capable of fully utilizing the gas stream as heating fuel, and producing a dry, hydrophobic fuel that can be immediately burned to produce electricity or stockpiled outdoors. The renewed interest in torrefaction technology starting in 2000 led researchers at several institutions in Belgium and the Netherlands to start small-scale experiments[65], and also resulted in the first commercial systems being built and operated in those countries including plants in Dilsen-Stokkem (BE), and now defunct plants in Duiven (NL) and Steenwijk (NL).

The first demonstration scale and commercial systems for torrefaction did not begin operation until around 2010; as of mid-2018 there are at least six operating plants in Europe and five in North America[66], with a global total capacity around 200,000 tonnes/annum (Table 2.5).

Several torrefaction plants have been planned/built in the past 10 years and have become cancelled, postponed, or dismantled within that timeframe. This is indicative that the market for torrefied biomass is very new, and the market for this type of product is somewhat unstable. Wind generation and photovoltaic solar generation technologies are quickly maturing, and economy of scale is bringing the cost of renewable electricity down very quickly. Power producers seeking market-ready zero-carbon electricity are therefore seeking out these mature/fixed cost technologies to reduce overall CO_2 emissions, before examining new technologies that go along with large logistical challenges for new fuel feedstocks (M. Kaytor – SaskPower corporation, personal communication, March 3, 2017).

Table 2.5: Operating/Planned Torrefaction Plants of Commercial/Demonstration Scale
(from source)[10,64,66,67]

Country	City/State	Company	Capacity t/a	Technology	Started
Canada	Becancour, QC	Airex	15,000	Entrained bed	2017
Belgium	Dilsen-Stokkem	Torr-Coal	35,000	Drum	2011
France	Mazingarbe	LMK energy	20,000	Moving Bed	2012
Finland	Mikkelli	CEG/Biocarbon	10,000		2018
UK	Derby	CEG/Biocarbon	30,000	Oscillating Bed	N/A
Denmark	Stenderup	ECN/Andritz	10,000	Moving Bed	2014
Sweden	Holmsund/Umea	Bioendev	16,000	Jacketed Screw	2016
USA	Larmaie, WY	River Basin Energy	(?)		
USA	Crockett, TX	Zilkha	(40,000)		?
USA	White Castle, LA	Teal Sales	10,000	Drum	?
USA	Quitman, MI	Solvay/New Biomas Energy	80,000	Screw Reactor	2013
Total Capacity			226,000		

This research project started in 2010, prior to the start of any commercial torrefaction plant operation. Despite a great deal of torrefaction research and development, the potential of torrefied biomass for immediate uptake, and the global need for renewable and carbon neutral fuel, the market for this product is unstable. This is partly due to the instability in chemical energy prices, economical alternatives in solar and wind, and because the many torrefaction technologies are each too disadvantaged in their own way to be economically robust.

2.4 Knowledge gaps

This project was undertaken with the premise that research and development into torrefaction was in the early stages and that the perspectives from process automation and fluidized bed design could be applied and add knowledge to this field. From an early point, it was observed that a reactor had not yet been designed around the particular process constraints and requirements of torrefaction. Rather, the process itself was being constrained within existing designs that were adapted to torrefaction. Likewise, the methods for measuring and evaluating the effect of torrefaction were based on paradigms from other

fields and industries. These simply did not fit well and resulted in very challenging qualitative and quantitative process control.

2.4.1 Torrefaction reactor designs

Foremost in the descriptions of torrefaction methods were the concepts of direct and indirect torrefaction, which can essentially be described as methods using conductive or convective heat transfer. The conductive heat transfer methods have inherently low heat transfer, longer residence times, and low throughputs, leading to a general lack of economic and process viability. However, these methods have such benefits as good throughput control, consistency, and process measurability. The direct or convectively heated methods on the other hand have very high heating rates and potential throughput rates but are usually constrained by poor throughput control, poor temperature control, and inflexibility around particle size and shape.

The missing element in the field of torrefaction reactors was thus thought to be the reactor/process that was constrained to torrefaction rather than the other way around. Such a process would be feedstock flexible, have high heating rate and thus low residence time, high throughput rates, and reliability in terms of throughput rate and temperature control. The gas and vapour phases produced in this ideal plant would also be produced in such a way that they could be more easily separated and concentrated near the point of release from biomass.

2.4.2 Expressing torrefaction severity

The other areas needing further investigation and research concerned the methods used to characterize and measure the extent or severity of torrefaction. None of the methods discussed in the literature provide a real-time picture of the torrefaction process, instead commercial systems rely on characterization of their process and narrow constraints on feedstock to produce a consistent high-quality product. Developing methods and correlations for estimating the severity of torrefaction based on directly measurable properties was thus the second identified area in the torrefaction field needing further work.

Numerous measures have been proposed as being suitable for quantifying the extents of torrefaction, primarily mass yield[68], and energy yield[50,69]. While mass yield can be reliably measured in batch and semi-continuous operations where the total mass can be measured before and after the operation, it is not a practical measurement for truly continuous, scaled processes. Energy yield would be a better measure

of the process as it can be used to adjust the process efficiency, but requires both the mass yield and calorific value of the output and input streams, and is therefore highly impractical. Hemicellulose yield has been proposed as a very effective method for quantifying extents of torrefaction[70], but the best known methods require either wet digestion of the sample or proximate thermogravimetry. Both methods are time consuming and impractical for providing feedback to an operating process. Given the practicality of measuring carbon content, by using high temperature combustion spectroscopy such as the Elementar Rapid CS Cube (DE)[71], the carbon content or carbon shift may be the most practical on-line measurement for torrefaction product quality assessment.

2.4.3 Direct measurement of torrefaction char quality and severity

Tools for rapidly assessing the quality of torrefied chars are lacking, relying on off-line analysis primarily, in addition to estimates based on process parameters (temperature, retention time) rather than output measurements. While torrefaction systems can be characterized for processing consistent, homogenous inputs, changes in the feedstock quality can result in process upset and variations in product quality, since direct measurement of the product and generating the associated process feedback is difficult. Since these direct measurement methods and correlations are lacking, this limits the ability for torrefaction processes to accept a wide range of feedstocks and to precisely produce the desired product.

While near-infrared (NIR) spectroscopy has been investigated as a method for direct measurement of torrefaction char quality[72], the results of that work were quite broad, extending the investigation to the far extents of pyrolysis with mass yields as low as 20 % (w/w). While that investigation was extensive, the dataset used was lacking in the domain of torrefaction with mass yields of 60 to 80 %. Further, the correlations developed relied upon a full spectrum of data with wavelengths from 1000 to 1500 nm and models which used a matrix of measurements within this range to estimate quality measures. This means that a practical measurement using this method would require full scans of the range of spectra and complex computation to predict quality measures. With a host of different absorbance features within such spectra, prediction of key quality measures should be possible using a specific, narrow band in the NIR region.

2.5 Hypothesis and research objectives

Hypothesis

By developing a process, evaluation, and measurement techniques around the constraints of the torrefaction process, continuous torrefaction can be used as a precision chemical process for changing the properties and characteristics of biomass to economically produce thermal char and high value chemicals.

Global objective

The objective of this research was to demonstrate a next generation torrefaction process by enhancing the form of biomass, developing a controllable, measurable and effective reactor around the torrefaction process, and to develop real-time torrefaction quality monitoring methods based on existing spectroscopic and analytical methods. By contributing such methods and knowledge to this field, torrefaction may shift from "roasting biomass to cause brittleness" to a rapid, cost effective, and well-controlled advanced industrial chemical process for converting low value, heterogeneous biomass into an array of higher value homogeneous products.

This global objective will be met through individual objectives in three specific areas:

1. Design and build a horizontal moving bed pilot plant based on the constraints and requirements of the torrefaction process. Demonstrate the efficacy of the technology through torrefaction of granular biomass. Characterize the output of the process by examining standard severity metrics in response to a range of temperature and throughput settings. Demonstrate the throughput capacity of the method, repeatability, and homogeneity of product for several feedstock types.
2. Investigate how the carbon content of torrefaction char changes relative to other measures of torrefaction severity, develop a correlation relating the change in carbon concentration (ΔC) to a standard torrefaction severity metric (mass yield). Validate correlation with data from literature by other researchers.
3. Map the NIR diffuse reflectance spectra for a range of raw and torrefied biomass, then investigate and develop a correlation between NIR reflectance/absorbance at specific or general spectra and chemical or physical quanta.

3.0 A novel torrefaction process method: horizontal moving bed

This chapter describes the pilot plant that was the primary apparatus used for this research project, including the conceptualization, design, build, and commissioning of this plant as well as development of ancillary equipment for biomass pre-processing. The development and characterization of this pilot plant was one of the major research objectives of this project. The pilot plant was also used to carry out many of the experiments for the other research objectives: developing alternative expressions for torrefaction severity and direct process measurement.

3.1 Rationale for an alterative gas-solid contactor

A review of commercial and pre-commercial torrefaction methods found that most of these methods are significantly constrained in ways that make their economic viability overly sensitive to market conditions. Low heating rate, low throughput, poor scalability, poor temperature and throughput control, constrained particle size, and poor flexibility are some of the issues with existing systems. This is in part because the reactor types currently used in torrefaction were adapted from other uses such as combustion, drying or gasification[64] and were not originally designed with torrefaction in mind. In those applications, the operating constraints did not limit the efficiency or optimization of their operation. However, for torrefaction chars to be produced at a cost that is competitive with coal, natural gas, or other renewable energy sources, the operation and maintenance costs must be minimized and throughput must be maximized. These specific requirements and constraints for the torrefaction process were used to develop a new torrefaction process method.

The constraints that were determined to be fundamental in developing a torrefaction process method included:

1. Biomass should be fully heated to the temperature setpoint with as short a residence time as feasible while achieving a high torrefaction severity.
2. Temperature should be measurable, reliable, and reflect the average temperature of the biomass.
3. Residence time should be consistent, reliable, and predictable.
4. System should be able to handle particles with a wide range of size and density, from 3 mm to 25 mm, and heat the entire size range of particles to the same final temperature.
5. Capital and operating costs for the process should be comparable or lower than other convective heated torrefaction methods

For feedstock particles smaller than 1 mm, fluidized beds are nearly ideal heat transfer mechanisms, as the rates of particle mixing and heat transfer are high[73]. For particles larger than this however, tower contactors, jacketed screw feeders, or drum reactors are traditionally used for commercial scale continuous heating[74]. Screw feeders have good flow and residence time control as the particles are propelled mechanically by the flighting through the shell of the conveyor[74]. However, the downside with jacketed screw feeders is the reliance on indirect heating, as it is a complex process with a relatively poor heat transfer rate[10].

The process that was envisioned for this project would combine the convective heating of a fluidized bed with the mechanics of a screw conveyor. This process concept is illustrated in Figure 3.1. This figure illustrates the segmented design; Temp #1 and Temp #2 can be set to different values, allowing control over biomass temperature in small sections, and adjustable temperature profile. This was the concept of the author (Campbell), originally developed in 2010. This was prior to the start of the Ph.D. program for which this dissertation serves as the culmination.

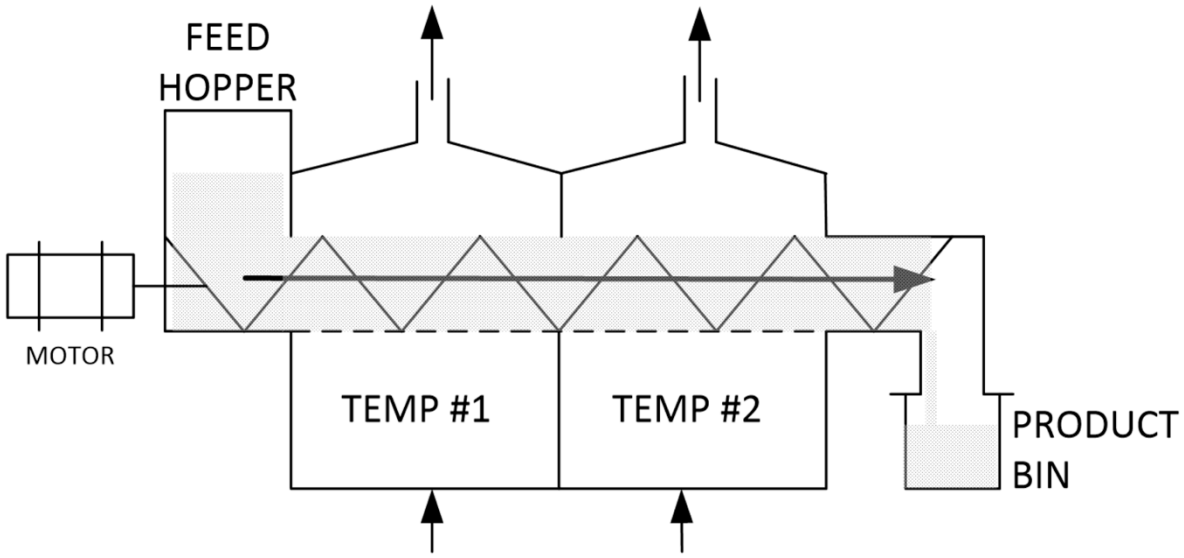

Figure 3.1: Conceptual diagram of Horizontal Moving Bed Contactor
Diagram illustrates segmented design, where Temp #1 and Temp #2 can be set to different values, allowing control of temperature profile.

Within this type of reactor, granular solids would be drawn from the feed hopper by a shaftless screw conveyor, while heated gas at just above atmospheric pressure would be injected across the screw though a perforated shell. The bottom of this shell would have a grid of holes similar to the distributor of a fluidized bed, while the top would have open ports acting as a freeboard and gas exit point. The

freeboard section would reduce the gas velocity, thereby reducing entrainment and carry-through of small particles with the exit gases. The injection holes would be designed to be small enough to prevent normal sized biomass from falling through and limited in number and size so as to have a significant pressure drop/gas exit velocity. By dividing the heated section into different zones, as indicated in Figure 3.1, the heating medium could be injected at different temperatures, thus allowing for direct and relatively precise control over the heating profile and final temperature. The rotational action of the screw would aid in mixing the solid particles, reducing process inconsistency. The heating rate possible with this apparatus was theorized to be sufficiently high to surpass most other reactor types in terms of short residence times and high throughputs, which are significant factors in terms of the economic viability of commercial torrefaction plants. The residence time in the apparatus could be closely controlled by adjusting the conveyor speed and would be quite consistent as particle position would be governed by the mechanical motion of the conveyor flighting as it would be in a screw feeder.

3.2 Process design

Beginning with the reactor concept, a pilot plant process design was undertaken that could accommodate larger scale experiments and occupy a small footprint so that it would fit in the pilot plant laboratory. The pilot plant design was based on a mass throughput rate range from approximately 1 to 10 kg/h, with a sufficient heating capacity to raise the biomass temperature to 300 °C at the highest throughput rate. This stated maximum mass flowrate range was based on coppiced willow granules, which have a volumetric density of 211 kg/m^3. The pilot plant was designed to heat the biomass in two stages so that heated air could be used to pre-heat and dry the biomass in Stage 1 and heated nitrogen from cylinders could be reserved for heating above 200 °C in Stage 2. Figure 3.2 illustrates the original process flow diagram for the plant. While Stage 1 was designed to have its heating medium warmed by a single 2 kW heater, Stage 2 was split into three independent heating segments. The temperature profile in the torrefaction section of the plant could thus be manipulated to a greater degree than in the preheating section.

An inert environment would be maintained in Stage 2 through three design and control elements:

1. Maintaining a full level in both conveyors whenever possible.
2. Maintaining a slightly higher pressure in Stage 2 to create a slight flow of inert nitrogen towards Stage 1.

3. Monitoring and alarming the differential pressure between Stage 1 and Stage 2 to ensure the higher pressure is maintained in Stage 2.

Despite using pressurized air and nitrogen as the convective medium, the pressure within the plant downstream of the gas flow controllers would be constantly maintained below 5 kPag, and during operation normally below 1 kPag. This meant that the mechanical design would not need to be pressure-rated and, more importantly, that combustible torrefaction gases could not become pressurized. This would keep the associated construction cost relatively low and ensure plant safety for operators and other occupants of the pilot plant laboratory.

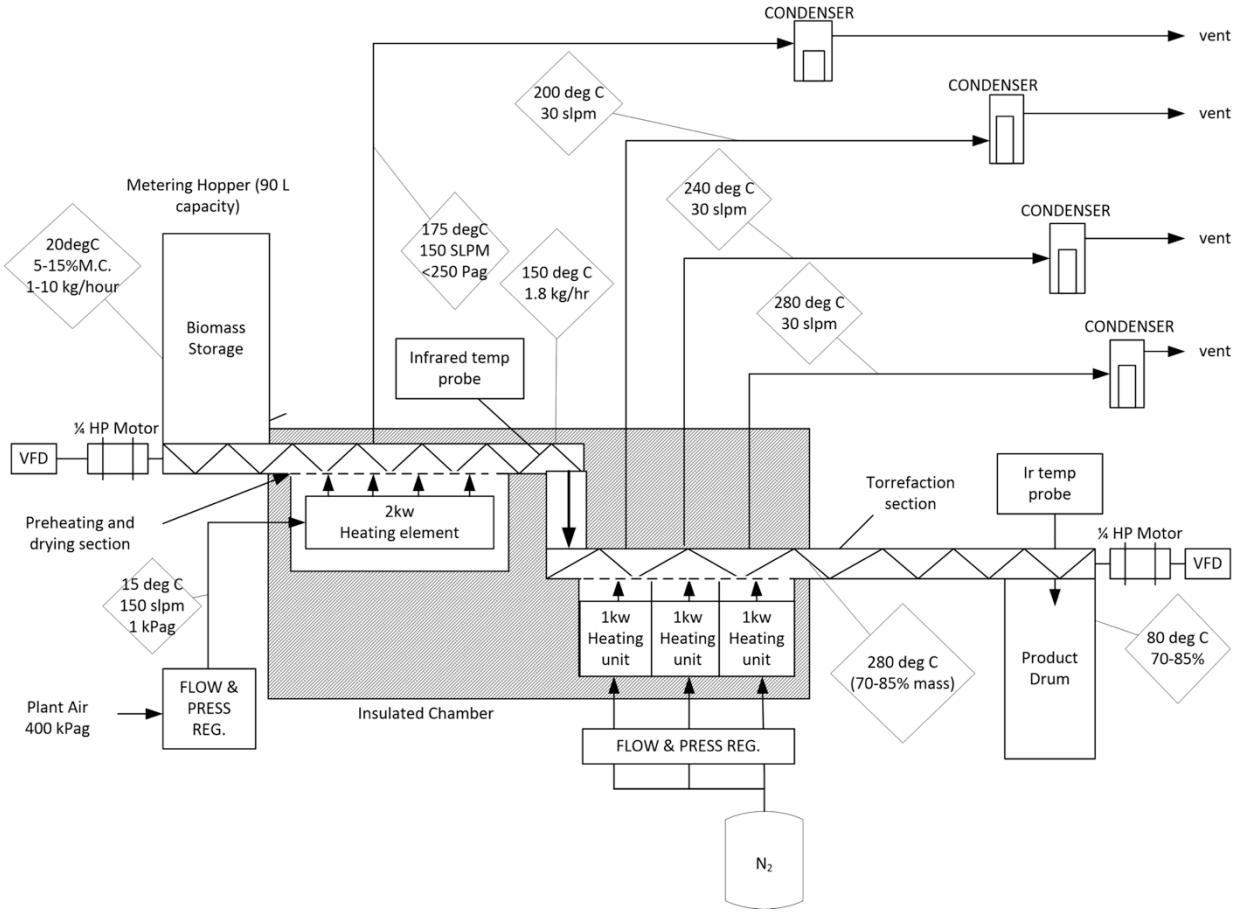

Figure 3.2 Torrefaction Pilot Plant Process Flow Diagram.
Annotations illustrate design flow conditions in for each stream; Temperature, volumetric flowrate (SLPM – standard litres per minute), mass flowrate (kg/hr), pressure (Pa / pascals), mass yield (% w/w).

3.3 Processing stem biomass into a homogeneous and flowable form

Following development of the plant concept, a key project issue was identified: lack of suitable biomass processing technology to produce enough raw feedstock for the scale of pilot plant and experiments envisioned. Wood chips produced using a drum chipper were found to have a broad particle size range; in one sample 13.7 % of particle mass was less than 3 mm in length and 36.4 % of particle mass was greater than 50 mm in length[75]. Feedstock produced in this way was completely unsuitable for use with the intended pilot plant design, both due to the wide range in particle size and the scale and fraction size of the largest particles. Similar problems were found with wheat and flax straw. To overcome this issue for early, small-scale experiments, biomass was manually prepared by cutting stems of willow, wheat straw, and flax straw using either pruning shears or a guillotine paper cutter. This method, though arduous, was able to produce consistently sized and intact particles from these stem biomass types.

With consideration that all biomass to be used for this research was in stem form, a process was developed that would produce consistently sized particles with higher sphericity and a narrow particle size distribution[75]. The developed apparatus, referred to as the "Rotoshear", consists of a rotating knife that is capable of continually cutting through a bundle of gravity-fed stem biomass, with sizing determined by an adjustable stop placed below the knife (Figure 3.3).

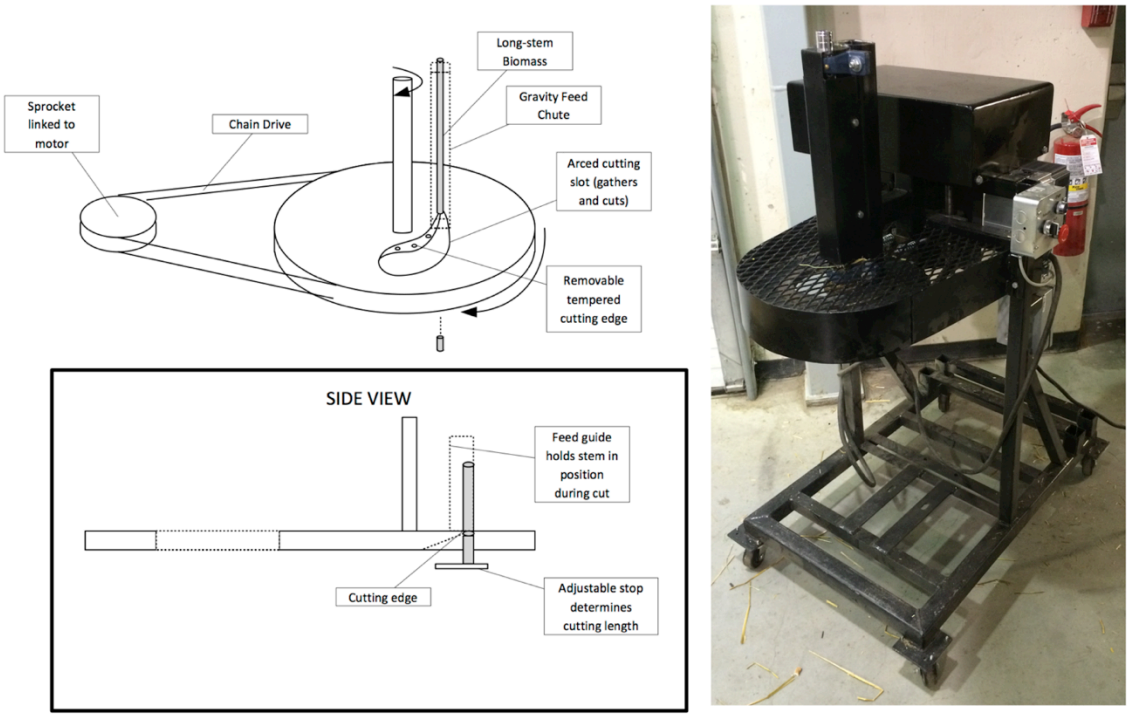

Figure 3.3: Biomass Segmenting Prototype: Rotoshear
Left: Conceptual Drawings Right: Photograph of prototype shaft/cutting wheel

The concept for this apparatus was adapted from the S3 Firewood Processor made by Bilke/Lehtoniemen Metalli Oy (FIN) in which waste lumber and small trees were segmented into firewood billets 0.2-0.55 m in length using a rotating cutting mechanism[76]. The Rotoshear is a scaled down and simplified version of the S3 that has been rotated to the vertical plane and is fed multiple stems through a narrow chute by gravity rather than a conveyor belt as is the case with the S3.

The Rotoshear could produce granules of willow, straw, and cattail in bulk quantities that would flow readily through the smallest screw augers used in the experimental work. Table 3.1 illustrates the average dimensions and sphericity of the willow particles prepared using the Rotoshear for a 40-granule sample. Photographs of examples of biomass granules produced by this system can be found in Figure 3.4.

Table 3.1: Dimensional averages for willow granules prepared using Rotoshear

Cylindrical Particles - Willow - 40 particle sample			
	Diameter (mm)	Length (mm)	Sphericity
avg	7.45	19.3	0.80
min	2	16	
max	14	22	
stdev	3.4	1.3	

Figure 3.4: Biomass granules produced using Rotoshear, from left; willow, wheat straw, cattails

3.4 Pilot plant design, build, and commissioning

Based on the process flow diagram design from section 3.2, a continuous torrefaction pilot plant with peak throughput of 10 kg/h was designed and built with the assistance of PAMI and the Applied Bioenergy Centre between 2013 and 2015. This plant was designed to utilize granular, solid feedstocks such as those prepared using the Rotoshear prototype, which could include cylindrical feedstocks cut into 10-20 mm lengths and up to 20 mm diameter. These parameters conformed to the maximum typical biomass feedstock dimensions for most other torrefaction processes[66], and would allow the pilot plant to be as feedstock flexible as possible.

3.4.1 CTU Stage 1

Design and construction of this plant began with Stage 1, which was used to test and demonstrate if the concept could be implemented in a single heating segment, and to refine the elements of the reactor before expanding the pilot plant to its full heating and throughput capacity.

Stage 1 was designed around a shaftless screw conveyor with an outer diameter of 0.037 m and a conveyor shell with an inner diameter of 0.048 m. Among the most critical elements of the Stage 1 design process was the gas injection/heating grid on the bottom side of the conveyor shell. This grid would need to deliver the heating medium to the flowing solids without compromising the strength of the conveyor shell or allowing small particles to fall into the distributor chamber. Figure A.3.1 in Appendix A illustrates the final design of the Stage 1 conveyor shell. The heating grid consists of 96 1-mm holes arranged in 4 rows spaced over a 0.912 m section of the conveyor. The holes are offset from the centre to reduce the amount of dust falling through the grid when gas flow is not present. There are four 25 mm diameter gas outlets evenly spaced along the upper side of the conveyor shell, which also act as temperature measurement points for the reactor. Figures A.3.2 and A.3.3 in Appendix A illustrate the design of Stage 1 and the arrangement of the internal heat distributors.

To ensure that a uniform pressure was present across the entire length of the grid, the convective medium flows through several stages. The convective medium first flows past an inline 2 kW electric heater, then into a first stage distributor before flowing out of that distributor into the ‘windbox’ which lies below the conveyor shell, as illustrated in Figure 3.6. The heater is operated by a Watlow (USA) EZ-zone digital temperature controller, which receives its setpoint from the operator, and its process value from the PLC control system. Since all of the thermocouples in the system are connected to the PLC, it was straightforward to enable the PLC retransmit either the internal distributor temperature or

the conveyor inlet temperature to the temperature controller. The operator thus has control over what part of the system temperature and what setpoint are used to control the heater output. This allows for a more 'controlled' pre-heating stage and reduces overshoot in bed discharge temperature.

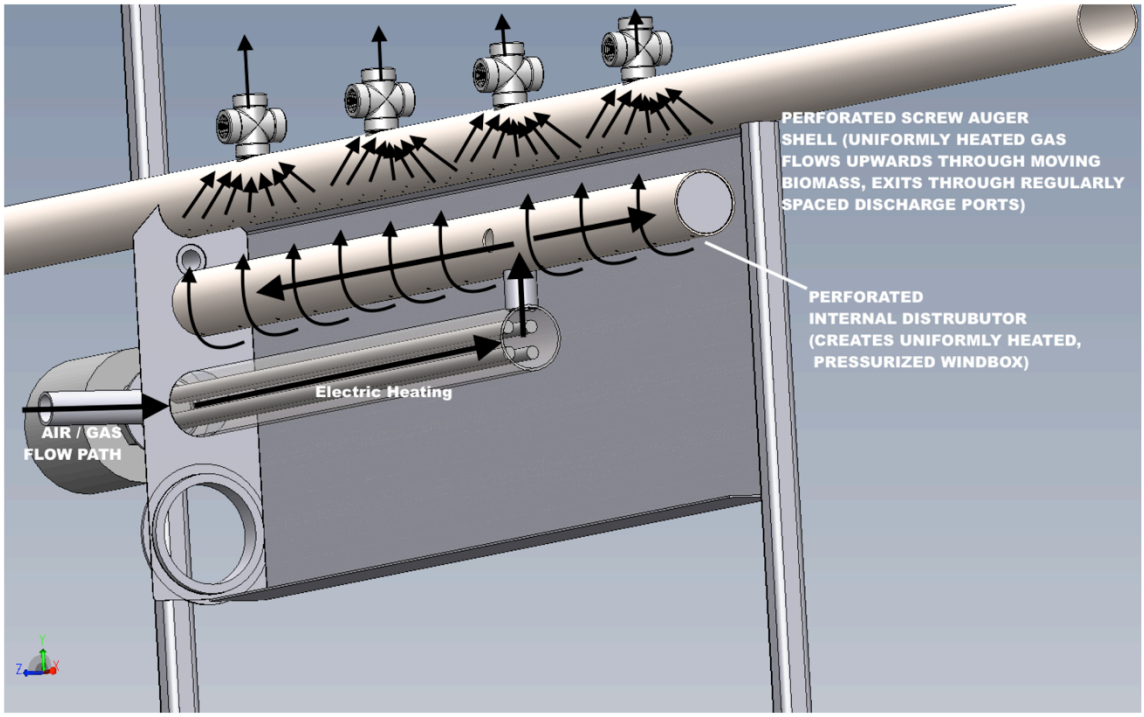

Figure 3.6: CTU Stage 1 "Windbox" internal detail with flowline illustration
(from 3-D rendering courtesy of PAMI)

This initial build was designed to be a completely functional part of the final pilot plant. Stage 1 was fully instrumented, including the 90 L metering hopper, operator touchscreen and PLC control system, full scale electrical distribution cabinet, and a single stage gas cooling tank as illustrated in Figure A.3.4 in Appendix A. Figure 3.7 illustrates the front and back of completed Stage 1 build.

Figure 3.7: CTU completed Stage 1 photographs (front/rear)

Along with controlling residence time in the heated section using the conveyor speed, the solids temperature is the most important measurement and control parameter for the reactor. The design of the horizontal moving bed relies upon indirect temperature measurement; temperature probes are mounted very near to, but not touching the moving biomass in the conveyor. Thermocouples are mounted in the exhaust ports on the upper side of the conveyor shell such that the measurement point is within the gas stream, less than 20 mm above the moving biomass in the conveyor. This is illustrated in Figure 3.8.

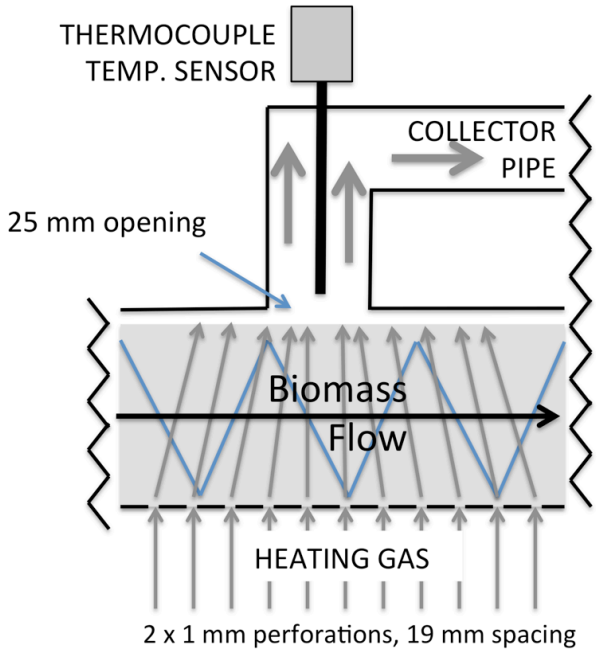

Figure 3.8: Illustration of horizontal moving bed in a localized section. Indicates temperature sensor mounting location, biomass flow path and heating gas flow path.

The temperature measured in this manner is thus the exhaust gas temperature, which is inferred to be very near to the average biomass particle surface temperature.

Testing of the completed Stage 1 prototype consisted of three experiments with coppiced willow granules having a moisture content of 9.2 % w/w. The conveyor was operated at two different rotational rates corresponding to approximately 1.5 kg/h and 3.0 kg/h dry feed-rate, and two air flow rates of 100 lpm and 150 lpm. Using a final airflow temperature of 188-196 °C, the willow granules were heated to a final temperature of 140-150 °C and after cooling were subsequently measured to be completely moisture free. Based on this result, the design of Stage 2 was undertaken using a similar heater inlet arrangement but split into three separate smaller segments.

3.4.2 CTU Stage 2 design and integration

Once Stage 1 of the CTU was tested and shown to heat granular biomass as expected, the planning and design for Stage 2 commenced. A simplified process and instrumentation diagram (P&ID) for both stages is illustrated in Figure 3.9. Detailed P&ID for Stage 2 can be found in Appendix A (Figure A.3.8). Like Stage 1, Stage 2 consists of a single shaftless screw conveyor, but with an outside diameter of 0.064 m in a 0.073 m internal diameter shell. This conveyor was designed with a greater diameter than conveyor 1 in order to facilitate a longer residence time range of 5-50 min while the heated section, like Stage 1, was designed to be 0.9 m in length.

While the purpose of Stage 1 was to dry the biomass feed and heat it to 150 °C, Stage 2 would contain the torrefaction part of the process. Stage 2 would thus need to meet other specific process constraints such as requiring an absence of oxygen, having a closely controlled and monitored temperature profile, and controlled residence time.

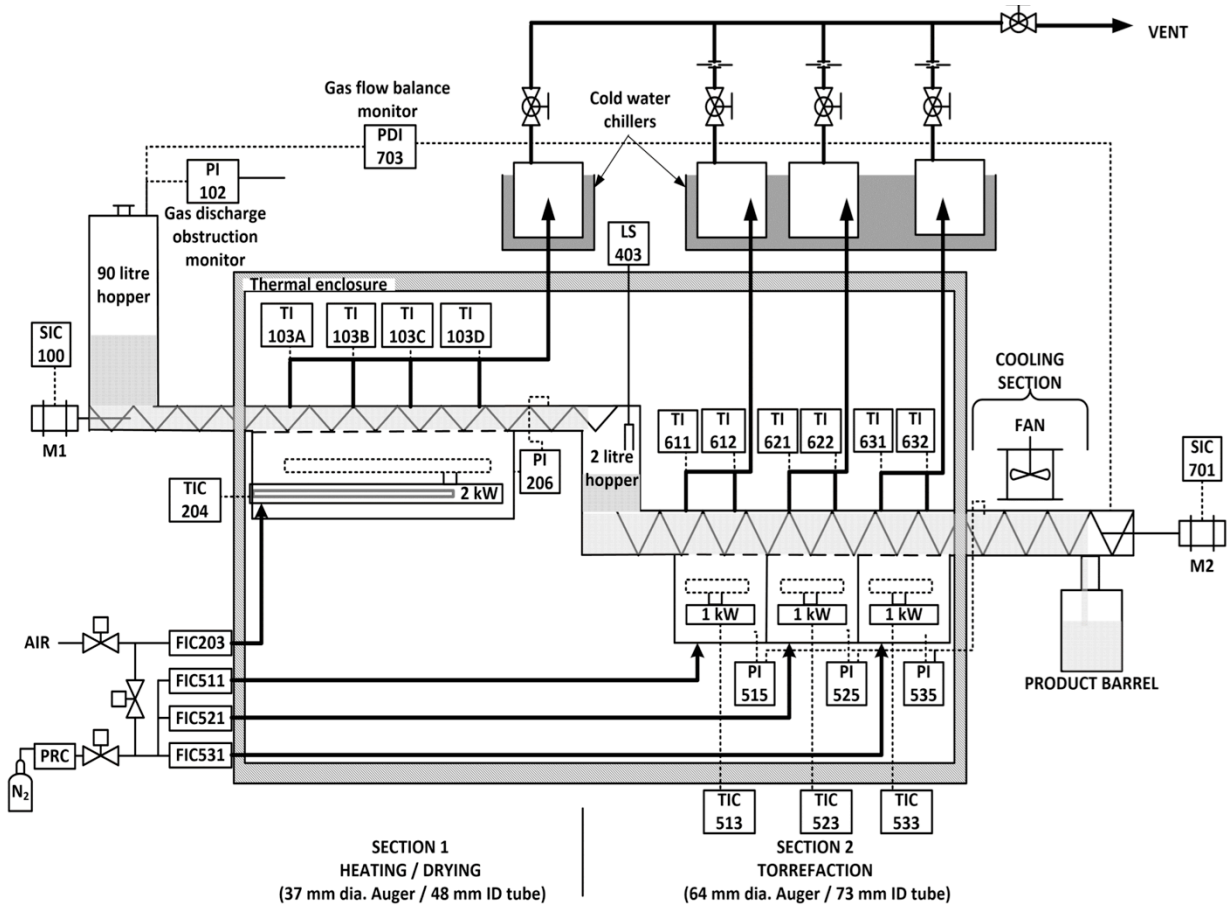

Figure 3.9: CTU Simplified P&ID.
Delineation between Stage 1 and Stage 2 is indicated, as well as 10 temperature probes on the upper part of the 'reactor' zones which infer torrefaction temperature.

3.4.3 Torrefaction residence time and plant throughput

The torrefaction residence time (t_{tor}) for the CTU was to be set based on the rotational rate of the torrefaction section conveyor, which is inversely proportional to the frequency setting of SIC-701 (Conveyor 2 variable frequency drive), as illustrated in Equation 3.1. This equation is used to calculate the required frequency (F) to set the reactor for a specific torrefaction time (t_{tor}).

$$t_{tor} = \frac{F_B}{F} \cdot \frac{GR}{S_F} \cdot \frac{L}{P} = \frac{214.3}{F} \xrightarrow{\text{yields}} F = \frac{214.3}{t_{tor}} \qquad (3.1)$$

The torrefaction residence time is defined for the CTU as the estimated time that a particle will be exposed to active heat in Section 2; this is a function of the operating frequency of the motor (F), which is transmitted from the variable speed drive. The other variables indicated in Equation 3.1 are constants in this system, including the gearbox ratio (GR), full speed rotational rate of the motor (SF), the active heating length (L), and the conveyor pitch (P). These and other key physical parameters can be found in Table 3.2.

Table 3.2: Pilot Plant Key Physical Parameters

Metering Hopper Volume	0.090	m^3
Stage 1 Conveyor Length	2.1	m
Stage 1 Heated length	0.91	m
Stage 1 Screw Diameter	0.037	m
Stage 1 Screw Pitch	0.032	m
Stage 1 Conveyor Tube ID	0.048	m
Stage 1 Conveyor Speed Range	1.7 – 28.8	RPM
Stage 1 Volumetric output range	0.06 – 0.96	lpm
Intermediate Hopper Volume	0.002	m^3
Stage 2 Conveyor Length	2.3	m
Stage 2 heated length (L)	0.90	m
Stage 2 Screw O.D.	0.064	m
Stage 2 Screw Pitch (P)	0.059	m
Stage 2 Conveyor Tube ID	0.073	m
Stage 2 Conveyor Speed Range	0.7 – 7.2	RPM
Stage 2 Volumetric output range	0.1 – 1.6	lpm

As indicated in Table 3.2, the maximum volumetric output range for Stage 1 is 0.06-0.96 lpm while for Stage 2 this range is 0.1-1.6 lpm. The overlap between the two conveyors is thus 0.1-0.96 lpm, very near to the 10:1 turndown ratio of the original design.

The purpose of the 0.002 m^3 intermediate hopper was to allow a full level to be maintained in Stage 2 by always having surge capacity available in this hopper. To facilitate this, the system was designed to have a level switch (LSH-403) in the intermediate hopper that would indicate when this excess volume was present. The system would start feed with conveyor 1 on and conveyor 2 in an auto-start condition; once the level switch triggered in response to biomass filling the hopper it would initiate conveyor 2 starting through the control system, and conveyor 1 would receive a lower speed setpoint. Once the level switch deactivated, conveyor 1 would again receive a higher speed setpoint. The low speed setpoint was always set to be less than the volumetric throughput rate of conveyor 2, while the high speed setpoint was set above this rate.

3.4.4 Plant heating and temperature monitoring

Because exceeding 200 °C and achieving a consistent, predetermined peak temperature in the torrefaction section are key characterization parameters, a significant part of Stage 2 design was to both measure and control the temperature at regular intervals in Stage 2.

The heated section of Stage 2 is divided into 3 segments, each of which has its own 1 kW heater and distributor and is sealed from adjacent segments. Individual digital temperature controllers control each of these heaters as well as the Stage 1 heater. Each temperature controller can use the temperature measured at either the heater discharge point or the just below the distributor grid. Figure 3.10 illustrates a cross-sectional representation of the horizontal moving bed, indicating the relative locations of the two temperature controller measurement points, as well as the process temperature measurement point. While the temperature measured just below the distributor would be very close to the temperature of heating gas as it enters the conveyor, the response time between the heater and this sensor would be relatively long. The heater discharge temperature, however, would respond very quickly to activation of the heater. Due to these response times, the heater discharge temperature would be used as the process measurement during initial pre-heating, while the distributor temperature would be used as the process measurement after the system is near operating temperature and steady state.

While Stage 1 has four temperature measurement locations in the drying section, there are two temperature measurement locations for each of the three segments in Stage 2, for a total of six probes. Referring to Figure 3.9, the four temperature probes in Stage 1 are tagged TE-103A-D, while those in Stage 2 are tagged TE-611/612/621/622/631/632. These temperature probes are Omega Engineering Inc. (USA) Type K 6 mm thermocouples, (KQXL-14). Figures A.3.5 and A.3.6 in Appendix A provide more detail on the arrangement of heaters, internals of stage 2 heating zones and discharge ports.

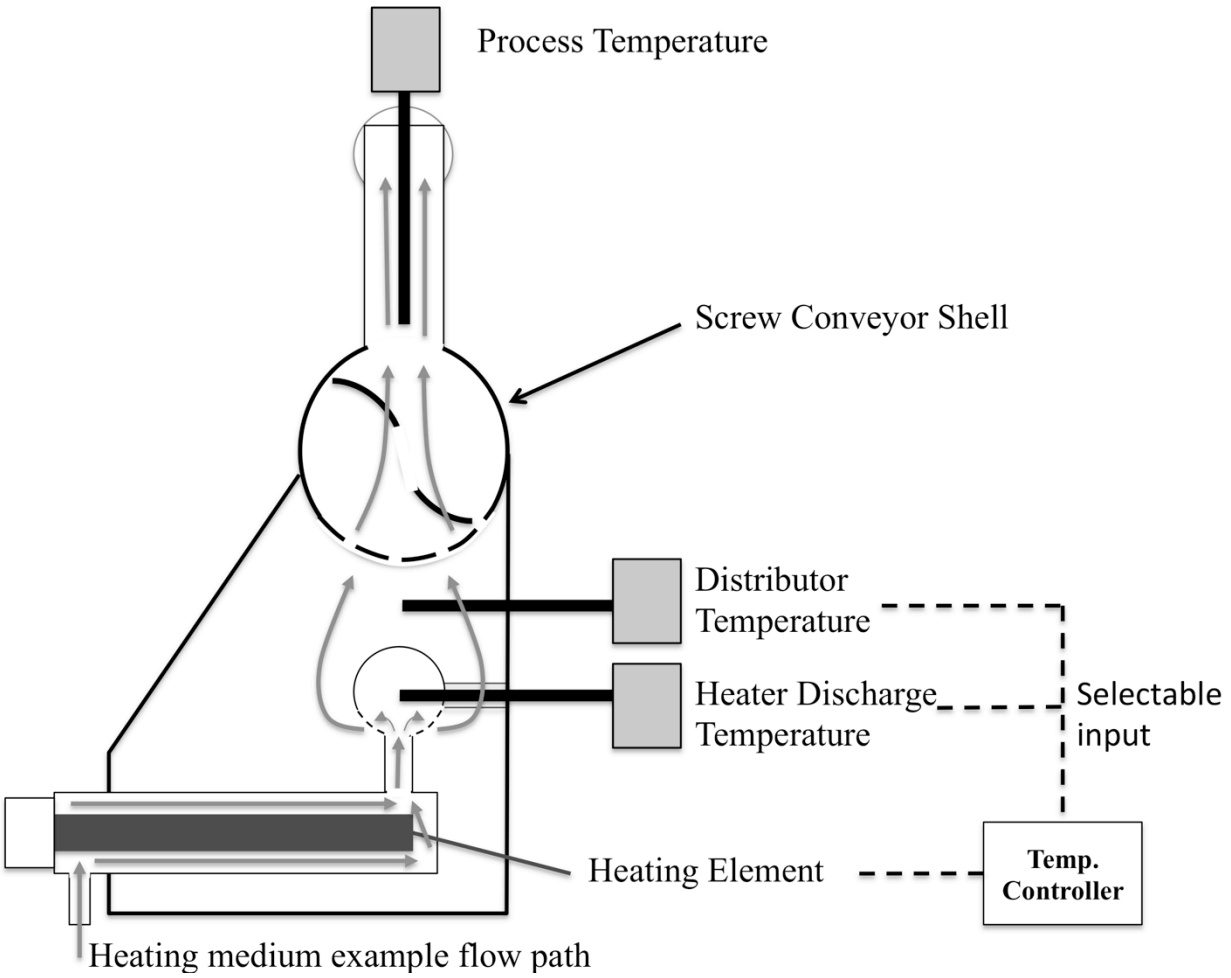

Figure 3.10: Cross section diagram of horizontal moving bed for CTU Stage 2.
Includes detail of temperature measurement locations and heating gas flow path.

3.4.5 CTU pressure monitoring and flow control

Pressure measurement serves two principal purposes for the CTU pilot plant. Pressure transducers (Series 616, Dwyer Instruments Inc., USA) monitor the pressure in the gas heating manifold, at each segment of the moving bed, and in the discharge streams of the torrefaction stage to monitor and balance the 3 legs in this stage. Pressure is also used for monitoring overall system air flow, routing and detecting blockages, detecting particle entrainment to discharge manifolds (higher pressures indicating high load of particles in manifold), and for balancing airflows in Stage 1 and Stage 2, and between the segments in Stage 2. The most critical pressure measurement in terms of process operation is the end-to-end differential sensor PDI-703, shown in the instrumentation diagram, which is used to monitor the net flow of gas from Stage 2 to Stage 1 and indicates how to adjust the gas flow rates, and when to adjust back pressure valves to ensure there is no net flow of air to that stage.

The flow of carrier gas in each of the four heating segments in the pilot plant is set and controlled by Omega (USA) FMA 5540 mass flow controllers. The Stage 1 flow controller has a maximum output of 150 lpm (air/nitrogen) while each of the Stage 2 flow controllers has a maximum output of 60 lpm.

3.5 CTU operator controls and automation

The CTU was designed to have as many measurement and control points as possible in order to inform the operator of all pertinent process conditions, to characterize the reactor for many possible combinations of variables, and to facilitate a wide range of experiments. Each of the 25 temperature and 10 pressure instruments are wired to a Modicon 340 PLC (Schneider Electric SE, France). Control algorithms and instrument calibrations are implemented in the M340. A desktop computer is used as a data acquisition and logging system; this PC receives instrument data from the PLC which is recorded to comma separated variable datafiles using LabView™ 10.3 (USA). The operator interface to the plant is a Magelis HMI-STU-655 touchscreen interface (Schneider Electric SE, France) with redundant monitoring and controls on the data-logging PC. The main operator control interface is indicated in Figure 3.11. This operator screen indicates all significant process measurements and conditions for temperature, pressure, and flow to the operator and has controls for motor speed/activation, valve control, and the flow and temperature controllers setpoints.

Hard-wired controls are also provided for the heaters and motors so that they can be easily deactivated if the touchscreen interface or PLC were to be disabled. Emergency stop buttons are wired to each of the variable frequency drives that initiate immediate motor shutdown, and each heater has operator switches that disconnect its activation relay. Each heater also has a pilot lamp that indicates when its control circuit is active. Figure A.3.9 (Appendix A) illustrates these operator controls on the main control panel, as well as the four digital temperature controllers.

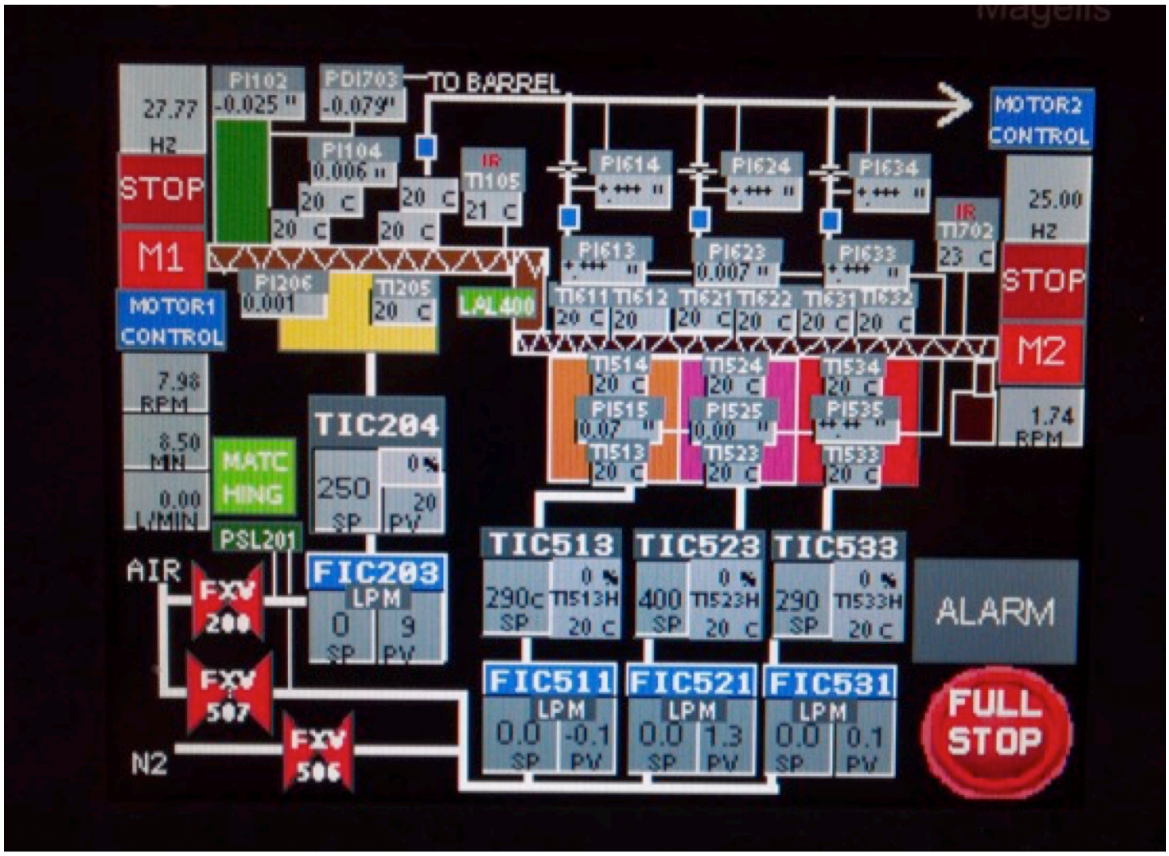

Figure 3.11: Primary Operator Interface Screen for CTU Pilot Plant

The operator controls for the CTU include the speeds of the two conveyors, the setpoints for the four temperature controllers that control the electric heating elements, and the four mass flow controllers that regulate gas flow to each heating zone. These rate controls are used to set and adjust the system parameters for each experiment.

Figure 3.12 is a photograph of the completed pilot plant during operation (mostly enclosed in thermally reflective rigid insulation), extending from the left edge of the frame (feed hopper, controls, and electrical cabinets, to near the right edge of the frame, where the white rectangular condenser tank for the torrefaction stage is visible. The plant occupies an approximately 6 x 1 m footprint in the pilot plant laboratory and is nearly 3 m in height at the metering hopper end. Figure A.3.7 in Appendix A illustrates the arrangement of Stage 1 and Stage 2. Additional photographs of the completed system are also included in Appendix A, from Figure A.3.12 to A.3.15.

Figure 3.12: Photograph of CTU pilot plant

3.6 CTU commissioning results

Coppiced willow granules prepared using the Rotoshear were selected for cold and hot commissioning tests with the finished CTU pilot plant.

The cold commissioning trials used a small number of willow granules and the system left at ambient temperature. These experiments were used to assess feeding and flow of the granules and to characterize the transit time for each conveyor at a given speed. Each conveyor motor was operated at a 50 Hz frequency (1/2 of the rated full speed for the motor) and the transit time for a single willow granule was measured from the feed point to discharge point for that conveyor. Based on these measurements, the travel rate for each conveyor was calculated to be 7 mm/s for Conveyor 1 and 4.1 mm/s for Conveyor 2, with estimated +/- 10% accuracy. These measurements were confirmed against the predicted values indicated in Table B.3.1 (Appendix B), within the noted accuracy range.

For the hot commissioning test, a 16 minute residence time (t_{tor}) was selected as well as a peak temperature parameter of 250 °C (T_{tor}). A quantity of willow granules totalling 3201 g with moisture content of 6.8 % was loaded into the pilot plant feed hopper. Accounting for the moisture content, the dry mass of this feed was calculated to be 2983 g. After pre-heating Stage 1 to above 150 °C and Stage 2 to 250 °C, Conveyor 1 was started at 25 Hz operating frequency (4 min total drying/pre-heating time). After Conveyor 1 had been running for 18 min, the level switch in the intermediate hopper tripped, indicating full level. Conveyor 2 was started at this point with a speed setpoint of 13.5 Hz (corresponding to 16 min torrefaction residence time). For this initial run, the speed of Conveyor 1 was lowered and raised manually, in order to find the optimal speed step-size. Figure 3.13 illustrates the temperature-time profile of this initial commissioning run. 35 min after Conveyor 2 had been started, the first particle was noted to have fallen into the receiving container by the distinct sound of the willow char striking the bottom of the receiving container. At 109 min after Conveyor 2 starting, it was determined that Stage 2 was completely empty, and complete shutdown was initiated. After cooling, the final mass of the char product was measured using the digital balance and was found to total 2339.3 g, for a dry mass yield of 78.4 % (w/w).

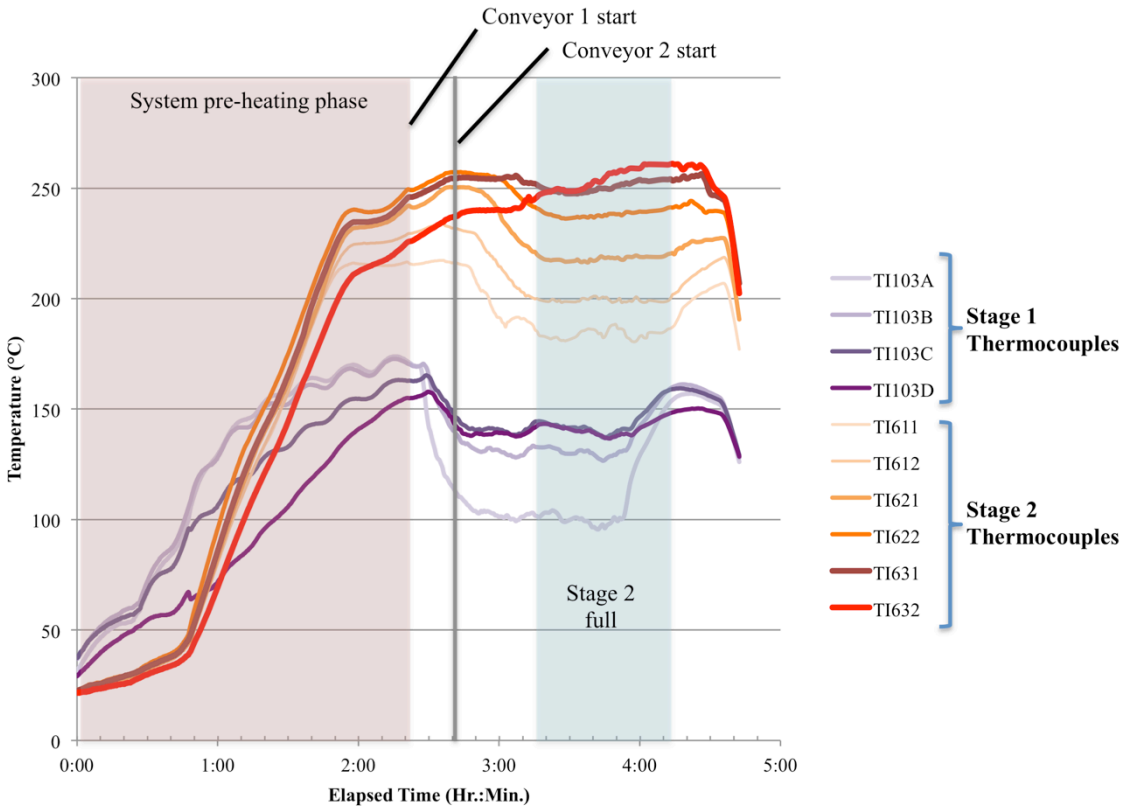

Figure 3.13: Time series data for 'hot' commissioning of CTU pilot plant (21 APR 2015)

The mass yield that was achieved in this initial commissioning test was significantly lower than predicted, as this value was below the average severity of torrefaction required in most reporting, which is 80 %. This was despite the fact that the temperature setting of 250 °C was in the middle range of capacity, and the residence time of 16 min, though already in the higher range for the CTU, was in the lower range for most torrefaction experiments. Along with the notable success of the operation in terms of the final result, two other procedural notes were made based on observations during the hot commissioning test. For most of the test, the temperature measured in Stage 2 sensor TE-611 did not exceed 180 °C, while the desired temperature for this point in the process should be 200 °C. This was presumed to be a direct result of the final temperature in Stage 1 (TE-103D) averaging 140 °C. With excess heating capacity available in Stage 1, it was noted that subsequent operations should increase the inlet distributor temperature setpoint, and ensure that Stage 1 final temperature should be at least 150 °C. Along with this change, raising the temperature setpoint for segment 1 of Stage 2 was noted as a required change to maintain 200 °C in Stage 2. This change would also improve the consistency of Stage 2 temperature in segments 2 and 3, which were noted to exceed the experimental temperature (250 °C) over the ‘steady state’ part of the experiment as a result of overcompensation/excess adjustment in the final segment.

4.0 Char quality response surfaces from torrefaction of coppiced willow in a horizontal moving bed pilot plant

4.1 Preface

The subject of Chapter 4 is the characterization and evaluation through experimental work of the horizontal moving bed pilot plant described in Chapter 3. Section 4.2 introduces the concept of torrefaction, as well as the project and the pilot plant, and the justification for why an alternative design is of interest. Section 4.2.1 illustrates why both the residence time and peak temperature are to be considered key parameters for a torrefaction process. This leads to the experimental design in 4.3.3 that is based on response surface methodology and uses a composite central circumscribed design. The feedstock used in this work was coppice willow, and the background and physical characteristics of this feedstock are described in detail in section 4.3.2. Finally, the results of the experiments are presented in section 4.4, where several quality measures including mass yield, energy yield, carbon content, and milling energy are presented as contour maps in which the residence time and temperature are the map Cartesian coordinates. The results illustrate how the horizontal moving bed can be used to reproduce experimental results with a high degree of confidence, and its operating range relative to the range of torrefaction severity is very high; an optimal output mass yield (80 % w/w) is achieved in the lower-middle coordinates of the experimental range. Section 4.5 makes these and further conclusions about the CTU operational results.

Chapter 4 was adapted (with permission) from the manuscript "Torrefaction Response Surfaces of Coppice Willow in a Horizontal Moving Bed", which has been published in the Canadian Journal of Chemical Engineering[26]. Sections 4.2 and 4.3 are amended from the published version as they cover details on the background of torrefaction and description of the pilot plant already discussed in Chapters 2 and 3. The experimental design, experiments and analysis described in this chapter were for the most part carried out by the candidate. The candidate was also the primary author of the manuscript, although the contributions of the co-authors are greatly appreciated: Dr. Kurt Woytiuk, Regan Gerspacher, Amy Coller, and Dr. Richard Evitts.

4.1.1 Additional results of CTU operations

What follows is a summary of work with the CTU pilot plant that was completed beyond the scope of the manuscript presented in this chapter. The results herein are presented to further the conclusions made

in Chapter 4 and provide additional context. Table B.4.1 in appendix B summarizes the results of all continuous torrefaction experiments conducted with the CTU. Figures A.3.10 and A.3.11 illustrate how the operator and process control had been improved over the course of the continuous experiments with coppice willow granules. The experiment illustrated in those figures (14-W) was a repeat of the central conditions (16 min / 250 °C). These were the same conditions as used in the initial hot commissioning run (Figure 3.13) and the main improvement when comparing the two time series is the stability and control of peak temperature in the torrefaction zone (TI622/TI631/TI632).

After the main experimental regime with coppice willow had been completed and the results compiled and analyzed, additional experiments were planned based on those results. These additional experiments were carried out to validate the response surface mapping results, and to confirm the conclusion that the CTU parameter control was resulting in repeat experiments with a very narrow range of torrefaction severity. Among those experiments, additional replicate experiments were conducted at 265 °C with 16 min residence time to validate the confidence interval measured for the original replicates. The results of these experiments are illustrated in Figure A.4.1 and Table B.4.2 located in Appendices A and B. The mass yield for each of these experiments was within 0.6 % of the expected value from the 'map' prediction, and the 95 % confidence interval of the replicate experiments was lower than that of the replicates in the original experimental design, 0.54 %.

Following completion of the continuous experiments with willow using the CTU pilot plant, wheat straw was subject to a smaller experimental regime where residence time was held constant at 8.6 min while the peak temperature was varied from 220 °C to 290 °C in six increments. The results of this work can be found in Figure A.4.2 (Appendix A), and have been presented at the ISBBB conference 2018 in Guelph, Ontario (July 24-27 2018). While these experiments did not test lower residence times, the range of temperatures evaluated illustrates both the very broad range of severity that is possible (from 54.2 % to 95.8 % mass yield (w/w)) and the degree of predictability that is possible where one parameter is fixed. The relationship between mass yield, carbon concentration, and fixed carbon concentration to torrefaction temperature each follow a quadratic equation with coefficient of determination 0.999, 0.998, and 0.943, respectively. These results not only show the reliability of the system with a given homogeneous feedstock, but the broader range of applications for the system outside of torrefaction.

Following the wheat straw continuous experiments, three other biomasses were examined, including cattail (*typha*), *moringa* leaf, and spruce (*picae*) pellets. A comparison of these experiments has been published in the conference proceedings of the 2018 Venice Symposium on energy from biomass and

waste (15-18 Oct. 2018)[77], and the major findings of that work were presented at that conference. A comparison of the feedstocks and char products from continuous torrefaction of these five biomasses using similar conditions in the CTU are illustrated in Figure A.4.3, A.4.4 and Table B.4.3 (Appendices A&B). These experiments illustrated the wide range of feedstocks that could be processed in a horizontal moving bed pilot plant, with the bulk density of these five materials ranging from 35 to 611 kg/m^3 and the average particle mass ranging from 0.002 to 0.318 g. The particle sphericity range between these feedstocks was also relatively broad. The key to success with these feedstocks was the flexibility of the plant; gas flow rates, throughput rate, temperature profile, and even the gas type per stage could all be adjusted to suit the feedstock. Torrefaction of the spruce pellets with a 10 minute exposure time, for example, required pre-heating with nitrogen instead of air and reducing Stage 1 speed so that Stage 2 would run partially full only. Using this method of operation, the residence time and mass throughput rate could be independent, facilitating a shorter residence time for high-density feedstock. Through this work, a preliminary relationship was presented relating biomass particle mass to torrefaction severity for a given set of conditions. While lower bulk density appeared to contribute to higher torrefaction severity, individual particle mass related to mass yield by a linear correlation for 4 out of 5 of the tested biomass types.

4.2 Introduction

Chapter 2 illustrated how torrefaction as a commercial process has been in existence for only the past 10 years or so, with fewer than 10 commercial scale plants operating worldwide in 2015 according to Thran *et al.*[67]. Commercialization remains challenging due to the narrow profit margins that are expected from most torrefaction plants. The sale price of product intended for use in electricity generation is tightly constrained to the sale price of electricity, which is often set by base-load generation types such as hydroelectricity, nuclear, wind, and natural gas. Because torrefaction plants are often constrained to small biomass particle size, low heating rates (long process time), poor control, poor capacity, and narrow feedstock flexibility[1,10,66], it is difficult for most to maintain optimum efficiency and flexibility in the face of such economic constraints. In consideration of the requirements of torrefaction, a system was designed with the notion of overcoming these shortcomings, and potentially expanding the types of products that could be produced and sold.

The horizontal moving bed reactor design outlined in Chapter 3 was undertaken with the goal of developing a hybrid system that could demonstrate the most favourable aspects screw conveyor and moving bed systems with few of the downsides. While counter and concurrent flow screw conveyor

reactors have been around for some time and have been used for torrefaction, these systems do not have the precise temperature control needed for thermal processing of heterogeneous solids.

This work concerns the evaluation and response characterization of a pilot scale horizontal moving bed torrefaction plant implementing this concept.

4.2.1 Process control parameters

The two process control variables that have the greatest influence on torrefaction severity are the maximum sustained temperature (T_{tor}), and the total torrefaction time (t_{tor}). Bergman *et al.*[41] defines the torrefaction time as the duration from the point where the biomass temperature exceeds 200 °C up until the point when the temperature drops below 200 °C. Through experimental work and analysis, many have defined the maximum biomass temperature for conducting torrefaction to be around 300 °C, but others have explored torrefaction temperatures as high as 350 °C[67]. Above this temperature range, rapid and extensive devolatilization occurs and the remaining energy value in the solid char is too low for it to be economical as fuel. The temperature range from 200–300 °C represents a normal range for torrefaction, with final torrefaction severity increasing through this range.

For a fixed torrefaction temperature, Prins *et al.*[49] demonstrated that severity will also increase with an increase in total torrefaction exposure time, but that severity will reach a limit after a long enough time interval. This interval is also observed to be significantly longer for temperatures near 200 °C than temperatures near 300 °C. Wannapeera *et al.*[78] demonstrated both of these aspects through a number of fixed bed torrefaction experiments, where similar torrefaction severity was achieved using different extremes of time and temperature combinations.

4.2.2 Comparing pilot scale torrefaction

This work concerns the evaluation of a small-scale torrefaction plant, referred to as the continuous torrefaction unit or CTU. The CTU was built to demonstrate the concept of a horizontal moving bed and to act as a general research tool. Comparable torrefaction plants include the bench-scale screw conveyor reactor at Ghent University (Belgium)[53] and the drum reactor pilot plant at Umea University (Sweden),[79] with maximum continuous feed rates of 2.5 and 20 kg/h, respectively. The Ghent University plant was reportedly tested from reactor wall temperatures between 275–375 °C and residence times from 5.75–16.7 min using commercial pine with maximum 6 mm dimension. Similar to other small scale screw conveyor torrefaction plants (Shang *et al.*[25] and Ohliger *et al.*[81]), that plant is indirectly

heated, and as a result these plants utilize either high temperatures (300 °C and above), long residence times (> 30 min) or both, in order to achieve torrefaction severity in the typical range of 80–90 % mass yield. The CTU was designed and built to demonstrate more rapid, controllable, and flexible torrefaction by combining the precise feedstock flow control of a screw conveyor with the heating rate and temperature control of convective or direct heating that is typically employed in vertical moving beds, cyclonic systems, and tray contactors.[10]

4.3 Materials and methods

4.3.1 Horizontal Moving Bed Torrefaction Plant: CTU

For details on the concept, design and theory of operation for the horizontal moving bed pilot plant, refer to Chapter 3.

4.3.2 Biomass – Short Rotation Willow

The feedstock used in this experimental work was 1-year growth of short rotation coppice (SRC) willow grown in Saskatoon, Saskatchewan, standing 2–3 m in height prior to cutting, which had a maximum diameter of 25 mm. A prototype rotary cutting system described in Gerspacher *et al*.[75] was used to reduce the stems into granular, uniform length pieces; a typical example is indicated in Figure 3. Examination of a random 40-piece sample found that the average particle dimensions for the cylindrical willow cuttings were 19.3 mm (length) and 7.5 mm (diameter), with standard deviation of 1.3 and 3.4 mm, respectively. The particle size distribution for the willow used in this work was relatively narrow and can be found in Gerspacher *et al*.[75] The granular willow cuttings were screened to remove any particles smaller than 3 mm, any pieces larger than 35 mm, and those that were non-cylindrical in shape, such as branch forks. The bulk density of the willow cuttings was measured to be 211 kg/m^3 (±2) (db).

4.3.3 Experimental design

In order to characterize the torrefaction plant through a representative range of operating conditions, an assessment of multifactorial experimental designs applicable to two control variables was undertaken. The primary control variables for a single feedstock type and particle size in a torrefaction plant are the peak temperature (T_{tor})[1] and the total torrefaction time (t_{tor}) from the point in time when the temperature exceeds 200 °C until it falls below that temperature.[10,41]

In this study, the time parameter was defined as the total residence time in the heated section of the torrefaction reactor, in order to satisfy precise experimental parameters. In order to understand the relative effects of residence time and temperature through a full range of conditions, experimental designs pertinent to response surface methodology (RSM) were investigated. A Box-Wilson central composite experimental design was selected to estimate the non-linearity of curvature of the response to residence time and temperature across as wide a range as possible. Given that both control variables are unconstrained aside from system and process limits, a circumscribed central composite (CCC) RSM design was selected, which requires five levels for each variable. The CCC design yields a spherical and rotatable response surface and can provide estimation of response curvature.[82]

Following initial experimentation with the pilot plant, which had mass yields near the targeted 80 % range, a central pair of process condition variables was selected: t_{tor} = 16 min and T_{tor} = 250 °C. The temperature parameter of 250 °C was selected as the centre of the design, as this temperature coincides with the approximate middle of the typical temperature range for torrefaction that is commonly given: 200–300 °C. The central torrefaction time of 16 min, on the other hand, was selected based on the physical operating boundaries of the reactor. To achieve the longest exposure time indicated, which was 24 min, the torrefaction conveyor motor had to be operated at 9 Hz, while the lower limit of operation was 6 Hz. It was considered prudent to avoid operating the drive and motor very near this limit, as operation reportedly becomes unreliable near this limit according to the manufacturer. The very shortest exposure time examined, which was 8 min, was limited in a different way by the expected heat transfer capability of the reactor. Increasing the feedstock temperature from the preheat temperature to the setpoint temperature was required to occur by the halfway point of the torrefaction section; 8 min total exposure time thus leaves 4 min to achieve the setpoint. This time was considered practical with this plant and for coppiced willow feedstock in the form indicated, but it was unknown from the outset if it was possible to do this in a shorter time. The torrefaction time steps of 8, 16, and 24 min were thus considered to be practical with this system and with this feedstock.

The factorial step sizes for the time and temperature variables are 5.7 min and 21 °C, respectively, while the axial steps were 8 min and 30 °C, resulting in the experimental factors listed in Table 4.1. Graphical representation of the CCC design is illustrated in Figure 4.1:

Table 4.1: Experimental design parameters

Block	X1	X2	T_{tor} (°C)	t_{tor} (min)
Factorial	-1	-1	229	10.3
Factorial	-1	1	229	21.7
Factorial	1	-1	271	10.3
Factorial	1	1	271	21.7
Axial	-1.414	0	220	16
Axial	1.414	0	280	16
Axial	0	1.414	250	24
Axial	0	-1.414	250	8
Centre	0	0	250	16
Centre	0	0	250	16
Centre	0	0	250	16
Centre	0	0	250	16
Centre	0	0	250	16
Centre	0	0	250	16

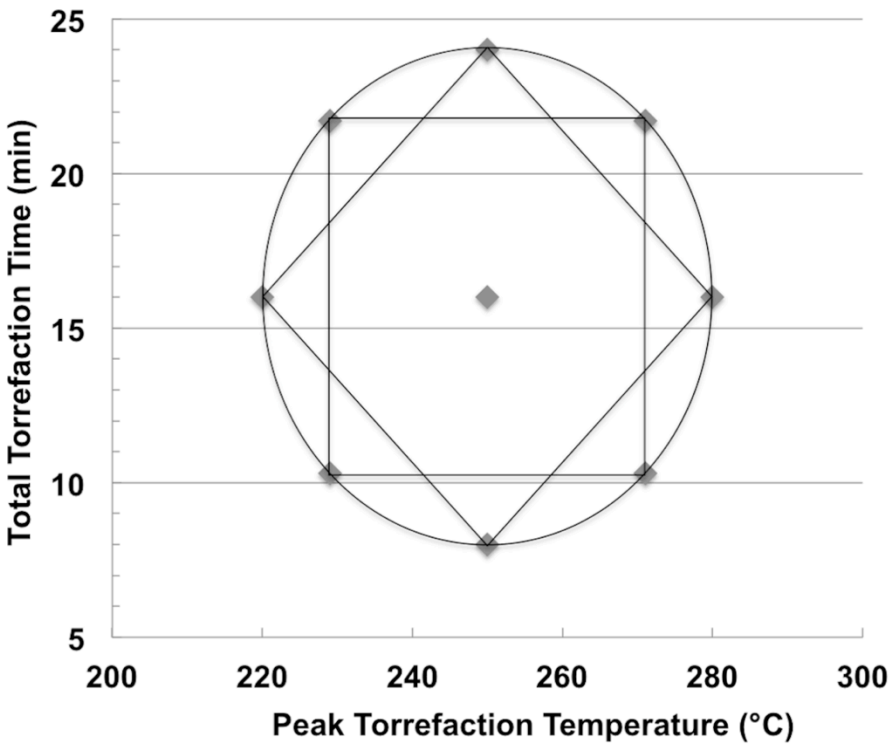

Figure 4.1: Central Composite Circumscribed Experimental Design. Illustrates the factorial and axial block settings as applied to the two main experimental variables (total torrefaction time and peak temperature).

4.3.4 Analyses

The main metrics used to assess the quality and severity of torrefaction for each experimental operation were the mass yield (Y_m), higher heating value (HHV), carbon content, energy yield (Y_E), and milling energy (E_g).

The mass yield (Y_m) of each torrefaction experiment was calculated from the measured initial mass of the biomass (M_i) as well as the final mass of the char (M_f). Mass measurements were made using a Mettler Toledo (USA) PB4002-S digital balance, which has a resolution of 10 mg.

Mass yield was calculated on a dry basis, requiring measurement of the initial moisture content of the biomass prior to the torrefaction experiment. This was performed using a Mettler Toledo (USA) HB43 halogen moisture analyzer with resolution of 0.01 %, with the average of three measures taken (MC_{avg}) from random samples in each experimental batch prior to loading. The expression for this calculation is given in Equation (4.1):

$$Y_m\,(\%, \mathrm{db}) = \frac{M_f}{M_i\left(1-\frac{MC_{avg.}}{100}\right)} \qquad (4.1)$$

Carbon, hydrogen, nitrogen, and sulphur (CHNS) composition was measured using an Elementar (DE) VarioEL III (v. 4.01, 2002) with a precision of ±5 % of the measured value and a Mettler Toledo (USA) XP6 micro-balance (±0.1 µg). Oxygen content was inferred as the remainder after combining the CHNS values with the ash concentration determined in the following TGA analysis.

Thermogravimetric analysis (TGA) was conducted on each sample to determine the moisture and ash content of each sample. A TA Instruments (USA) Q600 thermogravimetry analyzer (TGA) running software V20.13 (Build 39) was used for the analysis. The TGA microbalance has a sensitivity of 0.1 μg. The method used was the proximate analysis method described for use on all types of biomass by Stahl *et al*. in "Definition of a Standard Biomass" for the RENEW project[83]. The method consisted of 10 °C heating ramp in nitrogen to 105 °C, followed by isothermal heating at that temperature for 30 min. to ascertain moisture content. The sample was then heated at 5 °C / min to 700 °C and then held at that temperature for another 60 min to determine volatile matter content. The gas flow was then switched to air, initiating combustion of the remaining fixed carbon, temperature held at 700 °C for another 10 min. Finally, cooling was initiated at -5 °C/min. to return the sample to ambient temperature.

The elemental composition, ash, and moisture content of the samples were used to calculate the higher heating value of each biomass/char sample that was collected from the torrefaction run. The higher heating value was calculated using empirical correlations: the Nhuchhen and Afzal correlation,[23] illustrated in Equation (4.2), and the Channiwala and Parikh correlation,[30] illustrated in Equation (2.1), relating the energy content per unit mass of dry carbonaceous matter to the elemental/ash composition:

$$\mathbf{HHV = 32.793 + 0.005C^2 - 0.532C - 2.877H + 0.061CH - 0.240N} \qquad (4.2)$$

Calorific values are calculated using both correlations, since each provides a different approach to the relationship and both correlations have been shown to be useful in estimating higher heating value for biomass; between the sets of values a realistic range is established for the biomass/char. The Nhuchhen and Afzal correlation was specifically developed for torrefied biomass[23] and the paper presenting it illustrated a superior fit to measured heating value for torrefied biomass.

The energy yield would be calculated based on the mass yield, as well as the ratio of the new heating value to the original heating value (calculated on a dry basis, using the Channiwala *et al*. HHV value[22]), using Equation (4.3).

$$\mathbf{Y_E(\%, db) = \frac{HHV_{f,db}}{HHV_{i,db}} Y_m(db)} \qquad (4.3)$$

Grinding energy was calculated by grinding a 40 g sample of biomass using a #1 Wiley mill operated by a 0.75 kVA variable frequency drive (VFD) at 30 Hz/878 rpm, in two steps. The sample was first milled through a 6.8 mm screen, followed by a 1.8 mm screen. The biomass sample was fed to the Wiley mill by a screw conveyor with variable frequency drive (VFD) control. For each step of the milling operation, the feed mass and recovered mass (which had passed the indicated screen size) were both measured using a digital balance, with the final recovered mass used for the subsequent calculation of the grinding energy per unit mass.

A 0–5 V analog output (corresponding to kW power level) from the Wiley #1 Mill VFD drive was input to an Omega data acquisition module, and then was coupled to a LabView™ virtual instrument. The no-load power level (P_{nl}) was then subtracted from the grinding power signal ($P_{grinding}$), and the net grinding power signal was then integrated over the period where the mill was actively grinding the feed ($t_{grinding}$), resulting in the net energy value for the milling process. The final mass of ground sample meeting the size criteria for each milling operation (M_{milled}) was then used to calculate the grinding energy per unit mass of that step, as illustrated in Equation (4.4).

$$\mathbf{E_g} = \frac{\sum_{t=0}^{t_{grinding}} (P_{grinding} - P_{nl})}{M_{milled}} \quad (4.4)$$

4.3.5 Presentation of data

A contour plotting method was selected to visualize the response surface for the range of process conditions. The Wolfram (Champaign, USA) Mathematica ® 9.0 list contour plot function was used for this purpose, along with a grey-scale color scheme. This plotting method accepts a list of values along with their coordinates in the x and y-axes, as well as a list of which contours to include in the plot. The plotting method then reconstructs values between the entered values, and plots specific contour lines and the number of contour bands based on the input instructions. It was hypothesized that viewing the char quality measurements using this plotting method would reveal relevant patterns as well as highlight any outliers in the data which would appear as discontinuities in the image. Plotting response data in this manner has been shown to be very useful in characterizing continuous torrefaction processes such as the drum torrefaction plant at Umea University.[79] Contour mapping of response surface data often uses three-dimensional projections to present this type of data,[50,84] though this suffers from the expected difficulty with interpreting three-dimensional projections on a two-dimensional surface. The plots developed using this method were developed as specific indicators of the plant performance with a specific feedstock, to be used for estimating the process settings to achieve specific char qualities.

4.3.6 Experimental procedure

The pilot plant reactors are preheated using air as the heating medium. The temperature controllers are set to 150 °C in the pre-heat section and 200 °C in the torrefaction. As the system temperatures approach these values (approximately 60 min after starting the pre-heat sequence), specific setpoints per the experimental conditions are set on the temperature controllers. When the measured temperatures in the middle of section 2 are within 10 °C of the experimental temperature parameter value, the system heat and airflow are suspended and the pre-weighed quantity of biomass is placed in the metering hopper. After the metering hopper is re-sealed, the system heat and airflow are re-initiated. The metering conveyor is then started at 25 Hz (25 % of full speed). After 5 min of operation, the heating gas for section 2 is switched to nitrogen.

As heated feedstock flows into the stage 2 intermediate hopper, the level in that hopper will rise until the level switch LS-403 (Figure 3.9) is triggered. This automatically starts conveyor 2 at its pre-set speed, which corresponds to the desired exposure time (t_{tor}). Conveyor 1 now automatically switches to its low

speed setting. Once LS-403 switches off, conveyor 1 will switch to a high-speed setting to bring the level back up to trigger the switch again. The speed of conveyor 1 will modulate based on the output of sensor LS-403 in this manner until the metering hopper is empty.

The plant should enter steady state at this point, requiring only minor adjustments to temperature controllers to achieve the target torrefaction temperature, T_{tor}, until the batch of feedstock is consumed.

4.4 Results

The fourteen experiments where willow segments were torrefied in the CTU were conducted over a one-year period. Experimental results for mass yield, elemental composition, ash, moisture content, higher heating value, energy yield, and milling energy are listed in Table 4.2. These results are presented in the same sequence as outlined in Table 4.1. The six centre runs are listed last, followed by the average and 95 % confidence interval for each measure. The sulfur compositions are excluded, as these measurements are below 0.2 %, lower than or near to the limit of uncertainty in the measurements.

The mass yield values presented in Table 4.2 are the best illustration of the torrefaction severity, which ranges from 91.6 to a low of 64.7 % mass yield. Consistently, as the severity increases (mass yield decreases), the energy yield and milling energy decrease as well. Carbon content increases in a consistent manner as severity increases, while oxygen content falls at an inverse rate to the increase of carbon. Hydrogen content does not change with the same sensitivity but does fall as well at the higher range of severity, above T_{tor} values of 250 °C. The ash content is measured to be quite low in the raw willow sample (1.4 %), but does concentrate as the severity increases, rising to a maximum of 2.7 %. The ash content is somewhat variable across the range of experiments, however, as illustrated by the range of ash content in the six replicate experiments at 250 °C and 16 min. Moisture content in the raw sample was quite low (3.7 %) as all of the feedstock was air-dried following processing the stems into flowable granules.

Table 4.2: Torrefaction Chars Quality Parameters from Continuous Runs

Conditions T_{tor}/t_{tor} °C/min	Feed Rate Q_{input} kg/hr (db)	Mass Yield Y_m (% db)	Energy Yield Y_e (% db) Chan.[32]	Milling Energy Eg (kJ/g)	Ultimate Analysis (% db) C	H	O	N	Ash % (db)	M.C. %	HHV (kJ/g) (db) Nhuch.[31]	HHV (kJ/g) (db) Chan.[32]
Raw				1.34	49.4	6.3	42.5	0.4	1.4	3.7	20.2	20.2
229/10.3	3.4	91.6	94.4	0.35	51.2	6.1	41	0.2	1.4	2.9	20.8	20.8
229/21.7	1.6	85.5	91.2	0.25	53.1	6.1	39.1	0.3	1.4	2.4	21.5	21.6
271/10.3	3.4	75	83	0.2	55.1	6	36.9	0.5	1.6	2.3	22.3	22.4
271/21.7	1.6	68.9	79.8	0.18	57.3	6	34.7	0.4	1.6	2.7	23.2	23.4
220/16	2.2	89.9	92.2	0.28	51.5	5.9	40.3	0.6	1.6	1.6	20.8	20.8
280/16	2.2	64.7	74.4	0.18	58.4	5.5	33.7	0.7	1.8	1.8	23.3	23.3
250/24	1.5	75.8	83	0.2	55	5.7	35.8	0.7	2.7	2.5	22.1	22.2
250/8	4.4	87.5	91.3	0.29	52.5	5.8	38.7	0.5	2.4	2.6	21.2	21.1
250/16 (1)	2.2	77.9	84.9	0.19	54.9	5.7	37.3	0.5	1.4	3	22.1	22.1
250/16 (2)	2.2	79.5	86	0.22	54.4	5.8	37	0.5	2.3	2.4	21.9	21.9
250/16 (3)	2.2	78.3	87.1	0.29	55	6.1	36.4	0.5	2.1	2.1	22.3	22.5
250/16 (4)	2.2	78.5	87.7	0.16	54.7	6.2	36.3	0.4	2.3	2.1	22.2	22.6
250/16 (5)	2.2	78.5	88.1	0.23	55.1	6.1	35.9	0.5	2.4	1.9	22.4	22.7
250/16 (6)	2.2	79.6	90	0.2	55	6.3	35.7	0.5	2.5	1.8	22.4	22.9
Average of Replicates		78.7	87.3	0.21	54.9	6	36.4	0.5	2.2		22.2	22.2
95% Confidence Interval		0.7	1.9	0.05	0.3	0.2	0.7	0	0.4		0.2	0.4

The two HHV correlations produce values that compare very well for these samples: the raw biomass heating value is calculated to be 20.2 kJ/g, which increases to 20.8 kJ/g for the lowest severity experiment, and to 23.3 kJ/g for the highest severity. The average heating value of the replicated experiments was measured at 22.3 kJ/g, with only the uncertainty between these individual measurements indicating the difference between these correlations; the uncertainty of the Nhuchhen and Afzal[23] correlation for these replicates was 0.2 kJ/g compared to 0.4 kJ/g for the Channiwalla and Parikh[22] correlation.

Figure 4.2 illustrates the visual character of the char produced by the torrefaction plant; even at the mildest conditions, the carbonization/darkening is already considerable.

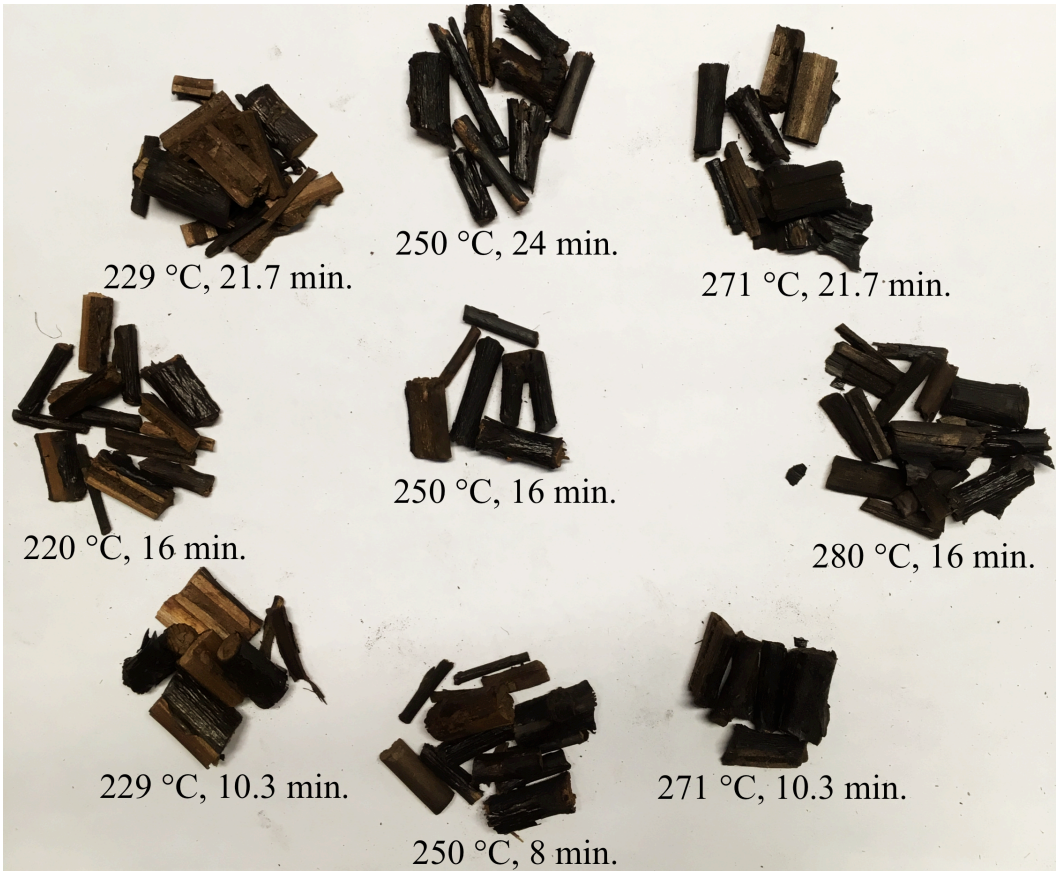

Figure 4.2: Torrefaction chars produced in horizontal moving bed pilot plant from willow. Torrefaction operating conditions (temperature/time) used in the CTU are indicated.

The variation in severity is quite clear from left to right, however, as the interior colouring of the wood changes from light to very dark brown. What is also of note is that the process appears to have low mechanical impact on the biomass particles, since they emerge from the process quite intact despite their significant brittleness.

The mass yield surface response is illustrated in Figure 4.3. The mass yield ranges from a high of 91.6 to a low of 64.7 %, with the highest yield result from T_{tor} = 229 and t_{tor} = 10.3 min and lowest from T_{tor} = 280 and t_{tor} = 16 min. Based on the lack of inflections and discontinuities in the contour pattern and the consistent density of the contour lines, there appear to be no significant outliers in any of the datasets, indicative that the step size between the control variable settings well exceeds any potential error/uncertainty. This also indicates that the pilot plant operates with sufficient reliability that it can produce char with predictable quality relative to the operating conditions.

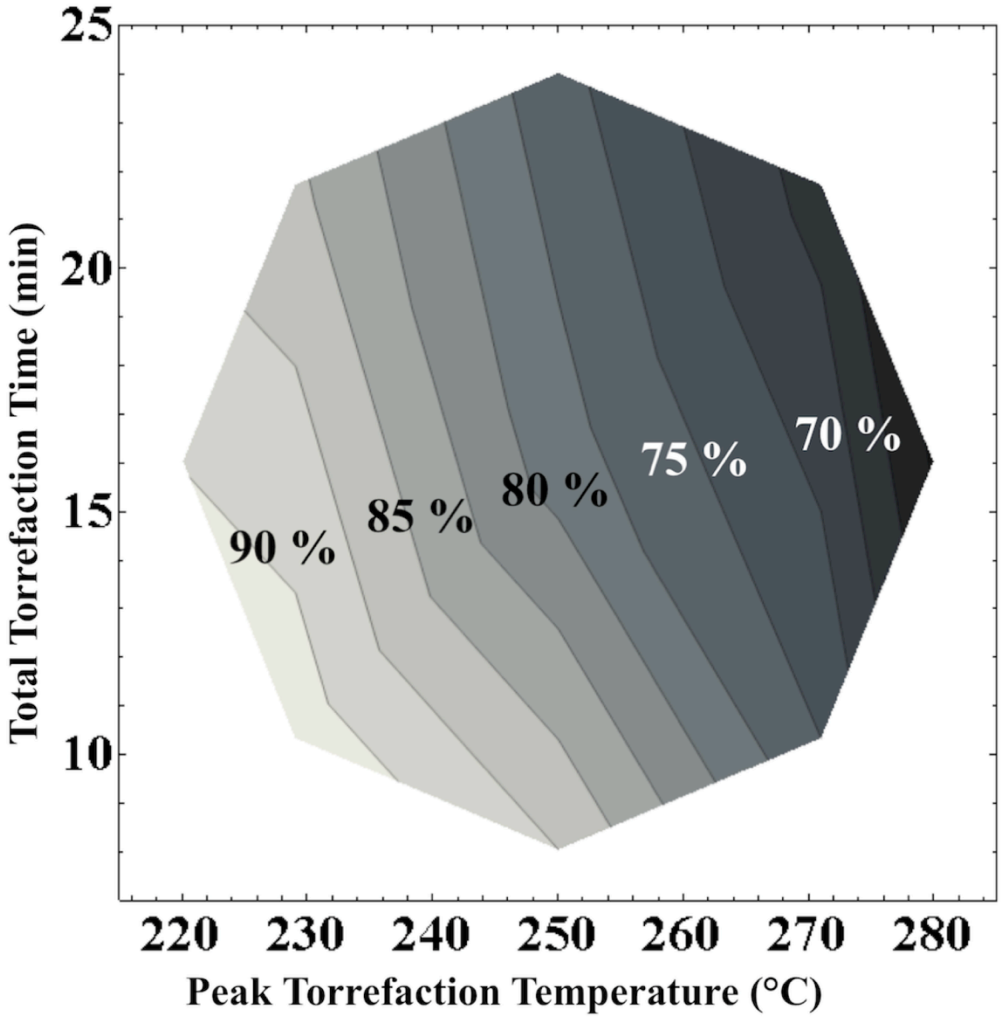

Figure 4.3: Contour plot of torrefaction mass yield.
Presented as a function of torrefaction time and peak temperature.
95% Confidence Interval = 0.7%.

Examining the experimental results at the central conditions of 250 °C and 16 min, the average value of the mass yield from the six runs conducted using these conditions was 78.7 %, with a 95 % confidence interval of 0.7 %. This level of repeatability in terms of response to the control parameters is illustrative of a reliable, predictable process and operation method.

Considering that most torrefaction processes are operated with around 80–85 % mass yield, a wide band of possible conditions is available for the CTU to produce char in with this severity; possible reactor settings vary in term of exposure time from fewer than 9 min to as high as 23 min, and a temperature

range of 230–265 °C. It would also appear that shorter torrefaction times/higher throughput rates are most likely possible, with an appropriate mass yield/severity of torrefaction a realistic possibility at 5 min exposure time.

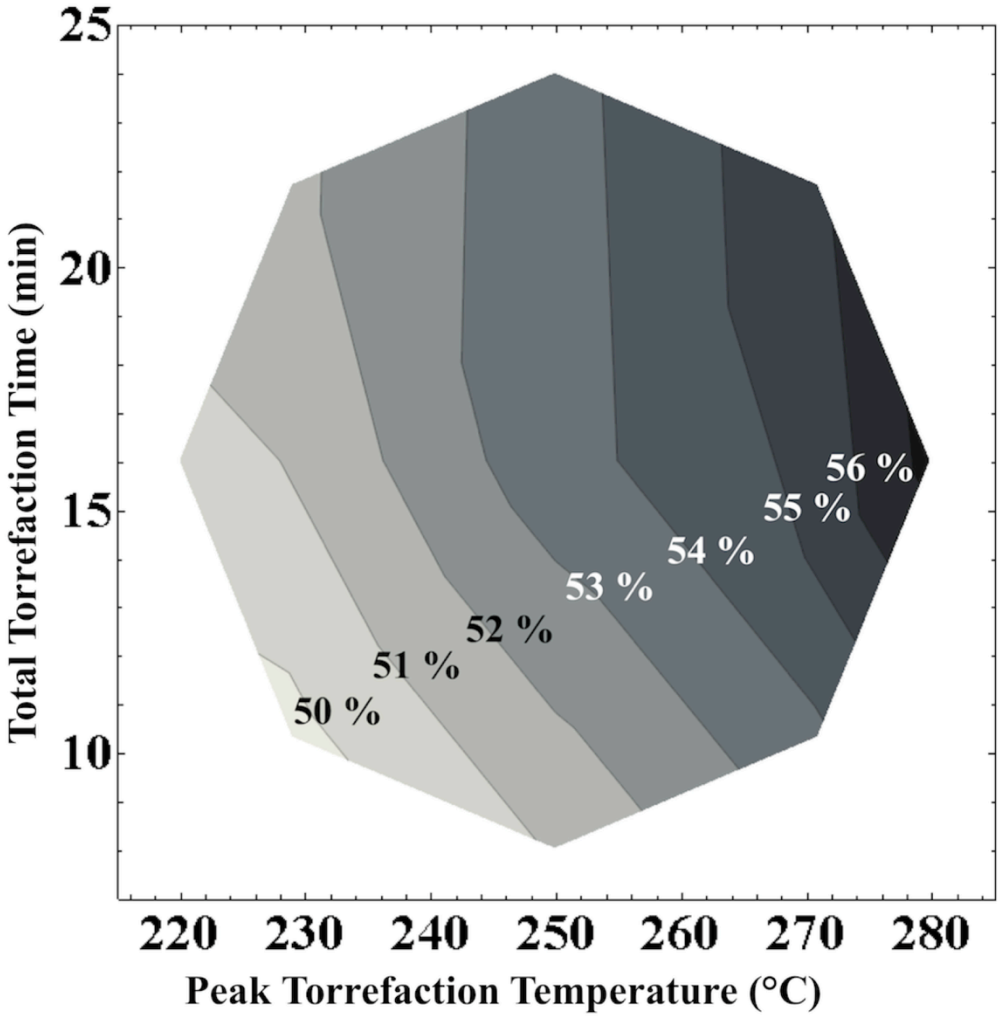

Figure 4.4: Contour plot of willow char carbon concentration.
Presented as a function of CTU torrefaction time and peak temperature.
95% Confidence Interval = 0.3%.

Other independent measurements include the carbon content, which is presented in Figure 4.4, and the milling energy, which is presented in Figure 4.5. Carbon content is a very useful indicator for torrefaction severity; this element contributes the most to the energy value for biomass (owing to its relative quantity), it changes very predictably and consistently with torrefaction, and its measurement is consistent and can be measured with an uncertainty of 0.5% (value) using CHNS analysis. The carbon content seems to increase in a very consistent fashion, with the band of 53–54 % corresponding to the 80–85 % mass yield range, which is the typical target range.

The plot of milling energy (Figure 4.5) illustrates that even at the mildest conditions, the milling energy has been reduced by 75 %, and that increasing the severity of torrefaction further provides only a marginal benefit in terms of milling to 1.8mm screen size.

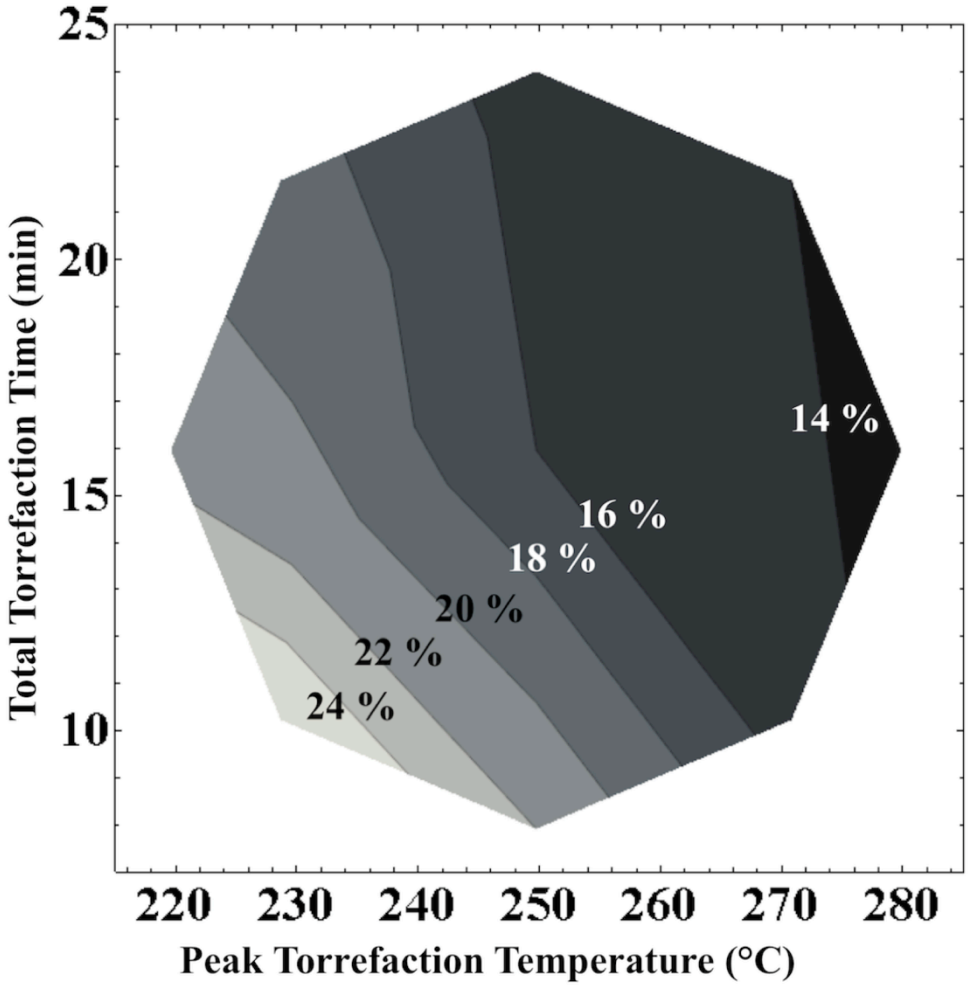

Figure 4.5: Contour plot of milling energy relative to raw willow granules.
Presented as a function of torrefaction time and peak temperature.

The energy yield (Figure 4.6) is a dependent variable, calculated using the mass yield as well as the higher heating value. The heating value is in turn calculated using a correlation to CHNS composition. While the energy yield is derived from the mass yield and estimated heating value, it does provide the best estimate of the operating boundary, which should be near Y_e = 90 %. Energy yields closer to 85 % would have the torrefaction gas energy content approaching the autothermal point; operating a torrefaction plant near the autothermal point would be atypical, because it is generally more cost

effective to use raw biomass as make-up heating fuel than to convert char to volatile matter for this purpose.[41] Since the milling energy has been reduced by more than 80 % along with a 90 % energy yield, the gains in increasing the torrefaction severity from this point become marginal.

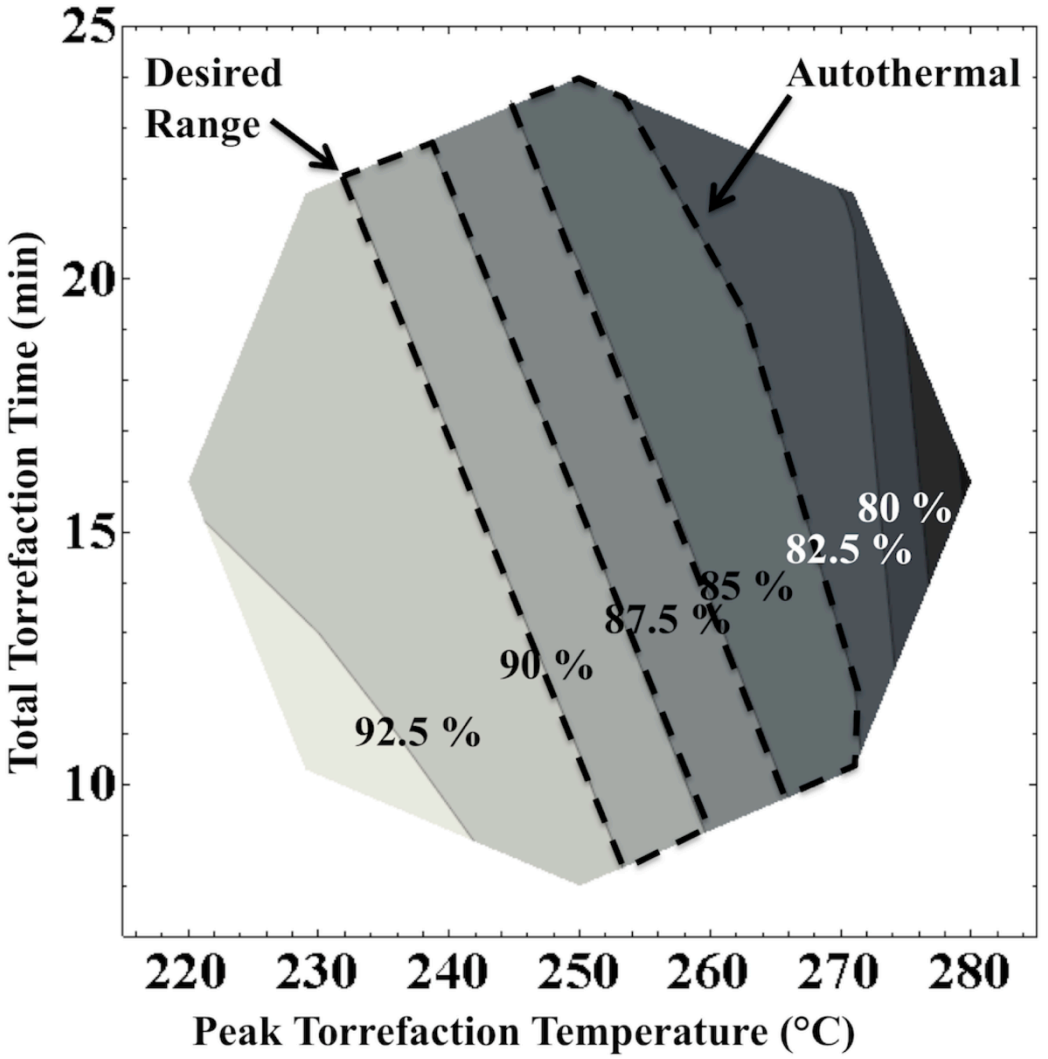

Figure 4.6: Contour Plot of energy yield as a function of torrefaction time and peak temperature. 95% Confidence Interval = 1.9%.

4.5 Discussion

Selected CTU operating results are suitable for comparison to those of similar pilot plants. Ohliger *et al*.[81] describe torrefaction experiments at Aachen University on beech woodchips using an indirectly

heated screw conveyor reactor. Experiments of 280 °C/20 min and 300 °C/15 min had mass yield values of 77.56 % and 76.23 %, respectively. Compared to the most extreme conditions with the CTU, where the temperature and time parameters were 280 °C/16 min, the mass yield was 64.7 %. Examining the surface response plot of Figure 4.3 the mass yield values reported by Ohliger *et al*.[81] would likely be achieved in the CTU with process temperatures of 270 °C/10 min, or with lower temperatures than this, but slightly higher exposure times. Examining the results of Strandberg *et al*.[79] where spruce chips were torrefied in a drum reactor, three different experiments were conducted using similar conditions: 260 °C/8 min, 260 °C/25 min, and 285 °C/16.5 min, which had mass yields of 97, 89, and 80 %, respectively. Comparable experiments with the CTU were conducted at 250 °C/8 min, 250 °C/24 min, and 280 °C/16 min, which yielded 87.5, 75.8, and 64.7 % mass, respectively. Both comparable pilot facilities using similar time and temperature parameters to those used with the CTU and willow feedstock are thus found to have a torrefaction mass yield that is higher by 9.5–15.3 %, illustrating that greater severity is achieved in the CTU using similar process conditions. The CTU employs direct convective heating that ensures rapid heat transfer, extremely even heating of the biomass, and allows for the biomass to be heated quickly enough to maintain the setpoint temperature for half of the total torrefaction time. This combination of properties is what allows this reactor to achieve greater severity than comparable continuous plants.

The contour maps of the char quality measurements provide significant insight into the relative strength of temperature and time on the torrefaction severity in this plant. Notably, above 15 min exposure time and 250 °C (upper right quadrant in all four figures), the effect of increasing t_{tor} is diminished, and thus the contour lines have a more vertical orientation compared to in the lower temperature/exposure time region. This is the predicted response inflection, indicating the char becoming stable more quickly at higher temperature.

The response surface contour projections developed through these experiments may be used to plan subsequent experiments. From any of the char quality response maps (Figures 4.3–4.6) a desired quality value can be used to select a set of time and temperature parameters to achieve that approximate value. For example, to achieve exactly 90 % energy yield could be achieved at 253 °C and 8.5 min exposure time, and would be associated with 21 % milling energy, 53 % carbon content, and 85 % mass yield.

4.6 Conclusions

A horizontal moving bed torrefaction plant was used to torrefy coppiced willow cuttings in fourteen experiments with parameters determined by RSM experimental design. The conclusions drawn from the results of this work are as follows:

1. For similar experimental times and temperatures, the severity of torrefaction chars produced with the CTU exceeds the severity of comparable torrefaction pilot plants. For example, for similar temperature and exposure times, the CTU produced coppiced willow char with a mass yield that was 13–15 % lower than the spruce char produced at Umea University in a drum reactor. This difference in severity can be attributed to the fact that the CTU utilizes direct/convective heating, while other mechanically conveyed processes generally rely on conductive/indirect heating.
2. Temperature has a greater influence than torrefaction time on severity for torrefaction of coppice willow in this plant for the respective ranges examined. The torrefaction temperature range was from 220–280 °C at 16 min exposure time, which produced char with a mass yield that varied from 89.9–64.7 %. On the other hand, varying torrefaction time from 8–24 min at 250 °C produced char with a mass yield from 91.3–83 %.
3. This torrefaction plant design is reliable with respect to char quality repeatability. The experimental conditions at the centre of the design space were repeated six times, resulting in mass yield measurements that agreed within a 95 % confidence interval of 0.7 %. Among the results of the other experimental parameter pairs, there were no significant or obvious mass yield outliers. This illustrates a very satisfactory uncertainty in controlling torrefaction severity by replicating process conditions.
4. The surface response maps of the different char quality measurements provide a method for accurately characterizing the char quality response of the pilot plant with a specific biomass for a broad range of conditions and process severity. This allows the selection of time-temperature conditions to produce specific char qualities, including specific mass or energy yield, milling energy, elemental composition, or heating value.

5.0 Determining the severity of torrefaction for multiple biomass types using carbon content

5.1 Preface

The research described in Chapter 5 proposes how the change in carbon content in torrefaction chars can be used to measure and infer process severity. Mass yield is typically used to represent torrefaction severity; however, this type of measurement is costly, complex, and has low reliability for large-scale continuous operations. Developing a method for measuring torrefaction severity using representative sampling was the driving force of this part of the research. In order to have a sufficient body of experiments to review, this work relied heavily on having completed many torrefaction experiments, including several completed very early on in the research project, and many experiments completed using the CTU pilot plant. The apparatus and experimental parameters for those experiments are discussed in section 5.3. Section 5.3.3 discuses the different feedstocks that were used in the experiments: coppice willow, wheat straw, and cattail. It was important for this research to examine a wide range of feedstocks so that the severity measurement tool could be broadly applied. Section 5.3.6 discusses how the data were to be normalized; this included expressing all experimental data on a dry, ash-free basis so that the masses and compositions considered were from the reactive part of the biomass. The expressions of ΔC (change in carbon composition), ΔM_c (change in carbon mass), and ΔM_t (change in total mass) are also discussed in terms of what they represent and how they are determined. Section 5.4 describes the results of this analysis, covering the experimental data, the carbon concentration correlation, the carbon mass correlation, and then introducing the literature data to both of these correlations. The carbon concentration correlation that is described is concluded to be suitable for developing a measurement method for continuous torrefaction, while the carbon mass correlation is illustrative of how the mass of carbon in the char changes relative to the total.

This chapter is based on the paper written at the Graduate Committee's request to fulfill the comprehensive exam requirement. That paper, titled "Determining the Severity of Torrefaction for Multiple Biomass Types Using Carbon Content" was subsequently published in the journal "Energy and Fuels" in August of 2018[85]. Reprinted (adapted) with permission from Energy and Fuels 32(9) Copyright (2018) American Chemistry Society. This chapter is an edited version of that manuscript, where redundant sections have been removed. Section 5.2 (Introduction) has been edited to remove content describing the torrefaction process (covered in Chapter 2) and the description of the CTU has been removed from materials and methods section (5.3.1) as it has been covered in detail in Chapter 3.

The assistance of Dr. Richard Evitts in preparing this manuscript for submission to Energy and Fuels is greatly appreciated, as well as in readying the major revision of the manuscript. The expansion of the analysis in this chapter to include loss in mass of carbon was at the suggestion of the manuscript reviewers. The reviewers felt that the contribution of this work would be improved by also illustrating the gross effect of torrefaction on the original mass of carbon, in addition to how the residual concentration is affected.

5.2 Introduction

Improving torrefaction process control through direct measurement of the severity of torrefaction is the subject of this chapter. Quantification of the mass of remaining solid matter (torrefaction dry mass yield) is normally how the extent or severity of torrefaction is reported at the lab and pilot scale, which relates well with other key criteria such as increase in heating value, energy yield, and friability[68]. On an industrial scale, accurate and continuous measurement of the mass yield would be complex and costly, requiring measurement of both the mass flow in and out of the torrefaction process; belt scales, nuclear mass flow meters, loss-in-weight feeders and Coriolis instruments would be the typical measurement systems [86].

This work examines the char carbon content as an alternative measure for evaluating torrefaction severity. The char carbon content has been shown to increase with the severity of torrefaction, as has been illustrated through a van Krevelen diagram such as Figure 2.2. Carbon can also be measured continuously and relatively rapidly using an automatically fed analytical instrument; an instrument that can automatically weigh, combust, and measure the relative production of CO_2 using NIR sensing can report the carbon content at a frequency of only several minutes [71].

An excellent example of how torrefaction extents relate to the change in carbon concentration is the research paper by Lestander *et al.* [72]. That study explored extremes of torrefaction and pyrolysis conditions for two biomass types (reed canary grass and Norway spruce) from above 95% to below 20% mass yield (w/w), where the residual carbon concentration increased from 50% to above 90%. Lestander *et al.*[72] concluded that a 2nd order polynomial correlation fit the relation between pyrolysis mass yield and residual carbon concentration for the experimental results analyzed. The rationale for a second order polynomial correlation relating mass yield to carbon concentration as illustrated by Lestander *et al*[72] is as follows; while part of the carbon will be released as volatile matter from heating, the 'fixed' carbon content cannot be volatilized and thus represents the lowest possible or boundary mass yield (daf basis).

Although some of the total carbon is lost as part of the gas/condensable organic matter during torrefaction, this fixed carbon content maintains an increasing carbon concentration as other mass is lost through volatilization. Further, the carbon concentration will approach 100% as the mass yield reaches its lower limit/boundary defined by the fixed carbon content, which is on average between 17.5-18.1% for woody and grass-like lignocellulosic biomass[87].

The study by Lestander *et al*[72] benefited from two biomass types with very similar raw ash-free carbon content, allowing a direct comparison of total carbon content that increased consistently through a wide range of pyrolysis conditions. There are many published examples of torrefaction experiments where carbon concentration clearly increases as mass yield decreases[15,52,53,62,78,79,81], but this relationship has not generally been defined mathematically, compared between a wide range of experiments, or proposed specifically as an indicator for severity of torrefaction. This research takes the work of Lestander *et al.*[72] and others to the next logical step; combining in-house data with other sets of torrefaction experimental results, normalization of the carbon data and determination to what extent the change in carbon correlates to torrefaction severity, as defined by the change in total mass.

The novelty of the work presented here is in how the results of many torrefaction experiments are distilled to a few normalized parameters that allow direct comparison of those experiments. First, the measured change in carbon concentration between raw biomass and torrefaction chars is compared to the process mass yield, a proxy indicator for severity of torrefaction. Secondly, using the same data, the mass change of carbon is compared to the total mass change for each experiment. Torrefaction experiments were conducted using both batch and continuous-flow apparatus', with willow, wheat straw and cattail feedstocks. The mass yield, ash and carbon content measurements from these experiments were used to develop an initial estimate for the carbon concentration and carbon mass change correlations. These correlations were subsequently refined and validated by introducing more than 60 datapoints from other published works on lab and pilot scale torrefaction experiments, with various wood and grass biomass types.

5.3 Materials and methods

This section describes the apparatus and method for conducting continuous torrefaction experiments, which yielded the majority of the data that were the subject of this study. The other experimental data examined included the results of 22 batch torrefaction experiments using wheat straw that had been previously published by Campbell *et al*. (2012)[88] as well as continuous torrefaction of coppiced willow

using a modified apparatus by Woytiuk *et al*. (2017)[51]. The details of those apparatus' and method may be found in the referenced publications.

5.3.1 Continuous torrefaction pilot plant

The torrefaction pilot plant (CTU) was used to conduct continuous torrefaction experiments that were examined for this research. For details on this apparatus, including concept, design, and operation, refer to Chapter 3.

5.3.2 Experimental parameters and method

As illustrated in Table 5.1, 27 in-house torrefaction experiments were completed using the CTU pilot plant, using willow, wheat straw and cattail feedstocks. Willow was used in 21 different experiments ranging in temperature from 220 to 280 °C, and a torrefaction time from 8 to 24 min. Starting dry mass for these experiments ranged from 1.3 to 6 kg. Wheat straw was similarly used in five experiments from 220 to 280 °C but at a consistent torrefaction time of 8.6 min, and an original dry mass of 0.52 to 0.55 kg. Cattail has thus far been only used in one experiment at 250 °C and 6.8 min torrefaction time, with a starting mass of 0.5 kg.

The parameters indicated were selected in order to characterize the torrefaction plant for a wide range of temperature and exposure time, and to produce torrefaction chars with a wide range of torrefaction severity for each biomass type.

Prior to each torrefaction experiment, the biomass moisture content was measured in triplicate, followed by measuring the required experimental mass using a digital balance. The plant was then pre-heated to the indicated temperature setting, followed by placement of the biomass in the feed hopper. Conveyor 1 was started at that point, running at a fixed speed until the level of the two-litre hopper fills to the level of the indicated level switch, automatically starting conveyor 2. The speed setting for Conveyor 2 was pre-calculated in order to meet the exposure time parameter indicated in Table 5.1. System programming automatically modulates the speed of Conveyor 1 to maintain a full level in the intermediate two-litre hopper, insuring a plugged flow condition in the torrefaction section.

Table 5.1: CTU Experimental Parameters

Temp °C	Time min	Replicate
SRC Willow (2015-2017)		
220	16.0	1
229	10.3	1
229	21.7	1
235	20.0	1
250	8.0	1
250	16.0	6
250	24.0	1
255	10.0	1
265	16.0	5
271	10.3	1
271	21.7	1
280	16.0	1
Cattail (2017)		
250	6.8	1

Temp °C	Time min	Replicates
SRC Willow (2014)*		
240	<10*	1
250	<10*	1
260	<10*	1
265	<10*	1
270	<10*	1
280	<10*	1
Wheat Straw (2016-2017)		
220	8.6	1
235	8.6	1
250	8.6	1
265	8.6	1
280	8.6	1

*For these experiments, 10 min. included heating, drying and torrefaction time

Once the main hopper and the conveyors had exhausted all of the available raw biomass, and the last of biomass had passed the final heating zone, the process heat and gas flow was discontinued. The char sample was then extracted and its mass was measured immediately while warm, to ensure it was as dry as possible.

5.3.3 Feedstocks

Two types of biomass were selected for the initial torrefaction experiments: short rotation coppiced SV1 willow and straw from hard red spring wheat. These biomasses were selected due to their proposed suitability as energy biomass in the western Canada; willow has been proposed as an energy biomass particularly suitable for marginal lands[5], while wheat straw is the most abundant agricultural residue in the region, with 2.7 to 11.7 million tonnes available in the province of Saskatchewan alone, after considerations and deduction made for soil maintenance and livestock usage[89]. With both biomass types having similar physical form as well, the same prototype apparatus "Rotoshear" could be used for converting the stem biomass into consistent, flowable feed (refer to Figure 3.4) for the continuous torrefaction process[75].

Typha spp., also known as cattail, has been selected for torrefaction experiments as well, for its local and wide availability as well as its notable absence in torrefaction literature as a potential feedstock. This

plant is a fast-growing thick-stemmed grass that grows throughout the world in wetlands. Cattail is used in constructed wetlands for wastewater management as it will uptake nutrient excesses and incorporate them into its structure[90]. *Typha spp.*, also having a similar physical form to willow and wheat straw also is converted to flowable granules quite readily, and was found to work well as feedstock for the continuous torrefaction pilot plant.

Referring to Table 5.2, the variation in elemental composition between the three biomasses examined is not insignificant; carbon content variation is more than 3 %, hydrogen 1 %, and oxygen 6 %. Ash content ranges from 1.4 to 7.6 %, and when torrefied will concentrate in the char product as volatile matter is removed. The difference in bulk density is noted as well, which is a particular challenge in flexible operation of a continuous plant; lower density feedstocks can be heated more rapidly but without characterizing each feedstock in advance it is difficult to predict the severity of torrefaction for particular temperature and residence times. The variation of material properties illustrates the need for a normalized torrefaction extent parameter, as well as on-line measurement techniques to ensure flexible, rapid high-quality char production.

Table 5.2: Chemical and Physical Characteristics of Raw Feedstocks

	C (%)	H (%)	N (%)	S	O*	Ash (%)	Bulk Density
Willow	49.4	6.3	0.4	0.0	42.5	1.4	210
Wheat Straw	46.2	6.0	0.5	0.2	39.5	7.6	47
Cattail	46.1	5.3	0.3	0.1	45.5	2.8	35

All reported measures expressed on a dry basis.

* Calculated by difference

5.3.4 Analysis Methods

The analysis methods used for the biomass samples examined in this work were consistent with those used for the research described in Chapter 4. Refer to section 4.3.4 for details on these procedures.

5.3.5 Literature data collection parameters

A review of published literature on laboratory, bench and pilot scale torrefaction experiments was conducted with the goal of collecting experimental data including mass yield, carbon content, and ash content for both raw and torrefied materials. The review was constrained generally to directly and indirectly heated, inert, near atmospheric pressure torrefaction apparatus' as the understanding of the

effects of hydrothermal and microwave torrefaction processes is less well understood and reported. The review only considered lignocellulosic biomass (non-food plant matter), and focused on homogenous feedstocks as much as possible. This review did attempt to cover a wide range of plant matter however, including hard and soft woods, grasses and agricultural residues. The review also considered a wide variety of torrefaction apparatus' and feed masses, encompassing experiments from several milligrams to many kilograms, and both small scale batch processes to continuously fed pilot plants.

5.3.6 Data normalization

In order to compare the results of different torrefaction experiments where the starting biomass may have very different relative compositions of moisture, carbon and ash, normalizing the mass yield and composition measures is required. Generally, most experimental results for yield and composition are reported on either a dry basis (db) or dry-ash free (daf) basis so that the relevant changes reported are concerned only with the reactive fraction of biomass.

When making comparisons between different experimental results, normalization of data using this method is sensible in order to express and compare the effect of the torrefaction process, where ash contents may vary between biomass types or growing conditions in different geographic areas. In particular, grasses, stems, seed hulls, shells, and other agricultural residues can have ash content varying from 5-10 % [25] which must be considered in comparing mass yields as well as elemental composition. In order to present the data in this format, sources were found which included data already on a DAF basis, or where the ash contents were specifically indicated. Where data were given on a dry basis only, mass yield or Y_m was converted to daf basis by Equation 5.1, which is derived as follows;

$$Y_{m(daf)} = \frac{M_f - M_{ash}}{M_i - M_{ash}} = \frac{M_f}{M_i} \frac{\left(1 - \frac{M_{ash}}{M_f}\right)}{\left(1 - \frac{M_{ash}}{M_i}\right)} \quad (5.1)$$

where M is the mass, with subscripts i and f referring to the mass before (initial) and after (final) torrefaction, while subscript ash refers to the mass of ash in the sample.

the percentage final ash content, denoted by A_f, relates to the final masses by Equation 5.2, or in in terms of the initial mass by Equation 5.3;

$$A_f = \frac{M_{ash}}{M_f} \quad (5.2)$$

$$A_f = \frac{M_{ash}}{M_f} = \frac{M_{ash}}{Y_m M_i} \rightarrow \frac{M_{ash}}{M_i} = A_f Y_m \quad (5.3)$$

this can also be expressed by Equation 5.4, which illustrates calculation of the dry, ash-free mass yield from just the dry mass yield and the final ash content of the char;

$$Y_{m(daf)} = Y_m \frac{(1-A_f)}{(1-Y_m A_f)} \quad (5.4)$$

where the sample carbon content was available on a dry basis, this was converted to daf basis by Equation 5.5;

$$C_{daf} = \frac{C_{dry}}{1-A_f} \quad (5.5)$$

Comparing the normalized change in carbon for different samples of torrefied biomass will be approached in two ways. The first method compares the change in carbon concentration (ΔC) to mass yield (Ym), while the second method calculates the change in carbon mass per 100 g biomass (ΔMc) and compares that value to the change in total mass per 100 g (ΔMt).

Many articles detailing torrefaction experiments report the mass yield of each experiment as well as the carbon concentration of the raw material and each char product. In general, the carbon content of the raw material will from 44 to above 50%[24], and will increase in value from that baseline with respect to increase in severity (decreasing mass yield). In order to compare many different biomass and different experiments, a normalization formula is used to 'zero' each dataset.

This normalization or 'zeroing' is conducted by subtracting the original carbon content (raw feedstock, daf basis) from the carbon content of the char product as illustrated by Equation 5.6. This calculation yields the normalized parameter of ΔC for each biomass type and each individual torrefaction experiment. It is from this normalization that arises the hypothesised correlation between change in residual carbon concentration (ΔC) and torrefaction severity (Y_m).

$$\Delta C_{daf} = C_f(daf) - C_i(daf) \quad (5.6)$$

The normalized change in carbon can also be expressed by calculating the loss of carbon per 100 g mass of biomass (ΔM_c). This parameter is calculated by taking the difference between the product of the mass yield (Ym) and final carbon concentration (C_f) and initial mass of carbon per 100 g of dry biomass (C_i), as illustrated in Equation 5.7:

$$\Delta M_c = 100 * (Y_m * C_f - C_i) \text{ (all daf)} \quad (5.7)$$

The mass change of carbon parameter expresses what ratio of the volatilized mass is carbon, and is that ratio consistent as severity increases. However, as a tool for measuring severity in real time, ΔM_c is not as helpful as ΔC as it requires the mass yield (Y_m) to be calculated. The ΔM_c parameter will be compared to the change in total mass per 100 g (ΔM_t), so that the two values can be directly compared. This value was calculated from the experimental mass yield (daf) by Equation 5.8:

$$\Delta M_t = 100 * (Y_m - 1) \text{ (all daf)} \quad (5.8)$$

5.4 Results and discussion

5.4.1 Experimental data: carbon concentration

The mass yields associated with each in-house torrefaction experiment are listed in Table 5.3 (daf basis), broken down into five sets based on biomass, apparatus and procedure. In addition to the experimental data from CTU experiments, two other previously published datasets are included from in-house experiments using other or modified apparatus. The procedure and apparatus of "CTU-Willow (2014)" were unique in that those experiments were completed when the CTU only consisted of its first stage and thus a unique procedure was used, described previously by Woytiuk *et al.*[51]. Procedural and apparatus description for "Batch-Wheat Straw (2012)" were also published previously (by author) as Campbell *et al.* [88]; this work consisted of torrefaction of 50 g samples of wheat straw segments in a tube reactor, for the time and temperature parameters indicated in Table 5.3.

Results are presented in order of ascending process temperature, and ascending torrefaction time so that in general, the results are also in ascending severity of torrefaction. A wide range of extents are represented in each set, covering a range from 55.6 to 96.7 % mass yield, which exceeds the typical 70-90 % mass yield range for this process.

The results of replicate experiments illustrate the uncertainty of each apparatus/method – the range of results from the earlier batch process replicates is significantly greater than from the continuous

experiments. The uncertainty in mass yield measurement for the same process parameters illustrates the potential benefit of continuous analytical measurement.

Table 5.3: Torrefaction experimental data (daf values)

Temp °C	Time min	C	Y_m	Temp °C	Time min	C	Y_m	Temp °C	Time min	C	Y_m
CTU - Willow (2015-17)				CTU - Wheat Straw (2016-17)				Batch - Wheat Straw (2012)			
RAW		0.50		RAW		0.50		RAW		0.49	
RAWø		0.51		RAW+		0.48		240	10	0.52	0.85
220	16.0	0.52	0.90	220	8.6	0.52	0.95			0.53	0.86
229	10.3	0.52	0.92	235+	8.6	0.52	0.90			0.52	0.88
229	21.7	0.54	0.85	250	8.6	0.55	0.83	240	20	0.54	0.80
235ø	20.0	0.56	0.83	265+	8.6	0.56	0.72	240	30	0.53	0.77
250	8.0	0.54	0.87	280	8.6	0.62	0.61	250	30	0.55	0.76
250	16.0	0.55	0.77					260	10	0.57	0.66
		0.56	0.79	CTU - Cattail (2017)				260	20	0.60	0.62
		0.56	0.78	RAW		0.47				0.57	0.68
		0.56	0.78	250	6.8	0.54	0.74			0.57	0.66
		0.56	0.78							0.57	0.70
		0.56	0.79							0.58	0.70
250	24.0	0.57	0.75	CTU - Willow (2014) [10]						0.56	0.65
255ø	10.0	0.57	0.82	RAW		0.50		260	30	0.56	0.68
265ø	16.0	0.58	0.73	240	<10*	0.51	0.96	270	10	0.60	0.59
		0.59	0.74	250	<10*	0.49	0.97	270	30	0.59	0.68
		0.59	0.73	260	<10*	0.51	0.92	280	10	0.59	0.63
		0.60	0.73	265	<10*	0.50	0.92	280	20	0.58	0.58
		0.59	0.73	270	<10*	0.54	0.85	280	30	0.62	0.56
271	10.3	0.56	0.75	280	<10*	0.54	0.81			0.59	0.60
271	21.7	0.58	0.69							0.61	0.58
280	16.0	0.59	0.64							0.63	0.61

*10 min included heating, drying and torrefaction time
ø/+Reference raw biomass sample for these torrefaction runs

The 54 experimental datapoints are illustrated in Figure 5.1, where the mass yield value for each experiment is expressed in terms of change in carbon concentration. The mass yield correlates well to change in carbon (ΔC) for all datasets between 70 and 90 %. Below 70 % mass yield, however, the relation for batch wheat straw torrefaction mass yields becomes increasingly spread out. This may be explained by the phenomenon described by Wannapeera *et al.* [78], where at mass yields of 60 % (and presumably lower), a high-temperature torrefaction pathway producing the same mass yield as a low temperature pathway will increase the carbon content by a greater amount, observed as a 2 to 3%

difference. Differences in measurement or sampling for the batch experiments may also have led to the data scatter present.

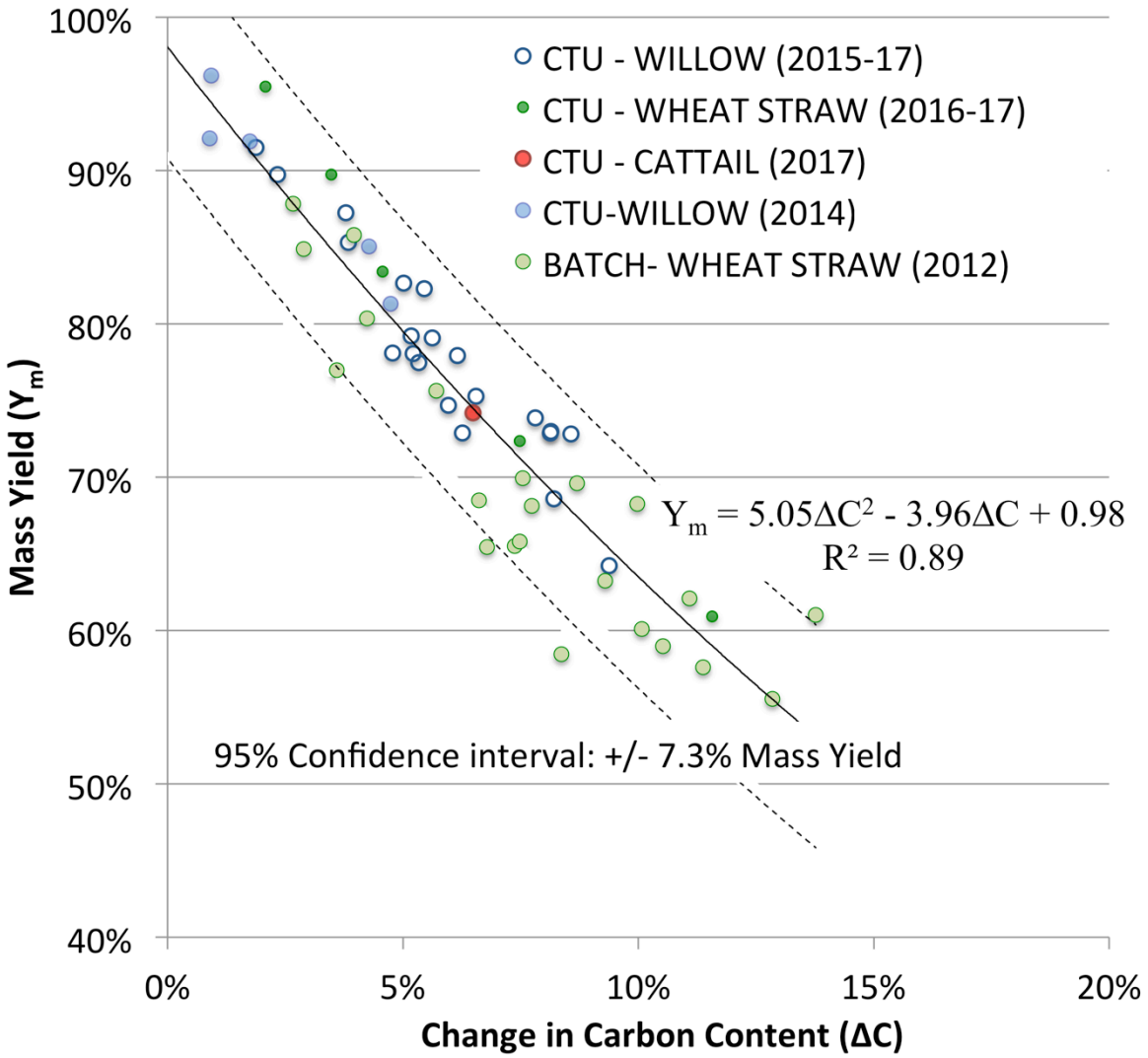

Figure 5.1: Mass yield with respect to change in carbon content for torrefaction experiments. (dry, ash-free basis). Symbol color code: Blue (Hardwood), Green (Wheat Straw), Orange (Softwood), Red (Reeds/grasses). Data for CTU-WILLOW (2014) from Woytiuk *et al.* 2017[51], BATCH-WHEAT STRAW (2012) from Campbell *et al.* 2012[88]. Polynomial correlation relating mass yield to ΔC is indicated.

The mass yields associated with "CTU-Wheat Straw (2016-17)" represent five experiments carried out using the CTU with wheat straw granules at increasing temperature settings, but with the same exposure time, and appear to be relatively linear with respect to change in carbon. The CTU-WILLOW data contain clusters of datapoints between 70 and 80%, which represent replications of the same experimental conditions, as well as alternate temperature-time pathways, which yielded similar mass yield and carbon measurements. Carbon content appears to increase at a regular rate with respect to decreasing process mass yield, and all five datasets generally overlap. Within the two largest datasets,

there is significant scattering between 70-60 % mass yield for the 2012 wheat straw (batch) data, and to a lesser extent in the CTU – willow dataset between 80-70 %. The datapoint for CTU-CATTAIL is included as it represents the most recent plant operation for which data are available, and is a relatively little examined type of biomass. Nevertheless, the datapoints for this single cattail experiment correlates extremely well to the others.

The polynomial regression for the combined experimental data is presented in Figure 5.1, which fits with a coefficient of determination of 0.89. The polynomial regression has also been constrained to ΔC = 40 % at 20 % mass yield so that the regression may continue to fit data outside of what is available; without this constraint the best fitting second order regression will reach its minima between ΔC values of 25 and 30 % and then begin to increase. A polynomial fit for mass yield as a function of ΔC is consistent with the findings of Lestander *et al.* [72]; though in that case the mass yield and carbon measurements were not normalized.

From Schenck[91], the 95 % confidence interval indicated around the regression curve on Figure 5.1 was based on ±2(SEE) band where SEE is the standard error of the estimate, or the error between the correlation equation and the datapoints. The SEE was calculated using Equation 5.9;

$$\mathrm{SEE} = \left\{\frac{\Sigma(\mathrm{Y}-\mathrm{Y}')^2}{\mathrm{n}-\mathrm{p}}\right\}^{1/2}, \qquad (5.9)$$

where Y is the measured value (mass yield in this case) and Y' is the mass yield estimate from the correlation equation. The denominator n - p represents the total degrees of freedom, or the difference between the number of estimates and the number of estimated parameters in the correlation.

5.4.2 Experimental data: change in mass of carbon

Figure 5.2 now illustrates the mass change of carbon with respect to total change in mass. While the previous section illustrates how the carbon concentration increases as mass yield decreases, the mass change of carbon and total mass change are both represented as losses.

The coefficient of determination for the best fit linear regression is indicated in Figure 5.2 as 0.96, while the linear regression itself is $\Delta M_c = 0.36\Delta M_t + 1.04$. This correlation illustrates through the X-intercept of -2.89 that the first 2.89 grams (or percent) of mass loss occur without consistent loss of mass of carbon, while the slope of the linear correlation illustrates that the subsequent loss rate of carbon is 36% of the total mass loss.

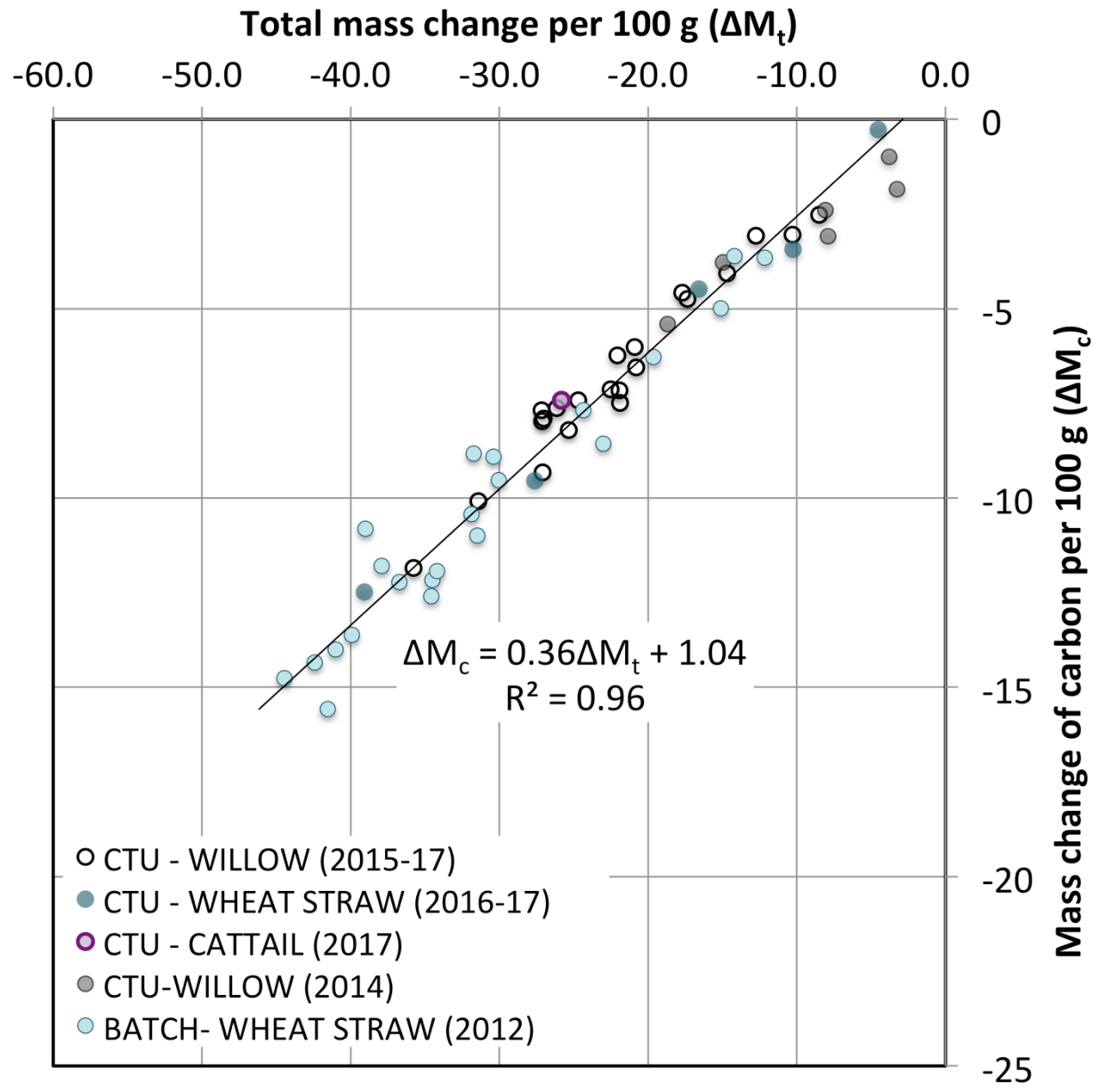

Figure 5.2: Relation between change in mass of carbon and total mass change per 100 g. For torrefaction experiments. (dry, ash-free basis). Symbol color code: Greyscale (Hardwood), Teal (Wheat Straw), Pink (Softwood), Violet (Reeds/grasses). Data for CTU-WILLOW (2014) from Woytiuk *et al.* 2017[51], BATCH-WHEAT STRAW (2012) from Campbell *et al.* 2012[88].

5.4.3 Literature survey data

Data from published torrefaction manuscripts was next collected to validate the in-house data and the correlation equations for ΔC and ΔM_c. While many published research papers reporting on torrefaction experiments include the mass yield and often also the carbon content, in many instances it was not possible to confirm or convert these values to an ash-free basis, lacking either the ash values for raw and torrefied samples, or lacking analysis of the raw material totally. Referring to Table 5.4, seven research papers have been reviewed and data from them have been included in this analysis. Where available, the process parameters for each experiment are listed along with the mass yield and carbon content (daf basis).

The values in Table 5.4 are reproduced from reported values in the manuscripts indicated, after converting the values to daf basis. The exception to this is the manuscript from Nachenius *et al.* [53]; the values in Table 5.4 were tabulated from a plot of carbon content and mass yield from that paper. The collected data include results from four sets of experiments using batch torrefaction apparatus (mainly tube reactors), and three sets using continuously fed systems (screw and drum reactors). There are five datasets for softwood, including three different experiments on pine, another on logging residues (also from pine) as well as Norwegian spruce. There are four sets on hardwoods; ash, beech, willow and leucaena, as well as four sets on grasses; wheat straw is represented twice, as well as reed canary grass and miscanthus. Overall, this is a good representation of the range of potential torrefied lignocellulosic biomass (non food plant matter).

The data also encompass a wide range of temperature pathways: Wannapeera *et al.*[78] in particular purposefully examined pathways ranging from 250 °C/1140 min. to 320 °C/6 min. at the same mass yield (60%) to determine if there are differences in char product. The range of temperatures examined spanned from 225 °C to 375 °C, though the relevance of temperature parameter was specific to each experiment given that in some cases it was the measured temperature of biomass surface (batch reactors) and in others it was the reactor wall or jacket temperature (screw reactors). The time parameter was varied a great deal as well, the most extreme being 1140 min. tested by Wannapeera *et al.*[78]., and several using fixed time parameters; 45 min. – Le Thanh *et al.*[52], 30 min. – Bridgeman *et al.*[62], Phanphanich *et al.*[15]. The experiments with a screw conveyor reported by Nachenius *et al.*[53]. tested the shortest torrefaction time (5.75 min.), while Strandberg *et al.*[79] tested 8 min. torrefaction times which were the next shortest. By including a wide range of pathways, processes and biomass, the change in carbon and severity of torrefaction may be evaluated independently of the process parameters.

Table 5.4: Torrefaction experimental data from literature survey. (daf values)

Bridgeman *et al.* 2008.[62]

TGA

Temp °C	Time min	C	Y_m
RCG	RAW	0.49	1.00
230	30	0.49	0.93
250	30	0.50	0.84
270	30	0.52	0.72
290	30	0.54	0.62
WS	RAW	0.47	1.00
230	30	0.49	0.91
250	30	0.50	0.83
270	30	0.52	0.72
290	30	0.56	0.55
WIL	RAW	0.50	1.00
230	30	0.51	0.95
250	30	0.52	0.90
270	30	0.53	0.80
290	30	0.55	0.72

Nachenius *et al.* 2015[53]

Screw Reactor

°C	min	C	Y_m
PINE	RAW	0.49	1.00
		0.49	0.96
		0.51	0.92
		0.53	0.84
		0.53	0.82
		0.53	0.82
		0.53	0.78
		0.54	0.78
		0.55	0.76
		0.56	0.71
		0.57	0.66
		0.65	0.43

Temp: 275 to 375C

Time: 5.75 to 16.5 min

Ohliger *et al.* 2013[81]

Screw Reactor

Temp °C	Time min	C	Y_m
BEECH	RAW	0.50	1.00
280	40	0.57	0.76
270	40	0.59	0.71
290	40	0.62	0.63
300	40	0.66	0.52
280	20	0.56	0.78
280	60	0.60	0.66
280	40	0.60	0.67
280	40	0.58	0.74

Strandberg *et al.* 2015[79]

Drum Reactor

Temp °C	Time min	C	Y_m
SPRUCE	RAW	0.51	1.00
260	8	0.52	0.97
260	25	0.54	0.89
285	16.5	0.55	0.80
285	16.5	0.55	0.80
310	8	0.56	0.77
310	25	0.70	0.46

Phanphanich *et al.* 2012[79]

Tube Reactor

Temp °C	Time min	C	Y_m
PINE	RAW	0.47	1.00
225	30	0.50	0.89
250	30	0.52	0.82
275	30	0.55	0.73
300	30	0.64	0.52
L-RES	RAW	0.48	1.00
225	30	0.51	0.88
250	30	0.56	0.81
275	30	0.54	0.70
300	30	0.68	0.51

Wanapeera *et al.* 2015[78]

Tube Reactor

Temp °C	Time min	C	Y_m
LEUC	RAW	0.48	1.00
250	120	0.53	0.80
280	5	0.53	0.80
300	0	0.53	0.80
250	480	0.56	0.70
280	40	0.56	0.69
300	5	0.55	0.70
320	1	0.57	0.70
250	1140	0.60	0.61
280	105	0.60	0.60
300	20	0.60	0.60
320	6	0.63	0.61

Le Thanh *et al.* 2015[52]

Tube Reactor

Temp °C	Time min	C	Y_m
PINE	RAW	0.52	1.00
250	45	0.52	0.82
280	45	0.55	0.71
300	45	0.60	0.55
ASH	RAW	0.50	1.00
250	45	0.53	0.77
280	45	0.57	0.64
300	45	0.64	0.47
MISC	RAW	0.50	1.00
250	45	0.51	0.84
280	45	0.57	0.66
300	45	0.67	0.47
WS	RAW	0.49	1.00
250	45	0.52	0.79
280	45	0.60	0.57
300	45	0.67	0.45

The torrefaction data collected from these papers do represent a wide range of torrefaction severity as well, from 97% mass yield to as low as 43%, which is well beyond normal torrefaction range. The carbon content of raw material ranges from 47% to as high as 52%, while the final carbon content of torrefied material ranges as high as 70%. These data should be illustrative if the mass yield and carbon content become non-correlated as the torrefaction severity increases past 60% mass yield as predicted by Wannapeera *et al.*[78]

5.4.4 Data and correlation validation: carbon concentration

The combination of the experimental data and survey data is illustrated in Figure 5.3. The source of each datapoint is indicated in the legend, along with the biomass type. Immediately it is clear that the correlation observed in the experimental data is both strengthened and weakened by the survey data. For several datasets, the torrefaction mass yield correlates to ΔC in the same manner as observed in the experimental data (Ohliger *et al.*[81], Nachenius *et al.*[53], Strandberg *et al.*[79]). In others, the severity of torrefaction appears to have a much weaker effect on the carbon content (Le Thanh *et al.*[52], Bridgeman *et al.*[62]), though some of these data overlap with the "Batch-Wheat Straw (2012)" data that was previously published.

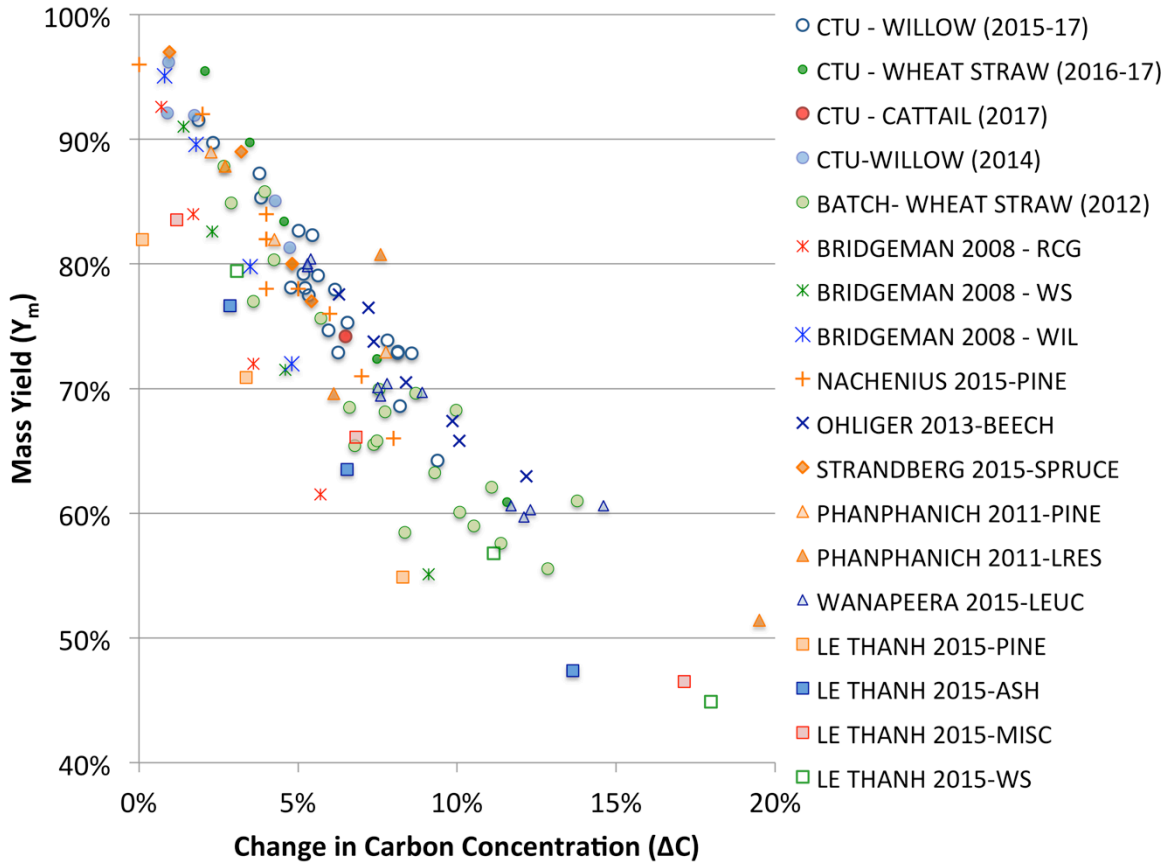

Figure 5.3: Experimental &literature torrefaction data for mass yield and change in carbon. (dry, ash-free basis).. Symbol color code: Blue (Hardwood), Green (Wheat Straw), Orange (Softwood), Red (Reeds/grasses) Data for CTU-Willow from Woytiuk *et al.* 2017[51], BATCH-WHEAT STRAW (2012) from Campbell *et al.* 2012[88], Bridgeman 2008[62], Nachenius[53], Ohliger[81], Strandberg[79], Phanphanich[15], Wanapeera[78], Le Thanh[52].

Notably, the experimental data from Wannapeera *et al.*[78] illustrate the point of that paper clearly; at 60% mass yield, the datapoint for their high temperature pathway illustrates a ΔC (15%) that is approximately 3% above the main cluster.

The variability in this total dataset is quite significant; particularly as lower mass yield values are reached. This dataset prompts several questions; is the apparent variability fundamental to the question, or is there a pattern of experimental bias/uncertainty in measurement of the mass yield or carbon content? As illustrated in Table 5.4, there are a wide range of experimental conditions represented, including different reactor/process types as well as time/temperature and experimental masses.

While presenting an array of different conditions is intentional, the range of experimental masses covers six orders of magnitude; the experiments of Bridgeman *et al.* [62] utilized initial masses of 25-35 mg while the experiments of Strandberg *et al.*[79] considered experiments with total feed masses of up to 50 kg. After review of the combined data, it was postulated that the smallest experimental masses may be susceptible to greater bias/uncertainty in the collection, measurement and calculation of mass yield values. It may also be possible that analyzing the carbon content from such small samples may be subject to error from non-homogeneity or other sampling error result from small sample sizes. In the case of 'logging residues' torrefied by Phanphanich *et al.* [15], which contained a heterogeneous mixture of bark, wood and branches, the effect is observed as a significant variation around the proposed correlation line. Such a mixture of different plant components would likely contain a broader range of 'baseline' carbon concentration than biomass from a narrow range of single species plant parts.

Narrowing the field of data to only experimental (starting) masses above 500 g (Figure 5.4), and removing the dataset based on non-homogenous biomass (logging residues) Phanphanich *et al.* [15], the variability in the field of values is reduced significantly. The correlation indicated may be valid for larger pilot scale experiments and potentially for commercial results, but not for laboratory scale experiments due to the higher uncertainty and potential for negative bias in mass recovery and measurement for experiments of 50 g and lower. The dataset from Wannapeera *et al.*[78]., notably, did correlate quite well despite having a relatively low torrefaction mass of 2.5 g, perhaps demonstrating that the effect of measurement uncertainty can potentially be minimized.

The polynomial regression indicated in Figure 5.4 is proposed to define the relationship between mass yield and change in carbon content for the 58 datapoints that remain. This regression is fixed at a ΔC

limit of 40%, where the mass yield is set at 20% based on the findings of Lestander *et al.*[72]. This correlation holds well for data from 97% to 60% mass yields, but below that range the correlation would likely be pathway dependent according to Wannapeera *et al.*[78]. In particular, high temperature short-residence time pathways at 60% mass yield and below would likely deviate from this correlation. Within this range however, the correlation illustrates well that the residual carbon concentration increases at a predictable rate with respect to mass yield, and does so following a second order correlation equation. This second order characteristic illustrates that the data fits with the assumption that the Δ carbon concentration very likely approaches a limit of 45% at the boundary of minimum mass yield which is near 20%.

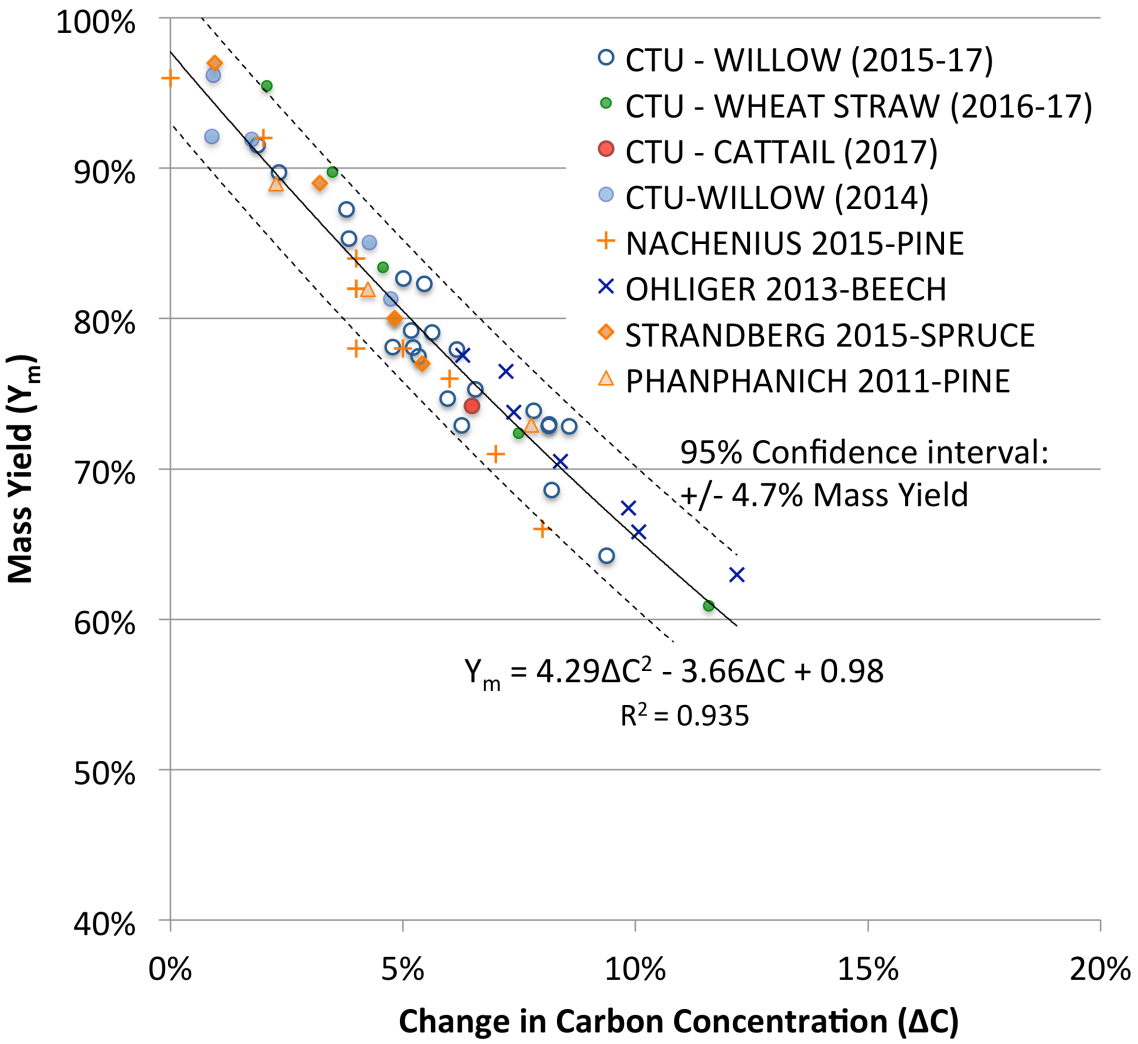

Figure 5.4: Correlation between mass yield and change in carbon content.
Includes selected experimental and literature data, limited to experiments of 0.5kg initial mass or greater. Symbol color code: Blue (Hardwood), Green (Wheat Straw), Orange (Softwood), Red (Reeds/grasses). Data for CTU-Willow from Woytiuk *et al.* 2017[51], Nachenius[53], Ohliger[81], Strandberg[79] , Phanphanich[15].

This boundary represents the most severe form of torrefaction/pyrolysis where the solid product consists of highly concentrated fixed carbon that is cannot be further reduced by this form of process. Though the data examined do not probe this far in terms of process severity, a correlation assuming this boundary does provide a good fit to the data.

In terms of predictive capability, the 95% confidence interval based on the sum of experimental error (SEE) in Y_m was found to be +/-4.7%. Examining the dataset used to generate the regression, a typical range for torrefaction severity defined by mass yield range of 70 to 90% would correspond to an increase in carbon content of 2.5 to 8.5% (daf basis). Simply knowing this range is a useful tool in developing processes for torrefaction chars where the composition, chemistry and stoichiometry are important.

5.4.5 Correlation validation: change in mass of carbon

Now combining literature data with experimental data for mass change of carbon, Figure 5.5 illustrates that the literature data corresponds well with the experimental data, with several outliers that were also seen in the ΔC validation. The four datapoints for logging residues (code = LRES) from Phanphanich *et al.* are highly scattered; this class of biomass may have significant variations in original carbon content since it may be a very heterogeneous mixture of wood, bark and possibly leaf matter. The data values for 'Pine' from Le Thanh *et al.*[52] appear to follow a linear pattern which is significantly offset from the main population of the data, and different from other pine wood and other softwood torrefaction experiments. This may be a normalization error originating from the reported value for raw biomass carbon content.

Table 5.4 and the original manuscript by Le Thanh *et al.* both illustrate that there was little or no change in carbon concentration between the raw biomass and the 82% mass torrefaction chars produced[52]. The carbon concentration reported by Le Thanh *et al.*[52] for the raw pine sample is inconsistent with other analysis of this material or with the torrefied pine carbon content reported in their work.

However, even including these outliers, the fit for the correlation is still very good, with an R^2 value of 0.93. This linear regression correlation is $\Delta M_c = 0.37\Delta M_t + 1.26$. This correlation illustrates the how the rate loss of carbon mass relates to the total mass loss from the solid biomass. Since all of the mass that is lost is converted to gas and volatile matter, this correlation also suggests what fraction of the gas/volatile stream would be comprised of carbon. On average, the first 3.4% of mass loss occurs with minimal loss of carbon, while subsequent loss of carbon representing 37% of total mass loss.

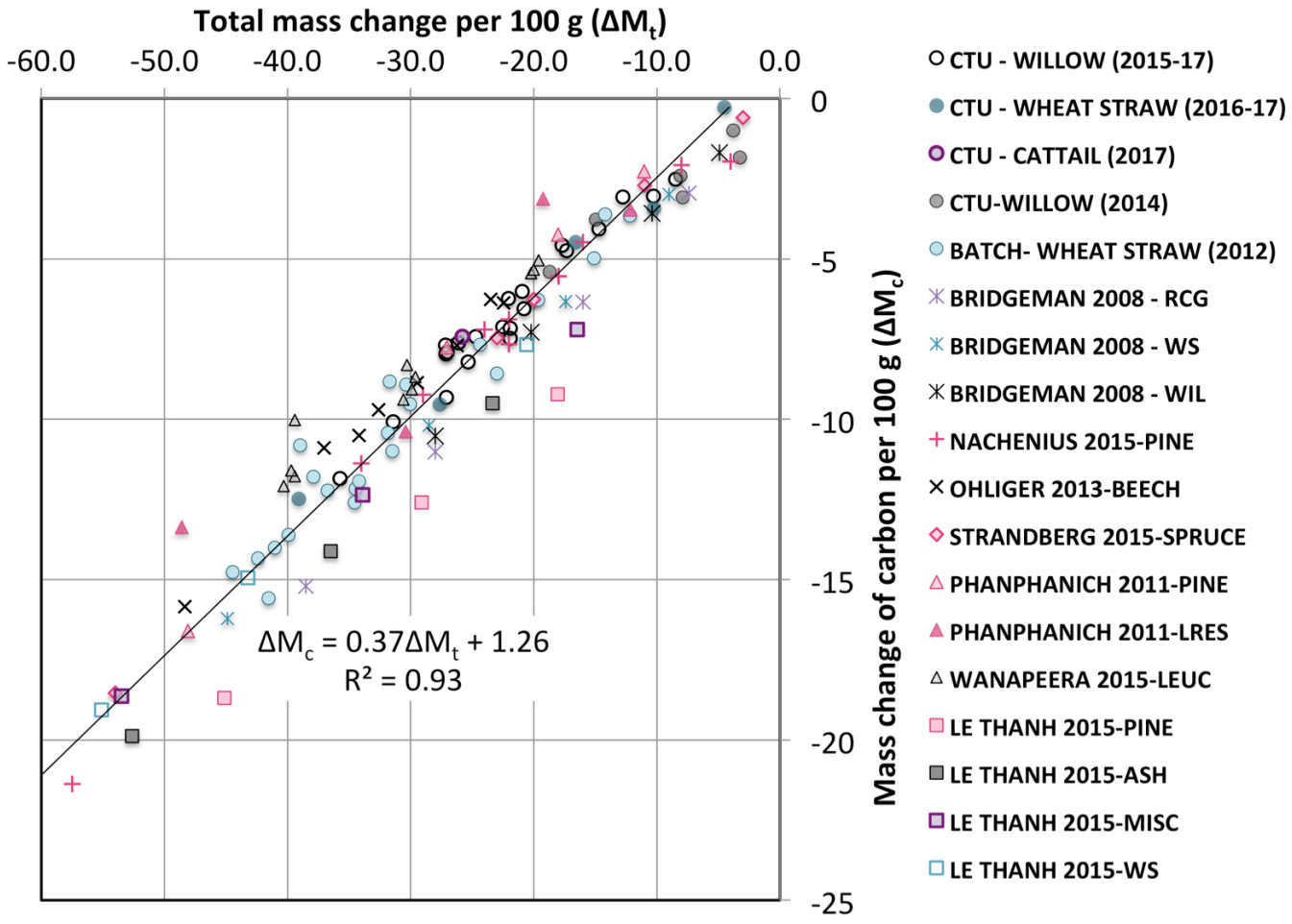

Figure 5.5: Experimental & literature data; change in carbon mass relative to total mass.
Symbol color code: greyscale (Hardwood), teal (Wheat Straw), Pink (Softwood), Violet (Reeds/grasses) . Data for CTU-Willow from Woytiuk *et al.* 2017[51], BATCH-WHEAT STRAW (2012) from Campbell *et al.* 2012[88], Bridgeman 2008[62], Nachenius[53], Ohliger[81], Strandberg[79], Phanphanich[15], Wanapeera[78], Le Thanh[52].

5.4.6 Application of Correlation

While the correlation based on mass loss of carbon can be used to understand the volatilization rate of carbon, the correlation between torrefaction mass yield and change in carbon concentration has the potential for application to continuous torrefaction process control, as illustrated by Figure 5.6. Since the daf mass yield of torrefaction follows the change in daf carbon content by a second order equation, as shown in 5.4.4, this correlation can be used to predict that mass yield where the carbon concentration values are directly and rapidly measured. Total carbon analysis could be applied to a continuous torrefaction process using off-the-shelf instruments (such as a UIC CM150 or an Elementar Rapid CS Cube).

By continuously sampling the carbon content of the raw biomass and the char, as well as regular sampling of the raw biomass ash content, an estimated ΔC value can be calculated and used by the correlation to estimate the mass yield in real time. The process can thus be regulated using PID control, adjusting temperature or residence time to meet a user setpoint defined either by a desired mass yield (Y_m) or specified change in carbon concentration value (ΔC).

Since the Y_m(ΔC) correlation is based on daf values, measuring and using the ash content to correct the ΔC calculation would be required to implement control in this manner. This would be important particularly for high-ash biomass types where the daf correlation would have poor fit with a (db) ΔC measurement. While the ash content of the torrefaction char would be ideal for this calculation, it would not be practical; a reasonable estimate of the char ash content can be made however, based on that of the raw material and an estimate of the mass yield.

Torrefaction with on-line compositional analysis and closed-loop control would thus be capable of producing chars with specific chemical composition and thus expand the potential for this technology beyond producing green coal to producing higher value bio-products in a biorefinery setting.

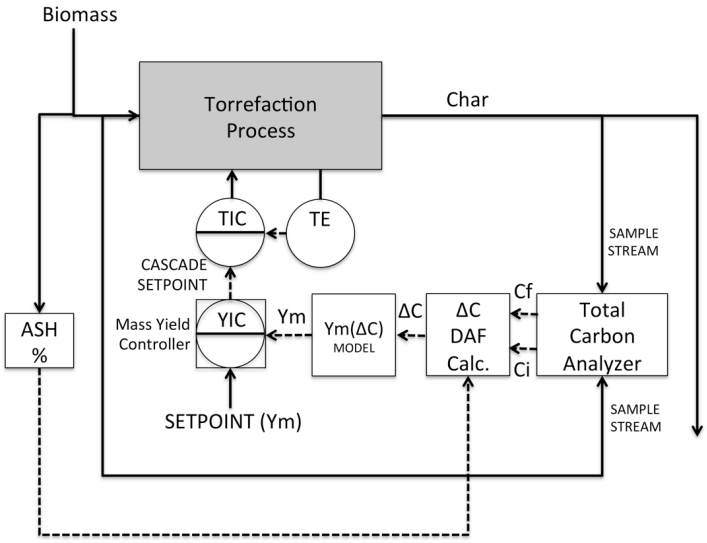

Figure 5.6: Process Instrumentation Diagram - Application of ΔC process control for a generic torrefaction process.

5.5 Conclusions

This work was carried out to determine if an empirical relationship exits between the change in carbon content and torrefaction severity. Both in-house experimental data as well as data generated by others were used to develop two correlations, one based on the change in carbon concentration, and another examining the loss in mass of carbon. Fifty-five in-house torrefaction experiments of three biomass

types were used to develop these correlations, which were then validated by introducing data from a literature review. The conclusions from this included:

1. The experimental data for change in carbon mass with respect to change in total mass yields a well fitting linear correlation: $\Delta M_c = 0.36\Delta M_c + 1.04$ ($R^2 = 0.96$). Combining the literature data validates the correlation with slight modification: $\Delta M_c = 0.37\Delta M_c + 1.26$ ($R^2 = 0.93$). This relation is illustrative of the fundamental effect that torrefaction has on carbon in lignocellulosic biomass; the initial 2.5-3.5% of mass loss occurs without significant loss in carbon, and subsequently carbon represents 37% of the total mass loss.
2. For in-house torrefaction experiments ranging from 55 % to 95 % (wt/wt) mass yield, the relation between mass yield (Y_m) and change in carbon concentration (ΔC) is described the equation $Y_m = 5.05\Delta C^2 - 3.96\Delta C + 0.98$ ($R^2 = 0.89$). The 95th percentile confidence limit for this correlation is ±7.3% (w/w). Introducing literature data to the correlation and narrowing of the dataset yields a refined correlation; $Y_m = 4.29\Delta C^2 - 3.66\Delta C + 0.98$ (($R^2 = 0.93$). The 95th percentile confidence limit for this correlation is ±4.6% (w/w). The data used to produce this correlation were from experiments with a minimum of 500 g of biomass and for mass yields greater than 60%.
3. Torrefaction experiments with small sample masses are observed to have higher potential uncertainty and negative bias with respect to mass measurement and representative sampling of elemental composition. Therefore, for small-scale experiments, the change in carbon correlation (ΔC) is not reliably predictive as it is for large-scale torrefaction experiments of 500 g and greater. However, this mathematical relation could be applied to a large scale continuous torrefaction process and used to provide control system feedback. This would require three continuous or regular measurements: continuous sampling of the carbon content of raw (1) and torrefied (2) biomass, along with regular sampling of raw biomass ash content (3).

6.0 Application of NIRS to the direct measurement of carbonization in torrefied wheat straw chars

6.1 Preface

This research presented in Chapter 6 is an investigation into how diffuse reflectance spectroscopy can be used to measure torrefaction severity. While coppiced willow was the main biomass examined in Chapters 4 and 5, wheat straw is examined specifically in this chapter, including wheat straw chars produced in both batch and continuous processes. Section 6.3.1 discusses in detail the form, origin, and composition of wheat straw used in these 15 experiments. The experiments conducted for this research used both batch and continuous processes. The continuous process utilized the CTU pilot plant as discussed in detail in Chapter 3, while the batch process is discussed in section 6.3.2. The theory behind diffuse reflectance is discussed in section 6.2, including why it is understood that diffuse reflectance of a solid material changes in response to thermal treatment. The results of elemental analysis for the 15 experiments are illustrated in Section 6.4, along with the diffuse reflectance spectra for each raw sample and char sample. It is observed that the most responsive and measurable part of the composition is the carbon content, which increases in response to torrefaction severity (as well understood from Chapter 5). The change (increase) in carbon concentration is selected to represent torrefaction severity, and the reflectance spectra are converted to absorbance spectra by ABS = log(1/R) so that both parameters ΔC and ΔABS are changing in proportion to one another. A series of linear regression analyses is then performed to determine at what wavelength the change in absorbance value can be best correlated to the change in carbon concentration.

This chapter is adapted from a manuscript that has ben submitted on Sept. 11, 2018 for publication in the journal “Biomass Valorization”.

6.1.1 Addendum

Torrefaction experiments conducted using willow and flax straw were also part of the early research in this area, results from those experiments are illustrated in Figures A.6.1 and A.6.2 in Appendix A. While 15 datapoints were used to develop a correlation for wheat straw, only 5 experiments were completed for willow/flax straw where the diffuse reflectance spectra were collected. In each case, the change in carbon concentration relative to change in absorbance follows a linear relationship with a very good fit, above an R^2 of 0.983 in both cases. For willow, the sensitivity (slope) relating absorbance to carbon appears to be more than 1/2 that of flax or wheat straw; a change in absorbance of 0.2 for flax straw or wheat straw would be associated with a 5% / 4% (w/w) increase in carbon concentration while

for willow this change in absorbance would only be associated with a 2% increase in carbon concentration. The conclusion from these different results was that each biomass will have its own sensitivity relating absorbance/reflectance to change in carbon content, but a linear relationship would be predicted in any case.

6.2 Introduction

While the severity of torrefaction is an important property for a continuous torrefaction process, measuring this value in real time poses significant challenges. Torrefaction severity is most often estimated based on the dry mass yield of the solid char product[1,68,72,79]. The mass yield from torrefaction relates well to other indicators of torrefaction severity, including the energy yield and heating value. While the mass yield is a suitable measurement for batch and small-scale torrefaction, it is not as convenient for commercial scale plants due to the complexity and cost involved in measuring large, solid mass flow rates. Other properties which change as a result of torrefaction include the milling energy[15], elemental composition, composition of volatile matter and fixed carbon measured from proximate analysis, and the amount of the macromolecule hemicellulose which diminishes significantly in response to thermal treatment in this temperature range[51,56]. Analytical measurements of these changes are very useful in assessing complex changes, but most are difficult to implement for real-time feedback to a process control system.

An example of a directly measurable physical property change pertinent to torrefaction is color; biomass will get progressively darker as torrefaction severity increases. The darkening/blackening observed in biomass that has been torrefied is the result of changes at the molecular level. Molecular bonds/structures between carbon, hydrogen, and oxygen that reflect specific wavelengths of light are gradually replaced by porous, amorphous carbon as oxygen and hydrogen are removed as the main fractions of the volatiles and gases that are produced from the process.

As a result, the solid structure of biomass char is less reflective of electromagnetic energy in the visible spectrum than raw biomass. This change extends into the near-infrared spectrum. Measuring the degree to which a solid sample will reflect light in these spectra is accomplished using diffuse reflectance spectroscopy, a type of near-infrared spectroscopy or NIRS.

The diffuse reflectance method of analysis is used to measure the surface properties of solids in the visible and near infrared spectra. For this method, a light source is directed towards a solid sample, then

the amount of light reflected back toward the sample for a specific wavelength is measured and compared to that of a baseline reflective material[92]. This procedure is then repeated for each wavelength in the band of interest, including the visible range from 400 to 700 nm, the near-infrared range from 700 to 1400 nm, and the short-wave infrared range from 1400 to 2500 nm.

Much of NIRS research with biomass examines the differences in reflectance or transmittance at different wavelengths. Specific types of molecular bonds in biomass reflect energy at certain wavelengths as a result of vibration/stretching behaviour in those bonds. For example, the energy reflectance at 1157 and 1171 nm is associated with C-H bond stretching in hemicellulose[93], the same type of macromolecule that is eliminated as a direct result of torrefaction. There is also a band from 1428 to 1597 nm that is dominated by reflectance from different O-H bonds in cellulose[93], a much more predominant macromolecule and one that does not experience thermal degradation until much higher temperatures[41]. The reflectance of biomass in the band from 740 to 1486 nm has been observed to diminish overall in response to thermal treatment, an extension of the color change observed in the visual spectrum.

NIRS has been demonstrated and applied to analysis of raw biomass and food products, providing on-line measurement methods for biomass moisture content[94], elemental composition, and quality measurement. For wheat straw specifically, Huang *et al*[95] examined the diffuse reflectance spectra for more than 100 samples of wheat straw, and correlated this spectra to elemental composition and heating value. Several methods have been developed and proposed where torrefaction chars are subject to diffuse reflectance analysis using NIRS allowing inference of changes in material properties. Lestander *et al.* examined a large number of torrefied/pyrolyzed spruce and reed canary grass samples and were able to develop multivariate calibration modelling for prediction of composition and heating value based on reflectance spectra from 950 to 1650 nm[72]. Considering the demonstrated potential of this measurement method and the potentially low cost of NIR measurement tools, a torrefaction and diffuse reflectance research project was developed. This would identify the most responsive wavelengths in the NIR band to torrefaction severity and attempt to develop a correlation between diffuse reflectance in a specific band or wavelength, relating that value to a measure of torrefaction severity that was appropriately sensitive.

The work presented here examines how NIRS can be used measure changes that result from the thermal treatment of wheat straw. A number of wheat straw char samples were produced through torrefaction, varying conditions for both temperature and residence time under two different torrefaction processes.

These samples were then examined using diffuse reflectance analysis and elemental analysis. The changes in diffuse reflectance were then compared to the changes in elemental composition and linear regression analysis was used to develop a correlation relating reflectance to specific changes in composition.

6.3 Materials and methods

6.3.1 Feedstock: wheat straw granules

Wheat straw is one of the most abundant types of biomass available in world. Worldwide yield of wheat in 2017 was 760 million tonnes[96], while wheat straw yields range in a ratio of 1-1.5:1 with the grain[89]. The recommendation for the amount of straw to remain on the cropland to protect it from erosion is around 1 tonne/ha or around 50% of production[89,97]. This means that a minimum of 500 million tonnes per year of wheat straw worldwide is available for other use, with chemical energy equal to 7 billion GJ or 1.2 billion barrels of oil equivalent (BOE). This makes wheat straw among the most abundant and underutilized sources of renewable energy worldwide. Enhancing the fuel qualities of wheat straw using torrefaction is therefore an excellent opportunity for further use of this material.

Figure 6.1: Segmented wheat straw sample.
Scale markings are 1 cm.

Straw samples of Canada Western Red Spring wheat (CWRS) were harvested from farms near Saskatoon, Saskatchewan. The straw was dried in the open air of the lab for a minimum of 3 months, followed by size reduction using a custom rotary cutting apparatus. This system is used for processing

stem biomass into highly consistent lengths, as illustrated in Gerspacher *et al*[75]. The result is wheat straw stem segments of 12 mm average length as illustrated in 6.1. The average bulk density of the segments was measured to be 47 kg/m^3, while the average particle mass was 0.003 g. These particles were used directly in the continuous torrefaction process, and for the batch torrefaction process were milled further using a #1 Wiley Mill to a maximum 0.88 mm particle size.

6.3.2 Apparatus: batch torrefaction unit

The batch torrefaction experiments were conducted in a 21 mm ID stainless steel tube reactor (Figure 6.2). Nitrogen gas provided from a compressed gas cylinder flows from a digital mass flow controller (FIC002) at a rate of 200 sccm into the reactor. The gas flows first through tubing wrapped in 200 W heating tape that is maintained at 200°C external temperature, then through the sample chamber which is within a 1140 W tube furnace. A porous plate distributor mounted within the tube supports the biomass sample, while the nitrogen passes through the sample and carries volatile matter and produced gases out of the reactor. A thermocouple probe is mounted so that its measurement point lies near the centre of the biomass sample.

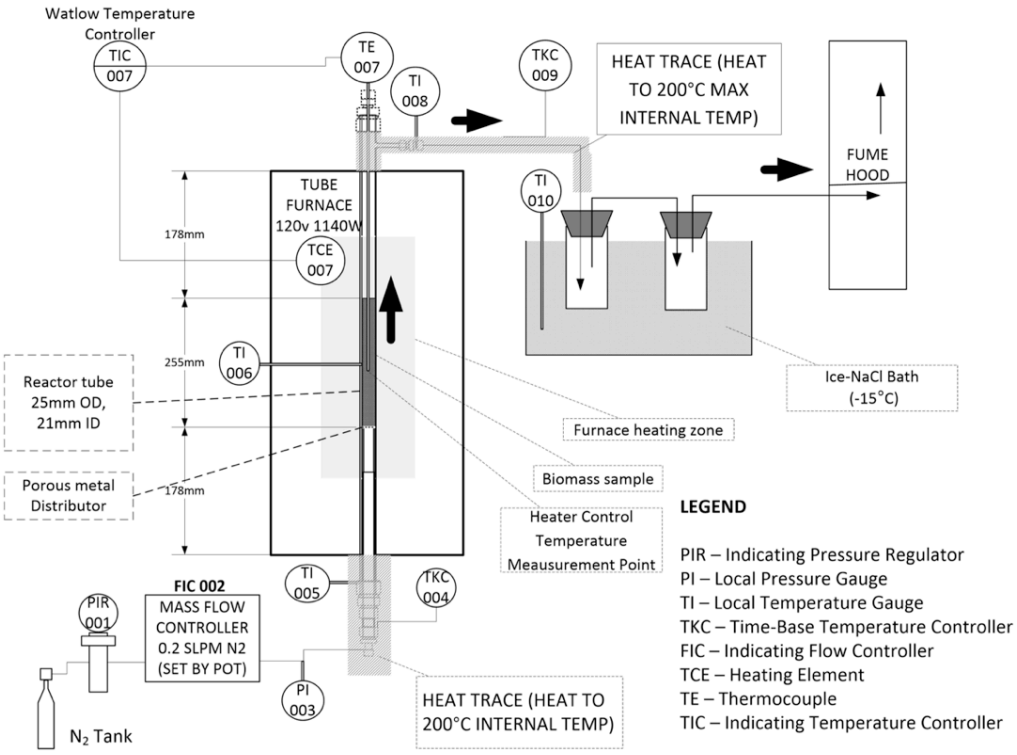

Figure 6.2: Batch torrefaction apparatus

The temperature measured at this point (TE007) is the process value for a digital process controller (TIC007), which activates the tube furnace in order to maintain the setpoint temperature that is entered by the operator.

Tubing immediately outside the sample chamber is wrapped in a 200 W heating tape, where the tubing temperature is maintained at 150 °C to prevent condensation in this line. Condensable volatiles are deposited in the ice bath pots, which are maintained at a maximum temperature of -15°C. Nitrogen and permanent gases flow out of the chiller pots to the fume hood.

The experimental procedure began with apparatus set-up followed by pre-heating of the system. An ice-bath was prepared by blending granular NaCl in the bath vessel along with ice, and a small volume of distilled water. This mixture was stirred until its consistency was homogeneous, and the liquid level was near the rim of the vessel. Clean condensate pots were then attached to the apparatus and lowered into the ice bath. The nitrogen tank valve was opened, followed by activation of the mass flow controller until the nitrogen flowrate hit the desired setpoint. Heating tape controllers were then set to the required tube exterior temperatures, which were 200 °C for the inlet tube and 150 °C for the outlet tube. The setpoint for the digital temperature controller (TIC007) was next set to 100 °C below the experimental temperature parameter (T_{tor}). Once this setpoint was reached within the sample chamber, the top of the reactor was removed and 20 g of wheat straw powder was inserted in the chamber using a funnel.

After closing the reactor, the temperature setpoint was increased gradually in increments of 20°C, waiting for the temperature to stabilize after each increase. Once the torrefaction temperature (T_{tor}) was reached, this value was held for 20 minutes. Cooling was then immediately initiated, in order to stop the torrefaction process. All active heating was halted aside from the discharge line heat tape, and the tube furnace was opened in order to direct the flow of air from a fan towards the sample chamber tube. Once the sample chamber was cooled below 80°C, the top of the sample chamber was removed and the wheat straw char was extracted.

6.3.3 Experimental setup: continuous system

Chapter 3 provides a description of the pilot plant used for the continuous torrefaction experiments, including detail on the rationale, design and operation methods. For more detail on how this apparatus

was applied to torrefaction of wheat straw, Campbell *et al.* 2016[98] illustrates three of the continuous experiments referred to in this work.

6.3.4 Experimental design and description

The torrefied wheat straw samples that were analysed were prepared from wheat straw from two separate harvest years, 2013 and 2015. Table 6.1 illustrates the sample groupings, apparatus, and conditions for each experiment.

The initial batch mode experiments included five different torrefaction temperature values (T_{tor}), from 180 to 300 °C in 30 °C increments. This temperature range overlaps the typical range of torrefaction temperatures both below and above, thus offering a picture of the char both before and after it reaches an ideal torrefied state. After subsequent evaluation of the results in this range, five additional experiments were carried out from 240 to 290°C to increase the number of datapoints in the temperature range where the changes in chemical composition and diffuse reflectance were most responsive.

Five experiments were carried out using the continuous torrefaction plant with wheat straw, ranging from peak temperature values of 220 to 280°C with a total torrefaction residence time of 8.6 min. These experiments were initially carried out to simply test the apparatus with that feedstock, and had already been subject to elemental and proximate analysis. Assessment of these chars using reflectance spectroscopy was carried out to further increase the number of datapoints that could be used to develop a linear correlation between carbon and reflectance.

In total, fifteen torrefaction experiments were conducted, including ten batch torrefaction experiments and five continuously fed torrefaction experiments conducted at various torrefaction temperature values, which are elaborated upon in Table 6.1.

Table 6.1: Torrefaction Experiment Details

Experiment Date	Harvest Year	Type	Temperature	Exp. Time
			°C	
21 Nov 2013	2013	Batch	180	20
4 Dec 2013	2013	Batch	210	20
4 Dec 2013	2013	Batch	240	20
4 Dec 2013	2013	Batch	270	20
4 Dec 2013	2013	Batch	300	20
3 Aug. 2016	2015 (a)	Continuous[98]	220	8.6
3 Aug. 2016	2015 (a)	Continuous[98]	250	8.6
4 Aug. 2016	2015 (a)	Continuous[98]	280	8.6
16 Aug 2017	2015 (a)	Batch	250	20
16 Aug 2017	2015 (a)	Batch	260	20
18 Aug 2017	2015 (a)	Batch	270	20
18 Aug 2017	2015 (a)	Batch	280	20
18 Aug 2017	2015 (a)	Batch	290	20
24 Aug 2017	2015 (b)	Continuous	235	8.6
29 Aug 2017	2015 (b)	Continuous	265	8.6

6.3.5 Chemical analysis

The intent of this work was to correlate reflectance to specific measures of torrefaction severity that could be accurately measured. The nature of the batch torrefaction experiments meant that the mass yield would be difficult to measure at better than ±5% precision. Therefore, the composition or rather, the change in composition relative to the change in reflectance. The composition of the char in the proximate and elemental domains were therefore those that were of focus.

The techniques for elemental and proximate analysis are described in detail in section 4.3.4.

6.3.6 Diffuse reflectance analysis

Each of the raw biomass and char samples was placed in a 40 mm diameter powder analysis cell (Figure 6.3) and subject to NIR-VIS reflectance spectroscopy using an Agilent Technologies Cary 5000 UV-VIS-NIR Spectrophotometer (Santa Clara, CA - USA) with external diffuse reflectance accessory.

Diffuse reflectance data were collected with 4 nm spectral bandwidth resolution in the 800 - 2500 nm range, and 1 nm resolution in the 400-800 nm range. The instrument baseline was set against a calibrated 75% reflectance Spectralon target (Labsphere, North Sutton, NH.), producing a total of 18 reflectance waveforms.

.

Figure 6.3: Agilent (USA) 40 mm quartz window sample powder cell loaded with mild char sample.

The second step in assessing the reflectance spectral data is in converting this spectrum to an absorbance spectrum, which is a standard practice in NIR analysis[99]. The absorbance is calculated from the reflectance according to Equation 6.1, which is simply the log of the inverse of reflectance.

$$ABS = \log\left(\frac{1}{R}\right) \qquad (6.1)$$

6.4 Results and discussion

The reflectance spectra for the 15 char samples and the 3 samples of original raw material are illustrated in Figure 6.4. Indicated are the visible band from 400 to 740 nm, near infrared (NIR) band from 740 to 1400 nm, and the short-wave infrared (SWIR) band from 1400 to 2500 nm. The reflectance in the NIR band from 740 to 1400 nm appears to have the highest sensitivity to torrefaction: a shift from 50-70% reflectance to 10-30% reflectance for the wheat straw char with greatest severity of torrefaction. There are significant changes in the reflectance at even small incremental changes in torrefaction severity. From 1400 to 1500 nm on the other hand, there is only an observable reduction in reflectance that occurs for the samples with the highest torrefaction temperatures / greatest severity. This is presumably the result of a significant reduction in the O-H bonds in cellulose that dominate this band[93]; significant thermal degradation of cellulose structures also reportedly only occurs at the hottest or most extreme torrefaction conditions[41], which lie beyond optimal operating conditions.

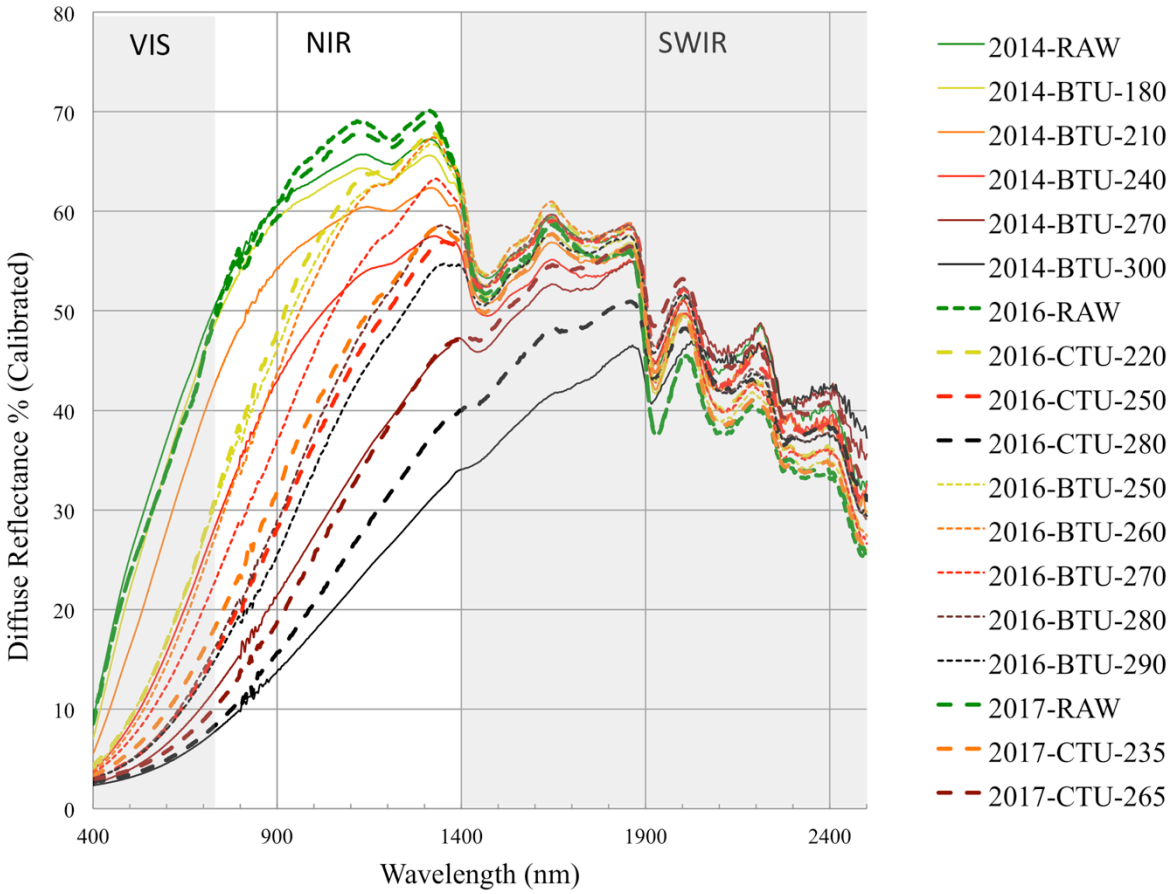

Figure 6.4: Diffuse Reflectance Spectra for wheat straw and char samples from 400 to 2500 nm. Samples are indicated in legend by harvest/batch year, continuous (CTU) or batch (BTU) process, and peak temperature (3-digit code). Signal color is assigned according to the torrefaction temperature used for that experiment group (green – raw), Yellow- mild, orange – medium-mild, red – medium, brown – medium-severe, black – severe. Shaded areas delineate the visible (VIS), near infrared (NIR), and short wave infrared (SWIR) spectra.

The char samples can be divided into 3 groups based on the batch and age of sample, this includes samples prepared/analyzed in 2014, 2016, and 2017. Table 6.2 illustrates the 18 samples, along with the dry, ash-free elemental composition of each.

Of note is the batch torrefaction experiments that were conducted in 2016; despite using similar conditions to some of the experiments conducted in 2014, the severity of torrefaction for the 2016 runs is significantly lower than would be expected. The disparity in results illustrates how different biomass harvests and different storage times can result in variation of torrefaction severity, even when using the same process conditions. This highlights the importance of having a form of real-time measurement of torrefaction severity.

Table 6.2: Elemental Analysis of Wheat Straw and Chars (daf basis)

GROUP	Sample	C	H	N	O
A	2014-RAW	50.5 %	6.2 %	0.8 %	42.2 %
A	2014-BTU 180	49.8 %	6.2 %	0.6 %	43.3 %
A	2014-BTU 210	50.5 %	6.2 %	0.7 %	42.5 %
A	2014-BTU 240	51.1 %	6.2 %	0.7 %	42.0 %
A	2014-BTU 270	57.4 %	5.9 %	0.8 %	35.8 %
A	2014-BTU 300	63.8 %	5.5 %	1.0 %	29.6 %
B	2016-RAW	50.0 %	6.5 %	0.6 %	42.8 %
B	2016-CTU 220	52.1 %	6.7 %	0.6 %	40.6 %
B	2016-CTU 250	54.5 %	6.7 %	0.6 %	38.1 %
B	2016-CTU 280	61.6 %	6.5 %	0.8 %	31.1 %
B	2016-BTU 250	52.9 %	6.1 %	0.7 %	40.3 %
B	2016-BTU 260	52.7 %	6.0 %	0.6%	40.6 %
B	2016-BTU 270	53.7 %	5.9 %	0.6 %	39.6 %
B	2016-BTU 280	54.9 %	5.7 %	0.6 %	38.8 %
B	2016-BTU 290	56.7 %	5.7 %	0.7 %	36.9 %
C	2017-RAW	48.4 %	5.9 %	0.6 %	45.1 %
C	2017-CTU 235	51.9 %	5.6 %	0.7 %	41.5 %
C	2017-CTU 265	55.9 %	5.7 %	0.6 %	37.7 %

The element for which the most measurable and observable shift occurs is carbon. Although the oxygen content is inferred to change by nearly the same amount as carbon, the calculation of oxygen content is not as straightforward. To calculate oxygen content, the difference between the total dry mass and the values found in CHNS analysis plus ash content is found. The carbon content, however, is calculated directly and is observed to generally shift upwards as the conditions of torrefaction become more extreme. The work of Lestander *et al.*[72] also illustrates a direct relationship between the change in carbon content and torrefaction mass yield, which is the main measure for expressing torrefaction severity. The limitation of this measure however, is that the total mass loss can be difficult to measure and calculate in some cases, which was the case with the batch torrefaction process used in this work. In particular, for small-scale batch experiments it can be difficult to transfer 100% of the remaining char from the experiment chamber to the balance to complete the mass yield measurement.

Expressing the reflectance spectra (R) as absorbance (ABS), illustrates how the absorbance in the NIR spectra increases incrementally as a results of increasing torrefaction severity (Figure 6.5). This now aligns with how the carbon content increases with torrefaction severity.

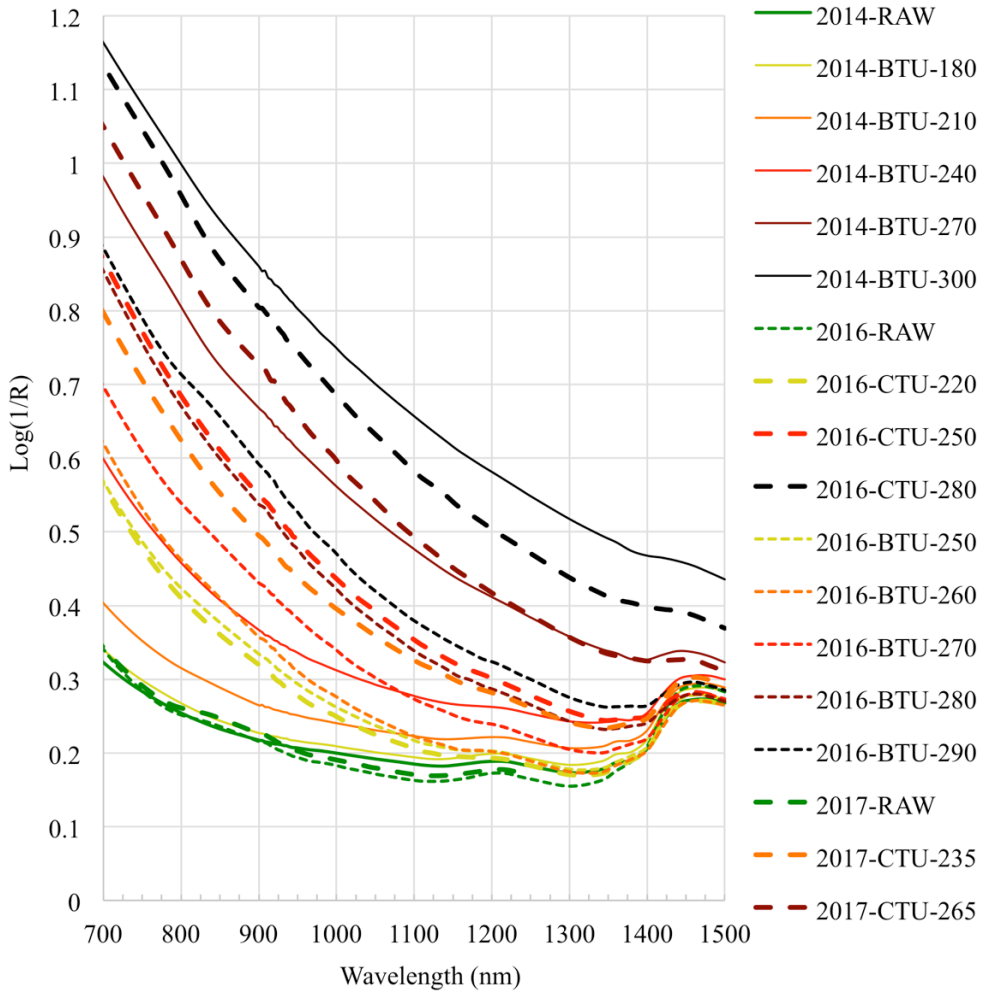

Figure 6.5: Absorbance spectra for wheat straw chars from 700 to 1500nm
Legend indicates sample harvest/batch year, continuous (CTU) or batch (BTU) process, and peak temperature (3 digit code). The color for each sample reflectance spectrum is assigned according to the relative severity of the temperature used for that experiment group (green – raw). Yellow- mild, orange – medium-mild, red – medium, brown – medium-severe, black – severe.

The next step in this process was to identify which wavelengths would best correlate the change in absorbance to the change in carbon content. For each of the three sample groups (A-C), the absorbance for the raw material is subtracted from the absorbance value for each char sample, creating a spectra for the change in absorbance. At the same time, an array of ΔC values were calculated for each of the three sample groups. For each wavelength from 700 to 1500 nm with a step size of 20 nm, a linear regression analysis was completed between the array of ΔC values and ΔABS values. The result is a set of linear regression parameters and coefficients of determination at each wavelength, based on the linear relationship of Equation 6.2.

$$\Delta C(\text{daf}) = A + B * \Delta ABS \qquad (6.2)$$

The coefficients of determination and parameters A and B for the linear regressions are illustrated in Figure 6.6. The regression fit is acceptable from 700 to 1400 nm, remaining above 0.9 for most of this range, however at 1400 nm it drops significantly, at the same point where the reflectance spectra for all the raw and mildly torrefied samples converge significantly.

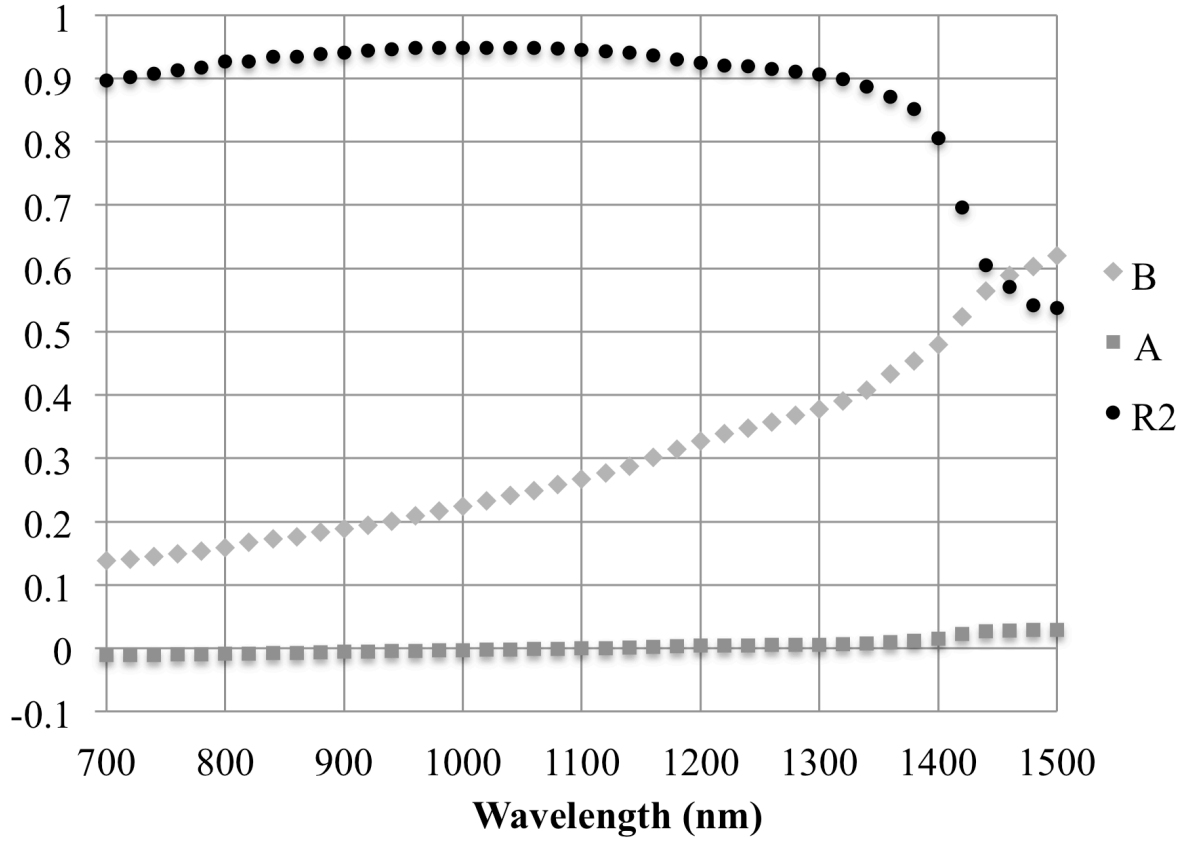

Figure 6.6: Coefficient of determination and coefficients for regression analysis.
Relation of ΔC to ΔABS, for wavelength interval of 20 nm.

For wavelengths 960 to 1060 nm, the coefficient of determination was between 0.947 and 0.949. By taking the average of ΔABS values in this range for each wavelength, a further linear regression was calculated, also having an R^2 of the maximum value, or 0.949. This may represent a more practical way to implement this technique in a practical or economical instrument where the reflectance is measured in a band rather than at a single wavelength. The results of that linear regression as compared to the data values for each sample are illustrated in Figure 6.7.

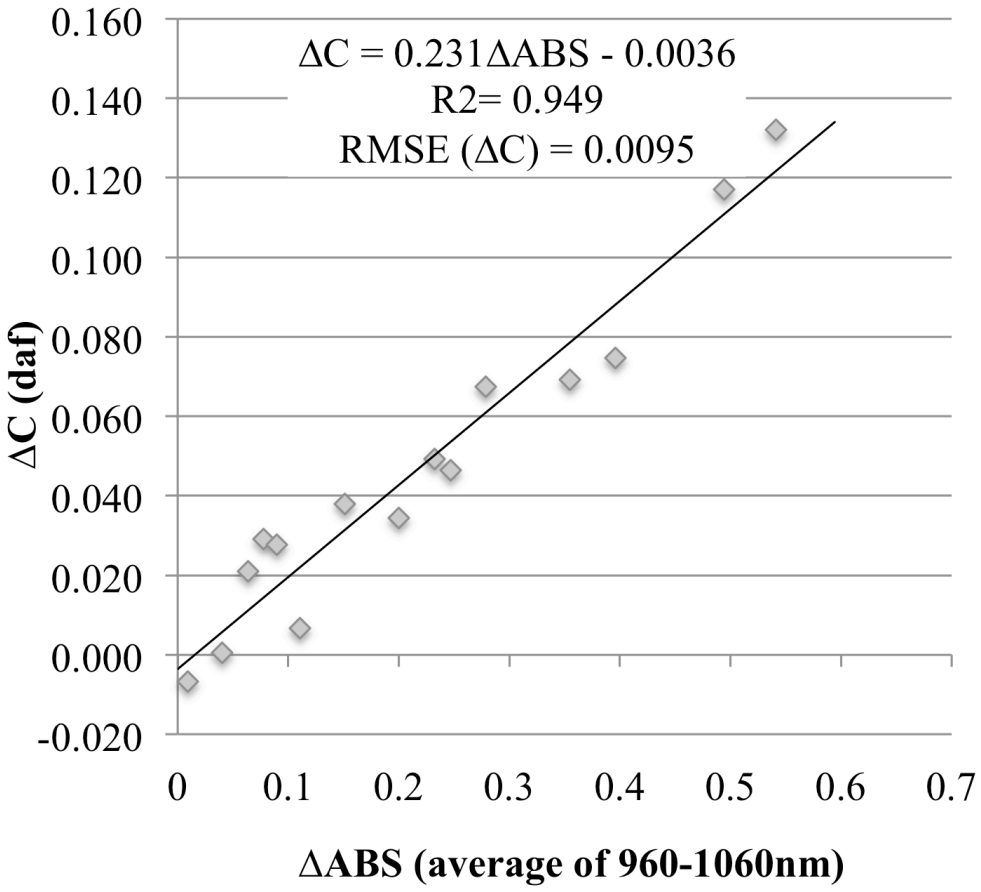

Figure 6.7: Linear regression analysis for ΔC and average of ΔABS in the band 960-1060 nm.

This correlation can also be expressed directly in terms of the reflectance, as in Equation 6.3:

$$\Delta C = 0.231\left(\log\frac{1}{R_{char}} - \log\frac{1}{R_{raw}}\right) - 0.0036 \quad (6.3)$$

6.5 Conclusions

An investigation was carried out where wheat straw was torrefied in 15 batch and continuous experiments using a wide range of conditions, then subject to diffuse reflectance analysis. The reflectance spectra for the raw samples and 15 char samples were then compared to each other and to the measured changes in the samples' elemental composition. Conclusions from this work include:

1. Wheat straw char absorbance in the 740 to 1400 nm band increases consistently and incrementally in response to increase in torrefaction severity as indicated by change in carbon content.
2. The absorbance in the 1400 to 1600 nm band responds strongly when the increase in carbon content exceeds 7%.

3. The band from 960 to 1060 nm has the closest correlation between increase in absorbance and increase in char carbon content, where the average increase in absorbance across this range correlates to the increase in carbon by equation $\Delta C = 0.231\Delta ABS - 0.0036$ for all samples with a coefficient of determination of 0.949.

7.0 Summary of research project

7.1 Primary findings

This research project was initiated to improve, develop, and evaluate process measurement and control methods that specifically support continuous biomass torrefaction. It was hypothesized that by making such improvements continuous torrefaction could be used as a more flexible and better-controlled chemical process that could economically produce char and high value products and chemicals.

This project started with the conceptualization of an untried gas-solid contacting method that was conceived based on the reported constraints of the torrefaction process (Chapter 3.1-3.2). The method was the hybrid of a screw conveyor and a fluidized bed, and was subsequently referred to as a 'horizontal moving bed'. This method led to the need for a process to reduce stem biomass to flowable granules, so that sufficient biomass in the correct form would be available to operate a pilot plant. The prototype developed for stem biomass processing was then built, called the 'Rotoshear' (Chapter 3.3). The detailed design of the 'CTU' pilot plant itself followed, as well as construction, integration, and commissioning (Chapter 3.4-3.6). A rigorous experimental design was then developed and carried out to evaluate and characterize the pilot plant using willow biomass (Chapter 4). Combining the results and analysis of continuous torrefaction of willow with subsequent results from wheat straw, cattails and previous batch torrefaction work with wheat straw led to an investigation into alternative methods for expressing torrefaction severity using change in elemental composition (Chapter 5). At the same time, direct measurement of torrefaction severity through diffuse reflectance analysis was also investigated, which led to the development of a correlation relating change in carbon composition to diffuse reflectance in the short-wave infrared band (Chapter 6).

As a result of this research project, the following contributions to the field of biomass torrefaction have been made.

7.1.1 Processing stem biomass into a granular form

A prototype system called the "Rotoshear' was developed for reducing stem biomass to a flowable format (Chapter 3.3). Granular feedstocks were then prepared from several biomass types using the Rotoshear prototype, for use in the continuous torrefaction pilot plant. More than 100 kg of willow granules were prepared and used in subsequent continuous torrefaction experiments (Chapter 4). Willow granules prepared with the Rotoshear were assessed in terms of particle size distribution and compared to willow processed in a drum chipper.

Wheat straw granules were also prepared for continuous experiments, more than 5 kg in total. Wheat straw prepared in this fashion could pass down through the pilot plant hopper and was able to be conveyed through the 37 mm and 64 mm screw conveyors.

This biomass processing method was not only relatively low cost (< $2000 CAD) but was able to produce highly consistent granules that were the ideal size for use in the CTU pilot plant. Development of this system was thus a key step before most of the subsequent experimental work could be completed (Chapters 4-6). This prototype was a highly valuable tool for working with this type of biomass, and for conducting continuous biomass torrefaction experiments.

7.1.2 Reducing continuous torrefaction residence time

One of the main observations from repeated operation of the CTU pilot plant was how even relatively short residence times in the torrefaction section would result in mass yields near or less than 80 % (w/w). As an example, torrefaction of willow was carried out at 255 °C and 10 min residence time, which resulted in a 82.6 % (w/w) mass yield and 90.6 % (e/e) energy yield. Since the energy yield value of 90 % is often quoted as a typical operating point for torrefaction, these results would seem to fit within a normal torrefaction plant operating zone. By comparison, screw conveyor and rotating drum pilot plants operated by Ohliger *et al.*[81] and Strandberg *et al.*[79] required residence times of 20-40 min and 16 min, respectively, to achieve similar mass yields. In both cases, the peak torrefaction temperature was higher as well. When low-density feedstocks such as wheat straw, cattail, and moringa leaf matter were tested in the CTU, residence times all below 10 min were associated with a high degree of torrefaction in most cases. For example, using wheat straw granule feedstock, a 54.2 % (w/w) mass yield was achieved with 8.6 min residence time at 290 °C and with cattail granule feedstock, a 75.3 % (w/w) mass yield was achieved with 6.8 min residence time at 250 °C. The conclusion from these experiments was that the CTU should be able to produce torrefied biomass with a residence time as low as 5 min. while still achieving an 80 % mass yield target for coppice willow or lower density feedstocks. This would place the horizontal moving bed process among the lowest residence torrefaction systems, which generally are constrained to small particle sizes or other issues of flexibility/operation. Since the torrefaction section of the CTU has a lower limit of 2 min residence time (Table B.3.1, Appendix B), this capability should be examined in the future.

7.1.3 Predictable control of process variables for continuous torrefaction

The CTU was used to carry out characterization experiments with coppiced willow feedstock which followed a response surface methodology that dictated very specific residence time and peak temperature parameters. The results of analyzing the char products from these experiments were used to generate contour plots of mass and energy yield, carbon content, and milling energy (Section 4.4), where the residence time (T_t) and peak temperature (T_T) defined the respective Cartesian axes. Review of these contour plots illustrated both how broadly yet precisely the process could be controlled; each step change in time or temperature resulted in a distinct change in each of the measures, resulting in contour plots without inconsistencies or inflections. A wide range of torrefaction severity was observed from these experiments, covering mass yields from 64.7 % to 91.6 % (w/w) despite only covering part of the pilot plant's potential parameter range. The parameter set in the middle of the design was used to conduct the same experiment six times, which resulted in mass yield values that had a 95 % confidence interval of only 0.7 % (w/w).

The mass yield contour map was subsequently tested and validated; three additional parameter sets were selected from within the response surface contour plots, such that the expected mass yield in particular could be estimated. Based on these three parameter sets, one set was used to conduct the same experiment five times, and the other two sets were each conducted once. For each of these three parameter sets, the resultant mass yield was within 0.6 % (w/w) of the expected result, within the 95 % confidence interval from the original analysis. For the new replicate experiments the 95 % confidence interval was less than the original set at 0.54 % (w/w), despite having one fewer replication than the original design.

These validation experiments illustrated that the control and measurement systems of the horizontal moving bed were sufficient to allow highly repeatable and precise torrefaction processing with predictable char quality and severity.

7.1.4 Feedstock flexible continuous torrefaction

The experiments carried out with the CTU began with only the coppice willow granules as feedstock, but later expanded to wheat straw, cattail, leaf matter, and commercial pellets. While the severity of torrefaction that was observed for these different materials varied significantly, the operation of the plant was nonetheless reliable in each case, once the specific requirements of each feedstock were well understood. For the feedstocks with very low density, the flowrate of convective gas medium was reduced by 80 % in order to reduce the possibility of entraining particles in the exit gas stream. After

operating the CTU with these widely varying materials, it was reasonably concluded that the goal of having a feedstock flexible reactor design was achieved.

7.1.5 Interpreting torrefaction severity through change in chemical composition

The change in carbon composition that results from solid biomass torrefaction was noted from the first experiments where char was analyzed and compared to raw biomass. Carbon content can also be measured using several techniques and the concentration of carbon increases reliably by 4-5 % for average torrefaction severity (80 % mass yield). After examining the results of more than 100 torrefaction experiments where the mass yield, carbon, and ash content were known, a direct comparison of all of these experiments was carried out (Chapter 5). This process began with normalizing the composition of many different biomass types (hardwoods, softwoods, grasses, agricultural residues) by calculating the change in carbon concentration (ΔC), and then further normalizing biomass with different ash content by converting the mass yield and ΔC to dry, ash free basis. The mass yield and ΔC values could then be compared on an equal basis for all types of biomass, and experiments with a wide range of torrefaction severity. This data was then expressed in two ways, with two different intended purposes. By examining the relative mass change of carbon with respect to the total, a linear correlation was developed that had a coefficient of determination of 0.93. That correlation equation ($\Delta M_c = 0.37\Delta M_t + 1.26$) illustrates the relative rate of carbon loss in torrefaction (37 % of total) and also illustrates that the first 3.4 % of mass loss occurs without significant loss of carbon. The other way this data was applied was in the development of a correlation relating the mass yield to change in carbon concentration. This polynomial correlation ($Y_m = 4.29*\Delta C^2 - 3.66\Delta C + 0.98$) fit well for larger scale and continuous experiments where the sample mass was at least 500 g, where it had a coefficient of determination of 0.935. This correlation was also very consistent with similar results published by Lestander *et al.*[72] that included non-normalized carbon content for larger scale torrefaction experiments with two biomass types, with experimental mass yield values as low as 20 %. The purpose of this correlation is that it could be applied to continuous monitoring of char carbon content as it is output from a torrefaction plant; by also monitoring incoming biomass carbon and ash content, the correlation could be used to estimate the mass yield of a torrefaction process in real time, and use that estimate to adjust process conditions to achieve a process setpoint.

7.1.6 Direct measurement of torrefaction severity using NIRS

Diffuse reflectance spectroscopy can be used to directly measure changes in torrefaction severity. The carbonization that occurs as a result of torrefaction will cause the color of chars to become gradually

darker with increasing severity. This is the manifestation of a change in the molecular structure that alters how that structure interacts with incident electromagnetic energy in the visible and short wave infrared bands from 400 to 1400 nm wavelength. This principle was investigated to determine if the change in reflectance in the short wave band could be correlated to any measurable change in char composition. After analyzing wheat straw chars from five continuous and 10 batch experiments for elemental composition and compiling the values for diffuse reflectance (R) through this spectrum, a linear correlation was developed to this end (Chapter 6). This correlation relates the change in carbon composition (daf basis) to the average change in absorbance (ABS = log(1/R)) in the band from 960 to 1060 nm. The equation $\Delta C = 0.231\Delta ABS - 0.0036$ expresses this relation, illustrating how measuring the diffuse reflectance in real time could be used to infer the difference in carbon content between the raw biomass and char.

7.2 Evaluating research objectives

The objectives of this research included the following: 1. Evaluate and characterize a torrefaction process based on horizontal moving beds, 2. Examine and develop a correlation relating change in carbon content to torrefaction severity, and 3. Investigate how diffuse reflectance spectroscopy could be used to directly measure severity of torrefaction.

7.2.1 Horizontal moving bed pilot plant: design, build, evaluate and characterize

The horizontal moving bed has been shown to be a suitable reactor design for continuous torrefaction. This operation was aided significantly by processing stem biomass into a consistent flowable form, which facilitated operating the pilot plant with willow, wheat straw, and cattail feedstocks. Characterization of the pilot plant with willow feedstocks illustrated the wide range of severity that is possible with this design; mass yield range was 64.7 % to 91.4 % for only a fraction of the potential operating range. Repeated operations using the same time and temperature parameters also illustrated that this reactor would produce a very reliable, repeatable result as the 95 % confidence interval for the mass yield at the repeated conditions was 0.7 %. The contour plots generated from the characterization experiments also illustrate how specific char qualities could be achieved using a wide range of possible residence time and temperature parameter sets. The contour map for mass yield was validated by selecting three additional parameter pairs and carrying out additional experiments; the mass yields for those experiments were all within 0.6 % of the expected value. This reactor design was also demonstrated to be very flexible, five different feedstocks with a wide range of particle size and density were examined and were each continuously torrefied successfully, resulting in a wide range of char severity that was dependent upon individual particle mass.

7.2.2 An alternative expression for torrefaction severity

Torrefaction of biomass results in a consistent increase in carbon concentration, which is related to mass yield by a second order equation. Analysis of experimental results and literature data confirmed this relationship, defined by the correlation equation $Y_m = 4.29\Delta C^2 - 3.66\Delta C + 0.98$. This equation which had a coefficient of determination of 0.935 was developed to fit the results from larger scale experiments specifically with 500 g experimental mass or greater. Smaller scale experiments appeared to have significant negative bias and/or uncertainty in terms of both mass yield and normalized change in carbon content, resulting in a 'cloud' of data which were distinct from the larger scale experiments. By implementing total carbon measurement on the input and output streams of a continuous torrefaction process, this correlation could be used to estimate torrefaction severity in real time. That value could then be used as a process feedback for a process control system, which could then adjust the torrefaction control parameter to achieve a specific severity/carbon setpoint.

7.2.3 Develop a correlation between NIR reflectance and chemical quanta for torrefaction chars

Diffuse reflectance spectroscopy can be used to infer torrefaction severity. This was demonstrated in greatest detail for wheat straw torrefaction chars but is applicable to any torrefied biomass. Specifically, by measuring the change in average absorbance of both raw and torrefied biomass in the short wave infrared band from 960 to 1060 nm, that value can be used to estimate the change in carbon concentration between the raw biomass and the char. For wheat straw chars, the linear correlation relating these measures is $\Delta C = 0.231\Delta ABS - 0.0036$, which fits the experimental data with a coefficient of determination of 0.95. Since the structure and composition that influence diffuse reflectance for each type of biomass are unique, the mathematical relation between absorbance and carbon concentration would be unique as well and require similar analysis and correlation development. Continuous measurement of torrefaction severity could be implemented by developing an instrument capable of continuously measuring the diffuse reflectance in the 960-1060 nm range, and using that instrument to monitor both the raw feedstock (input) and char product (output) of a torrefaction plant and comparing those values.

7.3 Future work

While a significant number of experiments were conducted with the CTU in order to characterize its operation and illustrate its function, there remain several aspects of the design that should be investigated. The lower limit of torrefaction residence time is as of yet untested. While a torrefaction residence time of 6.8 minutes was highly effective for torrefaction of cattail, this range should be examined for coppice willow as well, and reduced further. The minimum effective residence time is among the most important aspects of process throughput and thus determining how low this value could be would illustrate information such as scalability, and how the plant capital cost relates to output capacity.

The other aspect of the plant design to still be investigated is its potential for separating and concentrating the gaseous/vapour products. Stage 2 of the CTU pilot plant was designed with product separation in mind. Stage 2 of the CTU pilot plant has three temperature zones where the heating medium can be very precisely controlled in terms of flowrate and temperature, such that the temperature profile of the torrefaction zone can be varied per experiment or within the same experiment. This system is thus well suited to immediate implementation of in-line gas analysis at six different points along the length of the torrefaction reactor. A process mass spectrometer would be well suited to this purpose, and an instrument of this nature is available for such a project. This will require installation of heated sampling lines that tie into each of the six discharge ports of the torrefaction reactor, as well as switching manifold to change which line is active. The process-MS would then need to be calibrated to detect the expected products of torrefaction, which would include H_2O, CO, CO_2, CH_3OH, CH_3COOH, and the carrier gas N_2. Torrefaction experiments could then be carried out with various biomass and temperature profiles, where each of the six gas streams could be sampled during a 'steady state' timeframe of the experiment. The spectra recorded from each of the six discharge streams would then require analysis to determine what specific compounds can be confirmed from the spectrum. If the process-MS spectra from these gas streams can be interpreted properly, this data could be used to refine the conditions and temperature profile in the horizontal moving bed and potentially concentrate specific known products of torrefaction such as methanol or acetic acid.

The next step for the correlation relating carbon to torrefaction severity is to demonstrate its application for a continuous process. This would begin with the installation of an on-line total carbon sampling instrument on the input and output streams of a continuous torrefaction plant. This instrument could then transmit these values to the plant control system, which could compute ΔC and from that value estimate the mass yield and severity of the product. By introducing measurement and control capacity for a

torrefaction process such that it can produce char with precise chemical composition, the opportunity may be created for such a system to be part of more complex biorefining process.

To apply the correlation relating diffuse reflectance of torrefaction chars to change in carbon content, a dedicated instrument and sampling assembly would need to be developed for this purpose. Since the diffuse reflectance in the NIR band from 960 to 1060 nm is equally responsive to the change in carbon content, an NIR detecting instrument that was sensitive anywhere in this range or covering it completely, would be suitable. However, since infrared measurement technology is relatively low in cost, an instrument of this nature could be more economical than measuring carbon content directly for this purpose. The challenge would be in maintaining a continuous stream of powdered char with optical access for the NIR sensor and light source. For large-scale torrefaction processes however, the cost associated with such an instrument would be justified by the increase in control and product quality that may be possible.

References

(1) Tumuluru, J. S.; Sokhansanj, S.; Hess, J. R.; Wright, C. T.; Boardman, R. D. *Ind. Biotechnol.* **2011**, *7* (5), 384–401.

(2) BP. BP Statistical Review of World Energy 2017 https://www.bp.com/content/dam/bp/en/corporate/pdf/energy-economics/statistical-review-2017/bp-statistical-review-of-world-energy-2017-full-report.pdf (accessed Jun 27, 2018).

(3) *SaskPower Corporation 2016-2017 Annual Report*; Regina, SK Canada, 2017.

(4) NEB - Provincial and Territorial Energy Profiles - Alberta https://www.neb-one.gc.ca/nrg/ntgrtd/mrkt/nrgsstmprfls/ab-eng.html (accessed Jun 27, 2018).

(5) Amichev, B. Y.; Kurz, W. A.; Smyth, C.; Van Rees, K. C. J. *GCB Bioenergy* **2012**, *4* (1), 70–87.

(6) Amichev, B. Y.; Hangs, R. D.; Konecsni, S. M.; Stadnyk, C. N.; Volk, T. A.; Bélanger, N.; Vujanovic, V.; Schoenau, J. J.; Moukoumi, J.; Van Rees, K. C. J. *Soil Sci. Soc. Am. J.* **2014**, *78* (S1), S168.

(7) Hangs, R. D.; Schoenau, J. J.; Van Rees, K. C. J.; Bélanger, N.; Volk, T. *BioEnergy Res.* **2014**, *7* (4), 1074–1090.

(8) Hangs, R. D.; Schoenau, J. J.; J Van Rees, K. C.; Bélanger, N.; Volk, T.; Jensen, T. *Bioenergy Res.* **2014**, *7*, 1091–1111.

(9) Biomass | Definition of Biomass by Merriam-Webster https://www.merriam-webster.com/dictionary/biomass (accessed Jun 7, 2018).

(10) Nhuchhen, D.; Basu, P.; Acharya, B. *Int. J. Renew. Energy Biofuels* **2014**, *2014*, 1–56.

(11) Nakano, Y.; Yamaguchi, M.; Endo, H.; Rejab, N. A.; Ohtani, M. *Front. Plant Sci.* **2015**, *6*, 288.

(12) Chen, H. *Biotechnology of lignocellulose: Theory and practice*; Chemical Industry Press, and Springer Science and Business Media: Beijing (China), Dordrecht (Neth), 2014.

(13) Antongiovanni, M.; Sargentini, C. *Option Méditérranéennes* **1991**, *16*, 49–53.

(14) Stems & Vascular Tissue http://www.sciencepartners.info/module-7-plants-pollinators/an-introduction-to-plants-pollinators/stems-vascular-tissue/ (accessed May 19, 2018).

(15) Phanphanich, M.; Mani, S. *Bioresour. Technol.* **2011**, *102* (2), 1246–1253.

(16) Schell, D. J.; Harwood, C. *Appl. Biochem. Biotechnol.* **1994**, *45–46* (1), 159–168.

(17) Mani, S.; Tabil, L. G.; Sokhansanj, S. *Biomass and Bioenergy* **2004**, *27* (4), 339–352.

(18) Hydrogen Bonding (Purdue University) https://www.chem.purdue.edu/gchelp/liquids/hbond.html (accessed Jun 7, 2018).

(19) Wiley, G. R.; Miller, S. I. *J. Am. Chem. Soc.* **1972**, *94* (10), 3287–3293.

(20) Graham, S. Degradation of Biomass Fuels During Long Term Storage in Indoor and Outdoor

Environments. Masters of Science Dissertation., University of Nottingham, 2015.

(21) Abdel-Hamid, A. M.; Solbiati, J. O.; Cann, I. K. O. *Adv. Appl. Microbiol.* **2013**, *82*, 1–28.

(22) Channiwala, S. A.; Parikh, P. P. *Fuel* **2002**, *81* (8), 1051–1063.

(23) Nhuchhen, D.; Afzal, M. *Bioengineering* **2017**, *4* (7), 1–15.

(24) Clarke, S.; Preto, F. Biomass Burn Characteristics. Order# 11-033 Agdex 737/120. OMFRA/Canmet Energy Report. http://www.omafra.gov.on.ca/english/engineer/facts/11-033.htm (accessed May 5, 2018).

(25) Clarke, S.; Preto, F. Biomass Burn Characteristics. Order# 11-033 Agdex 737/120 http://www.omafra.gov.on.ca/english/engineer/facts/11-033.htm (accessed May 25, 2018).

(26) Campbell, W. A.; Woytiuk, K.; Gerspacher, R.; Coller, A.; Evitts, R. W. *Can. J. Chem. Eng.* **2018**, (10.1002/cjce.23229. Pub. Online 26 Apr.2018).

(27) Coal Facts | Essentials Facts About Coal And Smokeless Fuel https://www.coals2u.co.uk/basic-coal-questions (accessed Jul 4, 2018).

(28) Potter, O. E.; Keogh, A. J. *Fuel Process. Technol.* **1981**, *4*, 217–227.

(29) Optimizing the Use of Fly Ash in Concrete http://www.cement.org/docs/default-source/fc_concrete_technology/is548-optimizing-the-use-of-fly-ash-concrete.pdf (accessed Jul 4, 2018).

(30) Panagiotis, G. The Bioenergy System Planners Handbook – BISYPLAN http://www.bioenergyprof.eu/handbooks/bisyplan/html-files-en/handbook-intro.html (accessed Aug 10, 2018).

(31) Tosti, L.; van Zomeren, A.; Pels, J. R.; Comans, R. N. J. *Resour. Conserv. Recycl.* **2018**, *134*, 25–33.

(32) Pulp, Paper and Power | Pulp & Paper Canada https://www.pulpandpapercanada.com/news/pulp-paper-and-power-1001905763 (accessed Jun 15, 2018).

(33) Chemical Composition of Natural Gas - Union Gas https://www.uniongas.com/about-us/about-natural-gas/chemical-composition-of-natural-gas (accessed May 30, 2018).

(34) van der Stelt, M. J. C.; Gerhauser, H.; Kiel, J. H. A.; Ptasinski, K. J. *Biomass and Bioenergy* **2011**, *35* (9), 3748–3762.

(35) Radovic, L. R. *Energy Fuels Soc. Anal. Bills Media Reports* **1997**, No. 1, 114–136.

(36) Silamiķele, I.; Nikodemus, O.; Kalniņa, L.; Purmalis, O.; Kļaviņš, M. *Proc. Latv. Acad. Sci. Sect. B Nat. Exact, Appl. Sci.* **2010**, *64* (3–4), 159–166.

(37) Coal Structure and Composition http://butane.chem.uiuc.edu/pshapley/environmental/l4/2.html (accessed May 30, 2018).

(38) Vassilev, S. V; Kitano, K.; Vassileva, C. G. *Fuel* **1996**, *75* (13), 1537–1542.

(39) Heat values of various fuels - World Nuclear Association http://www.world-nuclear.org/information-library/facts-and-figures/heat-values-of-various-fuels.aspx (accessed May 30, 2018).

(40) Basu, P. *Biomass Gasification, Pyrolysis and Torrefaction: Practical Design and Theory*, 2nd Ed.; Academic Press: Amsterdam, Netherlands, 2013.

(41) Bergman, P. C. A.; Boersma, A. R.; Zwart, R. W. R.; Kiel, J. H. A. *Torrefaction for biomass co-firing in existing coal-fired power stations "BIOCOAL" Report# ECN-C-05-013*; Energy research Centre for the Netherlands, Petten, Netherlands, 2005.

(42) Lipinsky, E. S.; Arcate, J. R.; Reed, T. B. *ACS Div. Fuel Chem. Prepr.* **2002**, *47* (1), 408–409.

(43) Bridgwater, A. .; Peacocke, G. V. . *Renew. Sustain. Energy Rev.* **2000**, *4* (1), 1–73.

(44) Bridgwater, A. V; Meier, D.; Radlein, D. *Org. Geochem.* **1999**, *30*, 1479–1493.

(45) Kan, T.; Strezov, V.; Evans, T. J. *Renew. Sustain. Energy Rev.* **2016**, *57*, 1126–1140.

(46) Arcate, J. R. In *Bioenergy 2002*; Pacific Regional Biomass Energy Program, Boise, Idaho USA Sept. 22-26, 2002; pp 1–8.

(47) Acharya, B.; Sule, I.; Dutta, A. *Biomass Convers. Biorefinery* **2012**, *2* (4), 349–369.

(48) Bourgeois, J. P.; Doat, J. In *Bioenergy 84.*; Swedish Trade Fair Foundation and University of Goteburg, Goteburg, Sweden. 15-21 June, 1984; Vol. 3, pp 153–159.

(49) Prins, M. J.; Ptasinski, K. J.; Janssen, F. J. J. G. *J. Anal. Appl. Pyrolysis* **2006**, *77* (1), 28–34.

(50) Medic, D.; Darr, M.; Shah, A.; Potter, B.; Zimmerman, J. *Fuel* **2012**, *91* (1), 147–154.

(51) Woytiuk, K.; Campbell, W.; Gerspacher, R.; Evitts, R. W.; Phoenix, A. *Renew. Energy* **2017**, *101*, 409–416.

(52) Lê Thành, K.; Commandré, J. M.; Valette, J.; Volle, G.; Meyer, M. *Fuel Process. Technol.* **2015**, *139*, 226–235.

(53) Nachenius, R. W.; van de Wardt, T. A.; Ronsse, F.; Prins, W. *Biomass and Bioenergy* **2014**, *79*, 96–104.

(54) Schorr, C.; Muinonen, M.; Nurminen, F. *Torrefaction of Biomass. Publication 1/2012 - Miktech Oy.*; Mikkeli, 2012.

(55) Bergman, P. C. A. *Combined torrefaction and pelletisation - The TOP process. ECN Report ECN-C--05-073*; Petten (NL), 2005.

(56) Tumuluru, J. S.; Hess, J. R.; Boardman, R. D.; Wright, C. T.; Westover, T. L. *Ind. Biotechnol.* **2012**, *8* (3), 113–132.

(57) Ciolkosz, D.; Wallace, R. *Biofuels, Bioprod. Biorefining* **2011**, *5* (3), 317–329.

(58) Prins, M. J.; Ptasinski, K. J.; Janssen, F. J. J. G. *J. Anal. Appl. Pyrolysis* **2006**, *77* (1), 35–40.

(59) Ndibe, C.; Grathwohl, S.; Paneru, M.; Maier, J.; Scheffknecht, G. *Fuel* **2015**, *156*, 177–189.

(60) Ontario Power Generation. Thunder Bay generating station now fueled by advanced biomass https://www.opg.com/news-and-media/news-releases/Documents/150209TBFuelledbyAdvancedBiomass_FINAL.pdf (accessed Feb 5, 2018).

(61) Bergman, P. C. A.; Prins, M. J.; Boersma, A. R.; Ptasinski, K. J.; Kiel, J. H. A.; Janssen, F. J. J. G. *Torrefaction for entrained-flow gasification of biomass*; Report# ECN-C-05-067; Energy research Centre of the Netherlands, Petten, NL., 2005.

(62) Bridgeman, T. G.; Jones, J. M.; Shield, I.; Williams, P. T. *Fuel* **2008**, *87* (6), 844–856.

(63) Olivier, J. G. J.; Schure, K. M.; Peters, J. A. H. W. *Trends in global CO2 and total greenhouse gas emissions: 2017 Report*; 2017.

(64) Kleinschmidt, C. P. In *Central European Biomass Conference 2011*; Austrian Biomass Association. Graz, Austria. 26-29 January, 2011.

(65) Kiel, J. H. A. *Present. 16th Eur. Biomass Conf. Exhib. 2-6 June 2008, Val. Spain* **2008**, No. June, 2–6.

(66) Cremers, M.; Koppejan, J.; Middelkamp, J.; Witkamp, J.; Sokhansanj, S.; Melin, S.; Madrali, S. *Status overview of torrefaction technologies: A review of the commercialisation status of biomass torrefaction (2015). ISBN 978-1-910154-23-6*; IEA Bionergy, 2015.

(67) Thran, D.; Witt, J.; Schaubach, K.; Kiel, J.; Carbo, M.; Maier, J.; Ndibe, C.; Koppejan, J.; Alakangas, E.; Majer, S.; Schipfer, F. *Biomass and Bioenergy* **2015**, *89*, 184–200.

(68) Grigiante, M.; Antolini, D. *Fuel* **2015**, *153*, 499–509.

(69) Bergman, P. C. a.; Kiel, J. H. a. *Proc. 14th Eur. Biomass Conf. Paris, Fr.* **2005**, No. October, 17–21.

(70) Woytiuk, K.; Campbell, W. A.; Gerspacher, R.; Evitts, R. W.; Phoenix, A. In *Venice 2012, Fourth International Symposium on Energy from Biomass and Waste. Venice Italy, 12-15 Nov.*; 2012.

(71) Data Bulletin: Analysis of carbon and sulfur in coal using the rapid CS cube https://www.elementar.de/en/products/organic-elemental-analysis/rapid-cs-cube.html (accessed Jul 5, 2018).

(72) Lestander, T. A.; Rudolfsson, M.; Pommer, L.; Nordin, A. *Green Chem.* **2014**, *16* (12), 4906–4913.

(73) Basu, P. *Combustion and gasification in fluidized beds*; CRC/Taylor & Francis: Boca Raton FL, USA, 2006.

(74) Ulrich, G. D.; Vasudevan, P. T. *Chemical engineering process design and economics : a practical guide. 2nd ed.*; CRC Press: Durham (US), 2003.

(75) Gerspacher, R.; Campbell, W.; Woytiuk, K.; Evitts, R.; Phoenix, A. In *24th Canadian Congress of Applied Mechanics, Saskatoon Canada, June 2-6*; 2013.

(76) Firewood processor Bilke S3 http://www.bilke.net/en/bilke-s3-en (accessed Jun 22, 2018).

(77) Campbell, W. A.; Coller, A.; Evitts, R. W. In *Venice 2018, Seveth International Symposium on Energy from Biomass and Waste/ 15-18 Oct.*; Venice, Italy, 2018.

(78) Wannapeera, J.; Worasuwannarak, N. *J. Anal. Appl. Pyrolysis* **2015**, *115*, 279–287.

(79) Strandberg, M.; Olofsson, I.; Pommer, L.; Wiklund-lindström, S.; Åberg, K.; Nordin, A. *Fuel Process. Technol.* **2015**, *134*, 387–398.

(80) Shang, L.; Ahrenfeldt, J.; Holm, J. K.; Bach, L. S.; Stelte, W.; Henriksen, U. B. *J. Anal. Appl. Pyrolysis* **2014**, *108*, 109–116.

(81) Ohliger, A.; Förster, M.; Kneer, R. *Fuel* **2013**, *104*, 607–613.

(82) NIST/SEMATECH. e-Handbook of Statistical Methods http://www.itl.nist.gov/div898/handbook/ (accessed Nov 30, 2017).

(83) Stahl, R. (FZK); Henrich, E. (FZK); Gehrman, H. J. (CUTEC); Vodegel, S. (CUTEC); Koch, M. (BKG). *Definition of a standard biomass - RENEW Project - Renewable fuels for advanced powertrains. SES6-CT-2003-502705*; Karlsruhe, Germany, 2004.

(84) Na, B. I.; Kim, Y. H.; Lim, W. S.; Lee, S. M.; Lee, H. W.; Lee, J. W. *Biomass and Bioenergy* **2013**, *52*, 159–165.

(85) Campbell, W. A.; Evitts, R. W. *Energy and Fuels* **2018**, *32* (9), 9448–9458.

(86) Lewis, C. Accurately Measuring Dry Bulk Solids http://www.powderbulksolids.com/article/Accurately-Measuring-Dry-Bulk-Solids-01-04-2016 (accessed Aug 10, 2018).

(87) *Biorefineries*; Rabaçal, M., Ferreira, A. F., Silva, C. A. M., Costa, M., Eds.; Lecture Notes in Energy; Springer International Publishing: Cham, 2017; Vol. 57.

(88) Campbell, W.; Woytiuk, K.; Evitts, R. W.; Phoenix, A.; Gerspacher, R. In *Venice 2012, Fourth International Symposium on Energy from Biomass and Waste, 12-15 Nov.*; 2012.

(89) Sokhansanj, S.; Mani, S.; Stumborg, M.; Samson, R.; Fenton, J. *Can. Biosyst. Eng. / Le Genie des Biosyst. au Canada* **2006**, *48*, 39–46.

(90) Grosshans, R. E. Cattail (Typha spp.) biomass harvesting for nutrient capture and sustainable bioenergy for integrated watershed management. Ph.D. Dissertation, University of Manitoba, 2014.

(91) Schenck, H.; Hawks, R. *Theories of engineering experimentation*; Hemisphere Pub. Corp: New York, 1979.

(92) Skvaril, J.; Kyprianidis, K. G.; Dahlquist, E. *Appl. Spectrosc. Rev.* **2017**, *52* (8), 675–728.

(93) Schwanninger, M.; Rodrigues, J. C.; Fackler, K. *J. Near Infrared Spectrosc.* **2011**, *19* (5), 287–308.

(94) Lestander, T. A.; Johnsson, B.; Grothage, M. *Bioresour. Technol.* **2009**, *100* (4), 1589–1594.

(95) Huang, C.; Han, L.; Yang, Z.; Liu, X. *Waste Manag.* **2009**, *29* (6), 1793–1797.

(96) United States Department of Agriculture - 2018 Report on World Agricultural Production http://usda.mannlib.cornell.edu/usda/current/worldag-production/worldag-production-05-10-2018.pdf (accessed May 15, 2018).

(97) Nikolaisen, L.; Nielsen, C.; Larsen, M. G.; Nielsen, V.; Zielke, U.; Kristian, J.; Birgitte, K.; Nikolaisen, H. L.; Energi, S. K. *Straw for Energy Production Technology - Environment - Economy Second Edition*; 1998.

(98) Campbell, W.; Woytiuk, K.; Gerspacher, R.; Evitts, R. W.; Phoenix, A. In *Venice 2016, Sixth International Symposium on Energy from Biomass and Waste, International Waste Working Group. Venice, Italy. November 14-17*; 2016.

(99) Xiao, L.; Wei, H.; Himmel, M. E.; Jameel, H.; Kelley, S. S. *Front. Plant Sci.* **2014**, *5* (August), 1–10.

Appendix A: Supplemental Figures

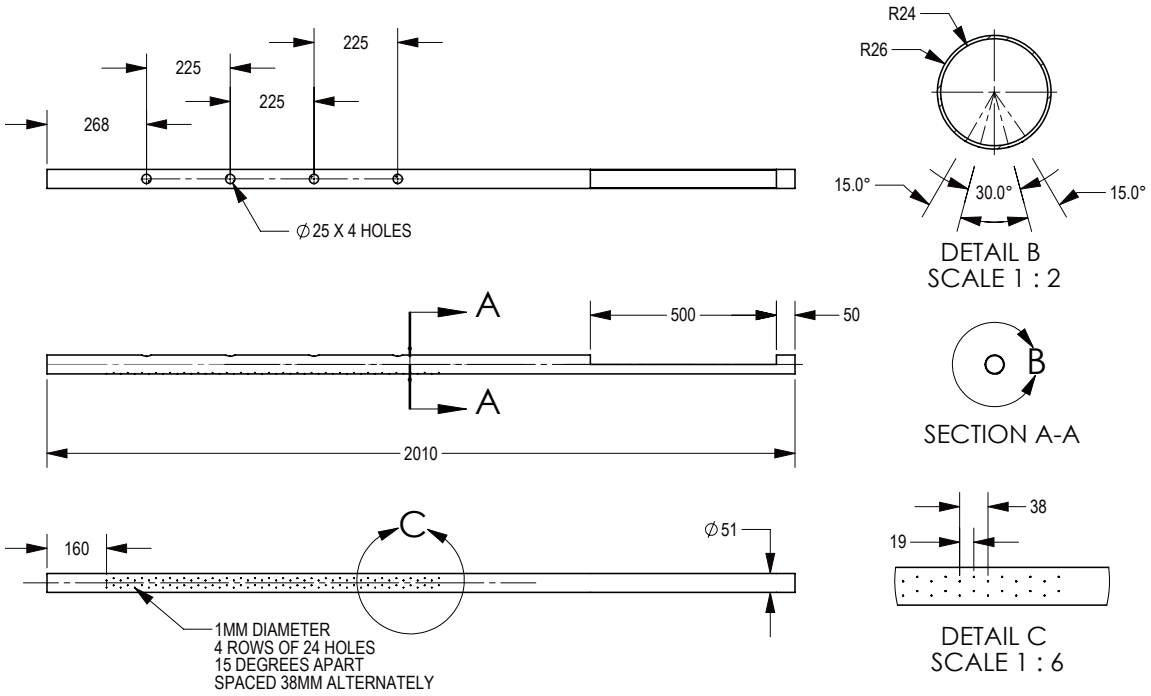

Figure A.3.1: CTU Stage 1 Conveyor tube, grid detail
(From production drawing courtesy of PAMI)

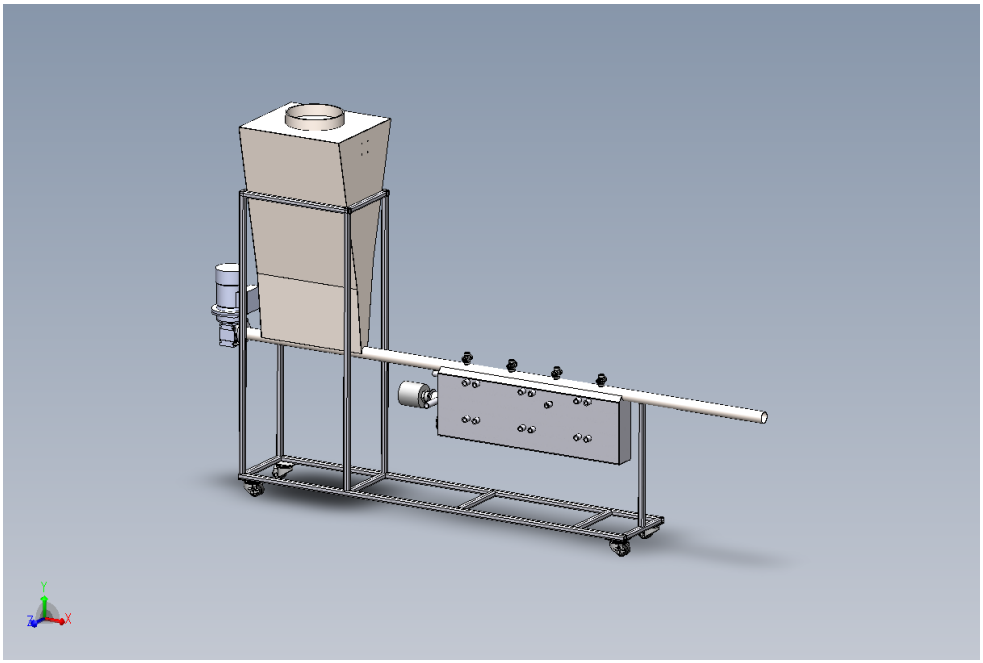

Figure A.3.2: CTU Stage 1 3D rendering

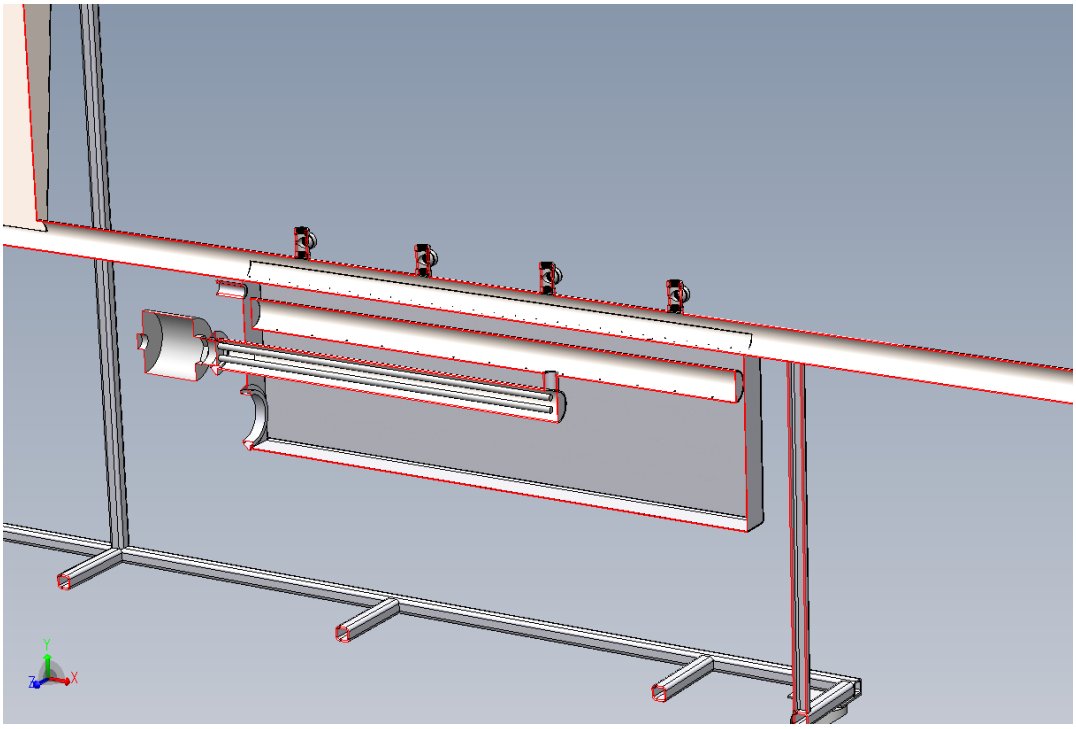

Figure A.3.3: CTU Stage 1 3D rendering: section view of internals (PAMI)

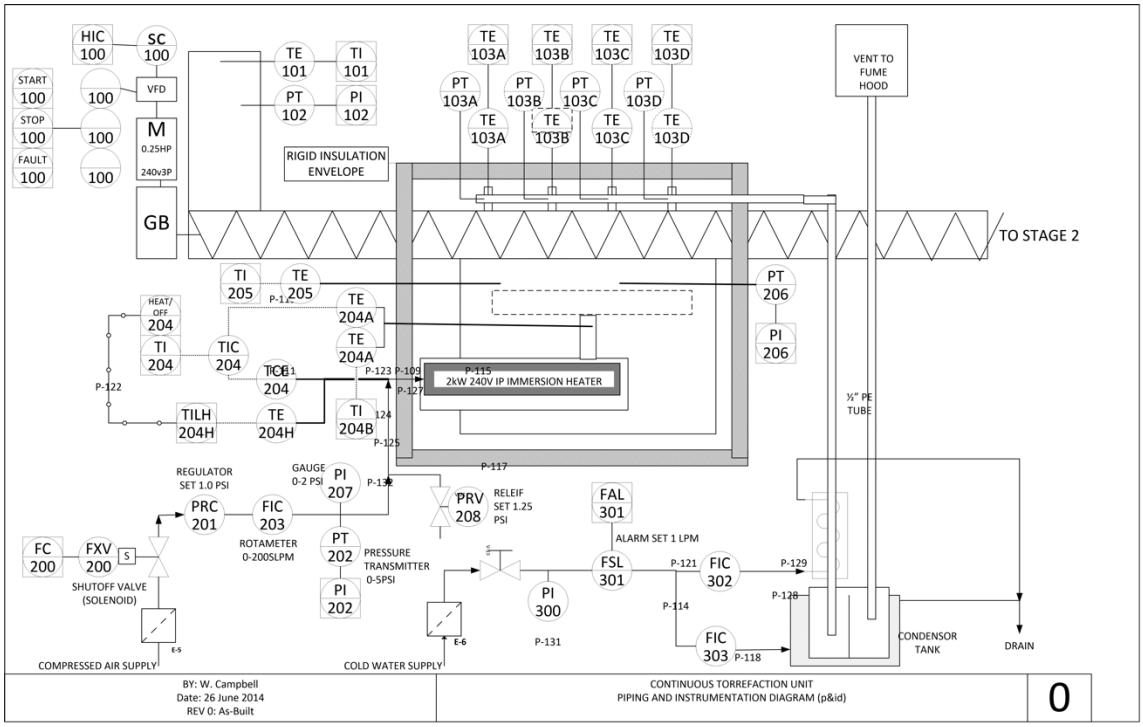

Figure A.3.4: Piping and Instrumentation Diagram of CTU Stage 1

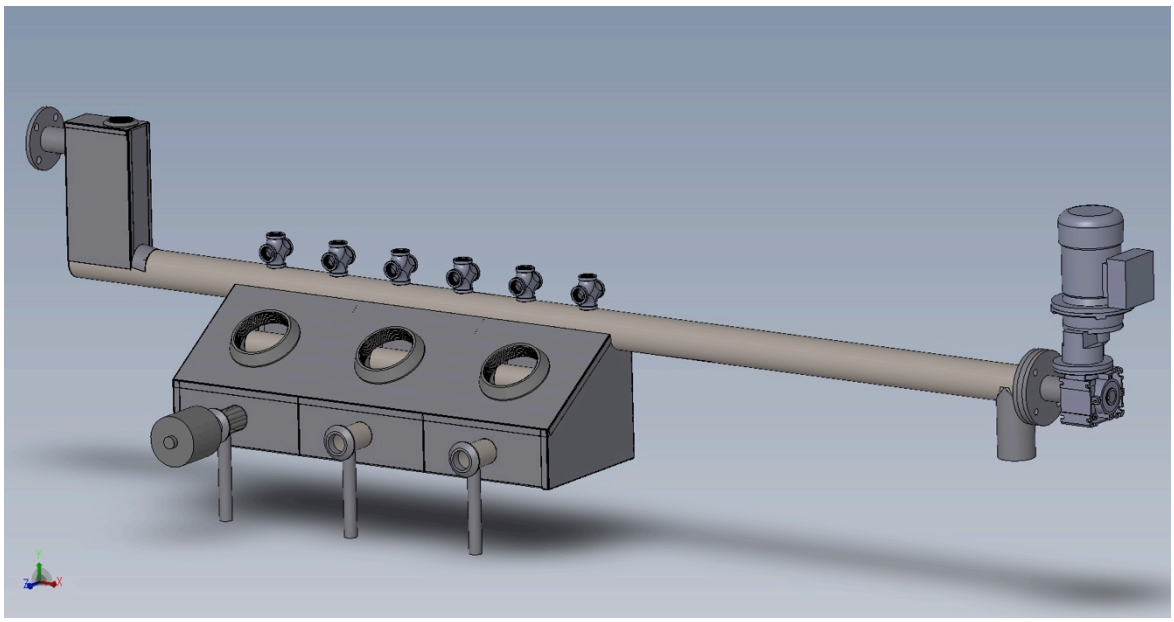

Figure A.3.5: CTU Stage 2 3d Rendering (PAMI)

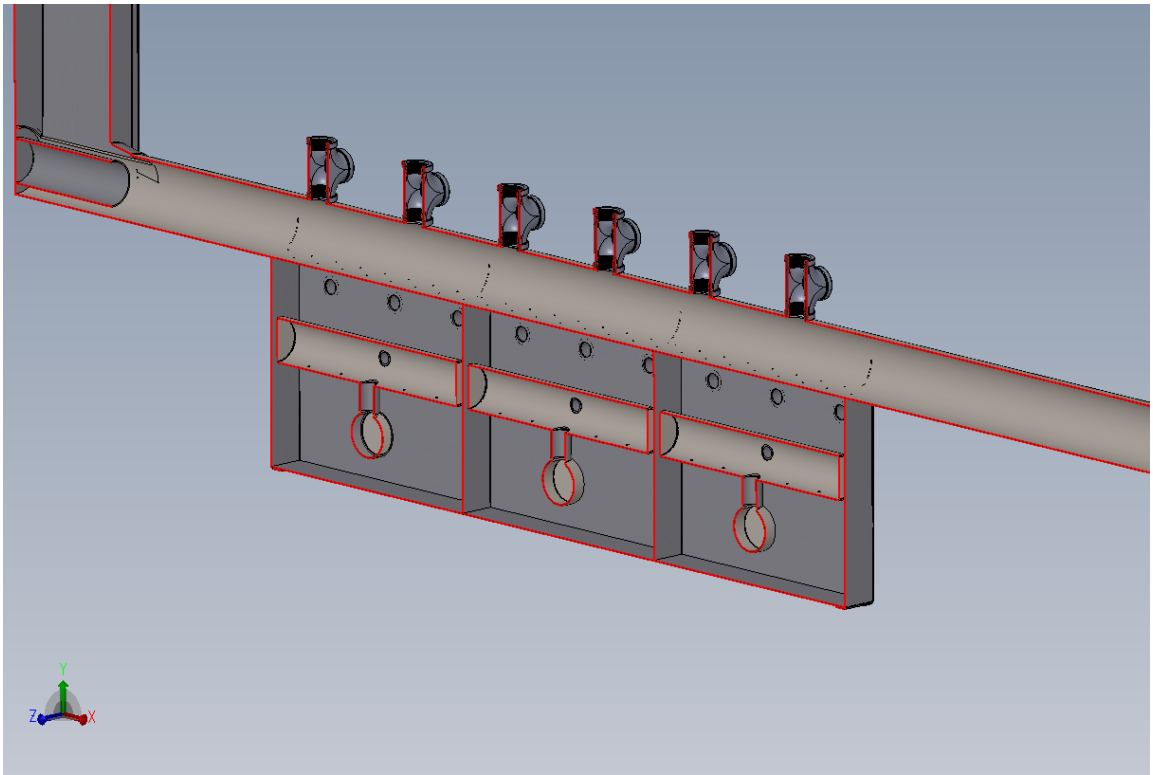

Figure A.3.6: CTU Stage 2 3d Rendering, section view of heat path. (PAMI)

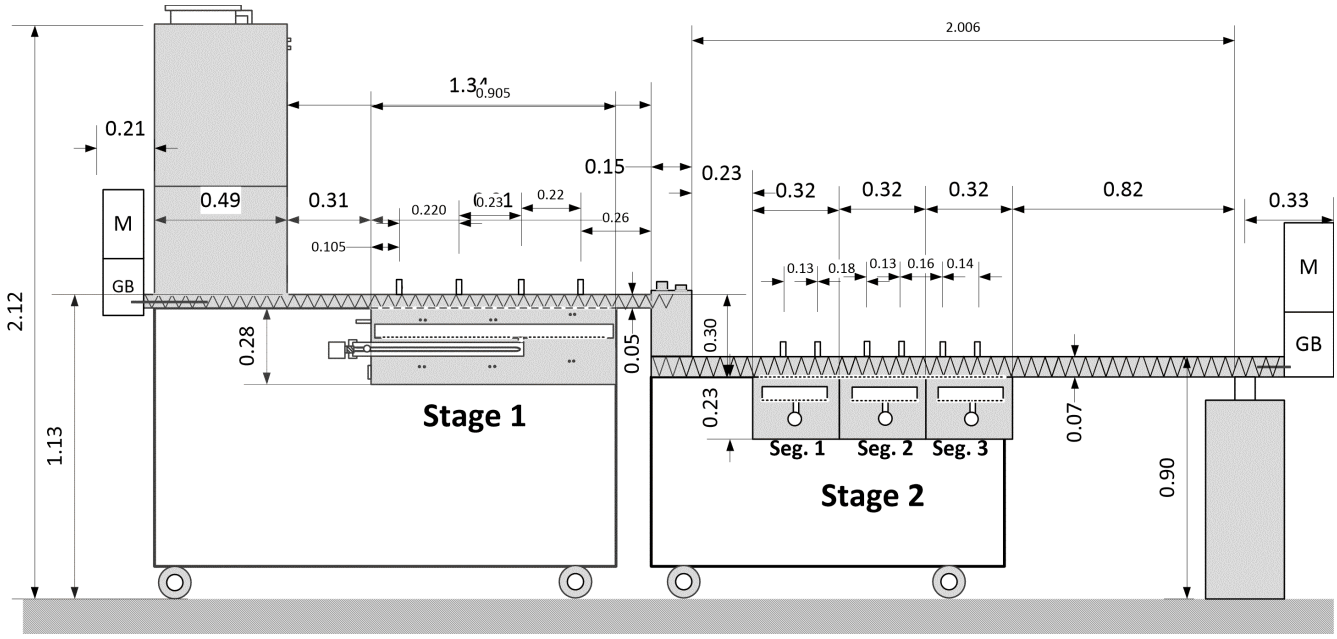

Figure A.3.7: Plan View Assembly Diagram of CTU.
(dimensions indicated are in metres)

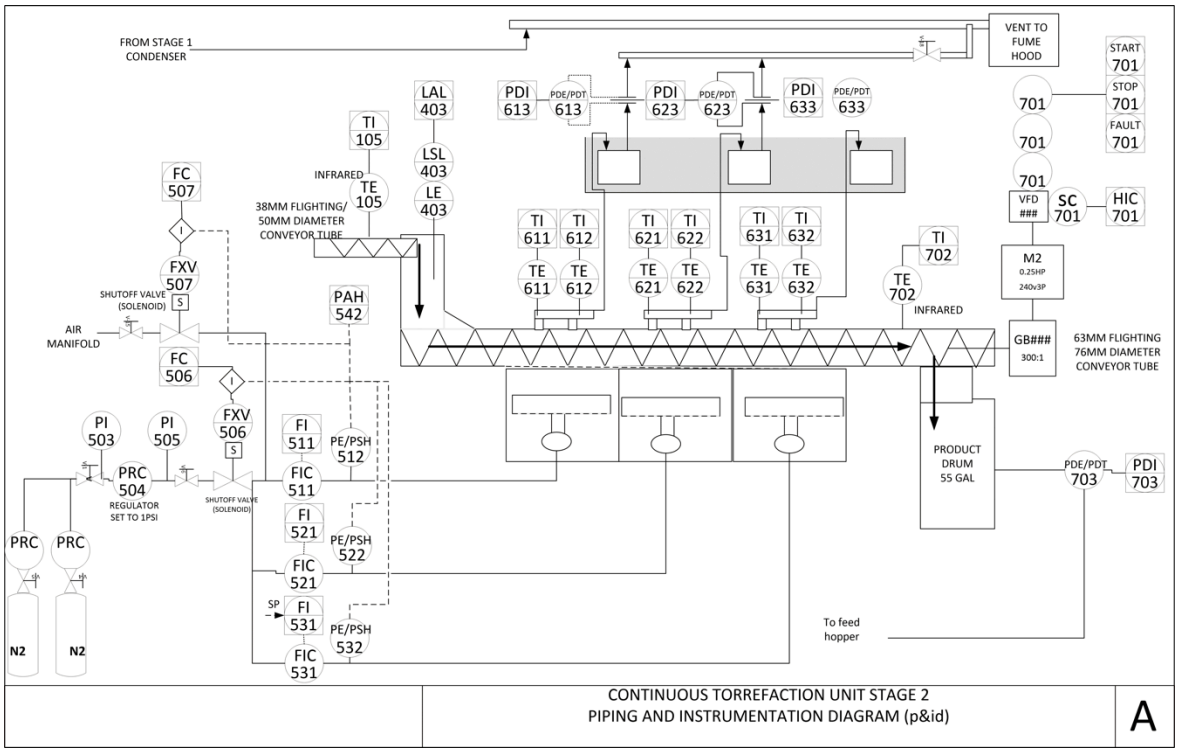

Figure A.3.8: Torrefaction Pilot Plant Stage 2 P&ID Diagram

Figure A.3.9: CTU Control Panel

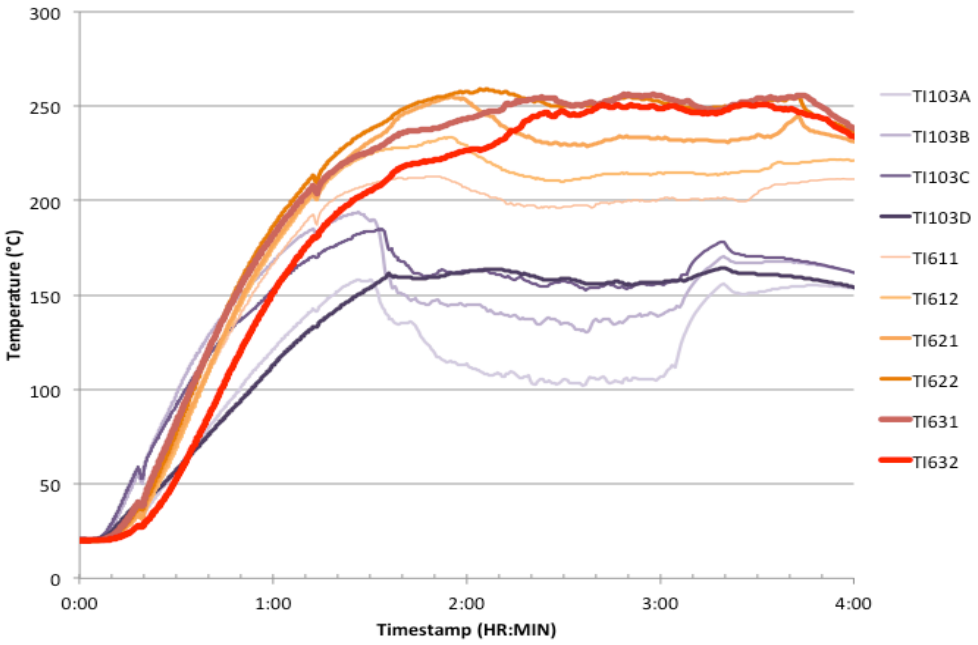

Figure A.3.10: Smoothed time series temperature measurements for CTU experiment 14-W. (coppiced willow granules, 2 Feb 2016).

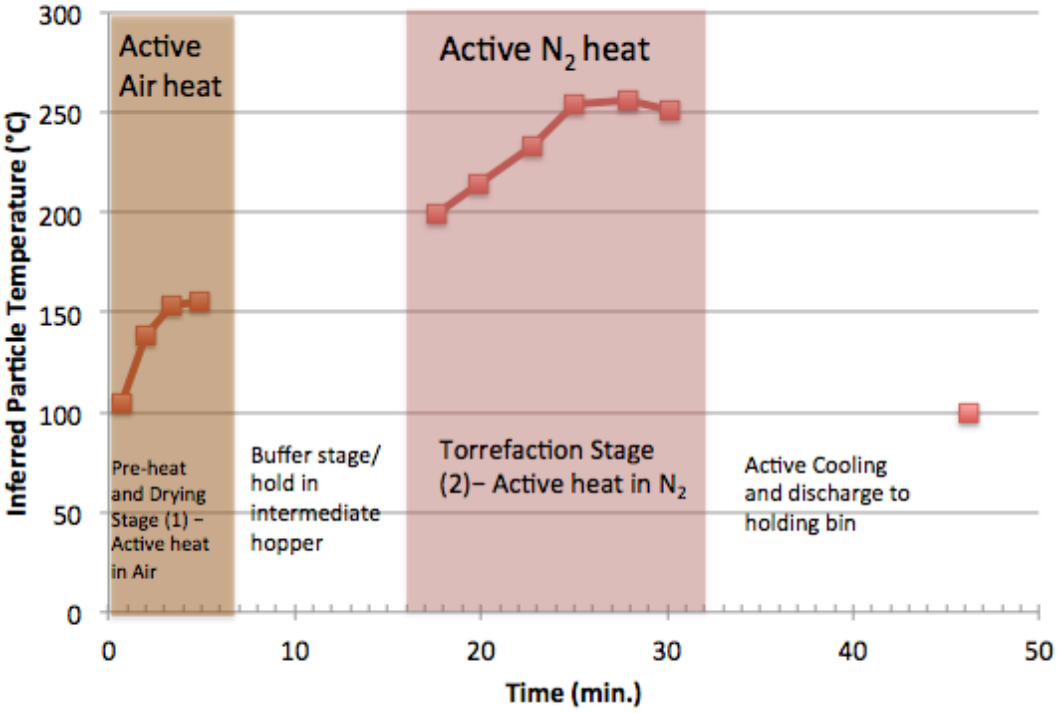

Figure A.3.11: Single particle Temperature Series
(21 APR 2015

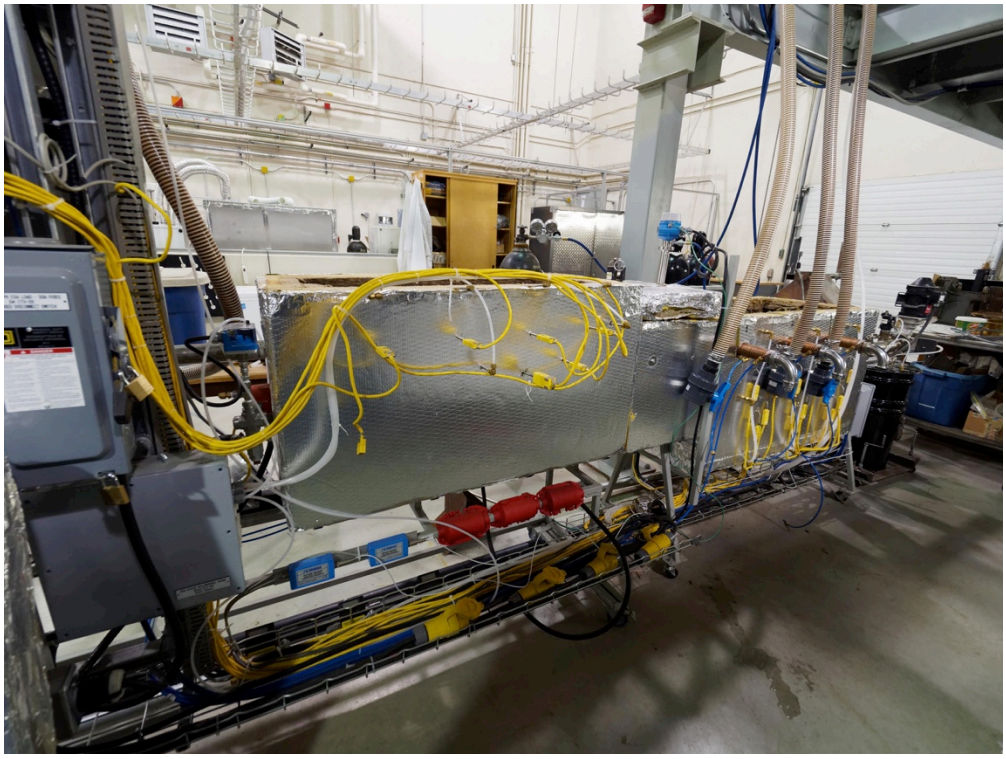

Figure A.3.12: Photograph of CTU pilot plant: Stage 1 external.

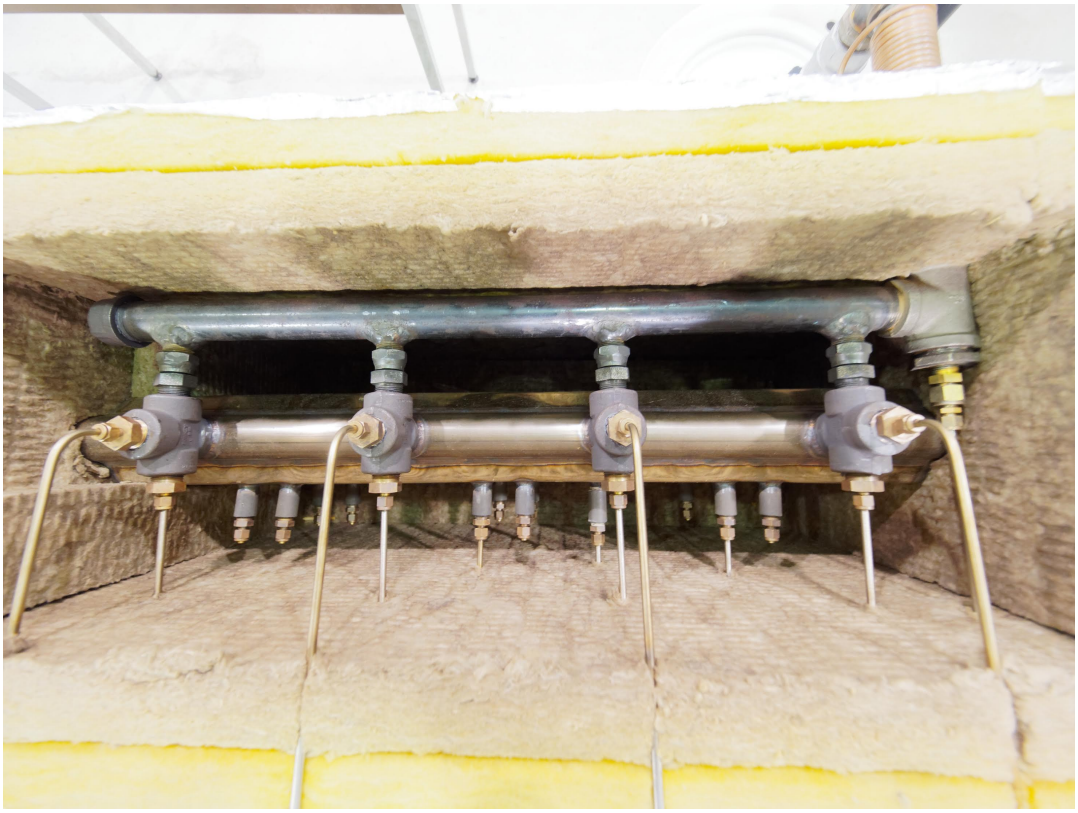

Figure A.3.13: Photograph of CTU pilot plant: Stage 1 manifold and auger shell.

Figure A.3.14: Photograph of CTU pilot plant: Stage 2 manifold and auger shell.

Figure A.3.15: Photograph of CTU pilot plant: Stage 2 discharge end, receiver and Motor 2.

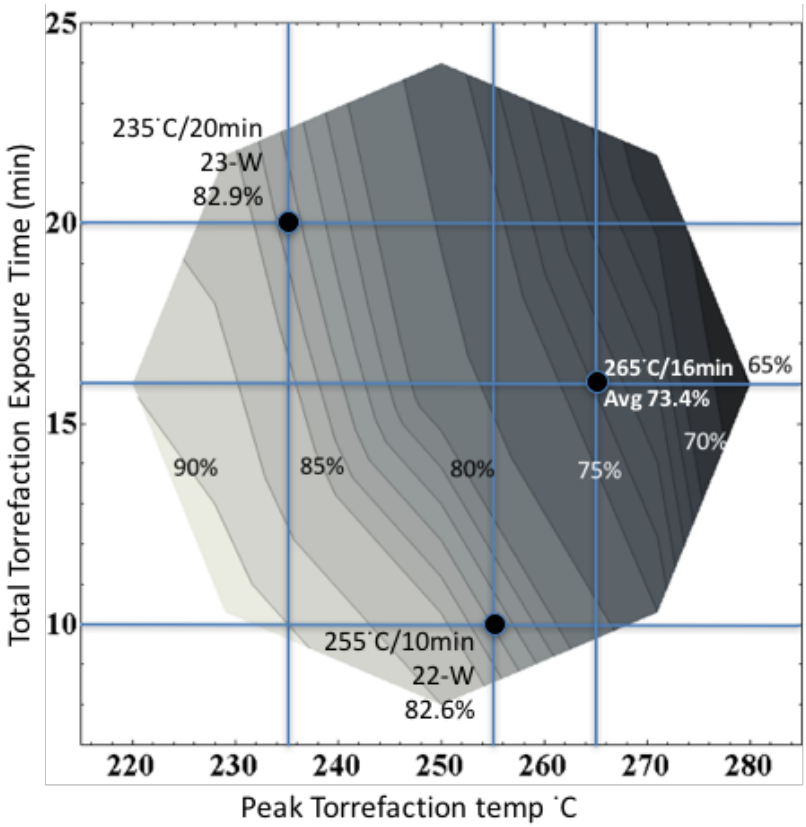

Figure A.4.1: CTU Pilot Plant Response surface validation results

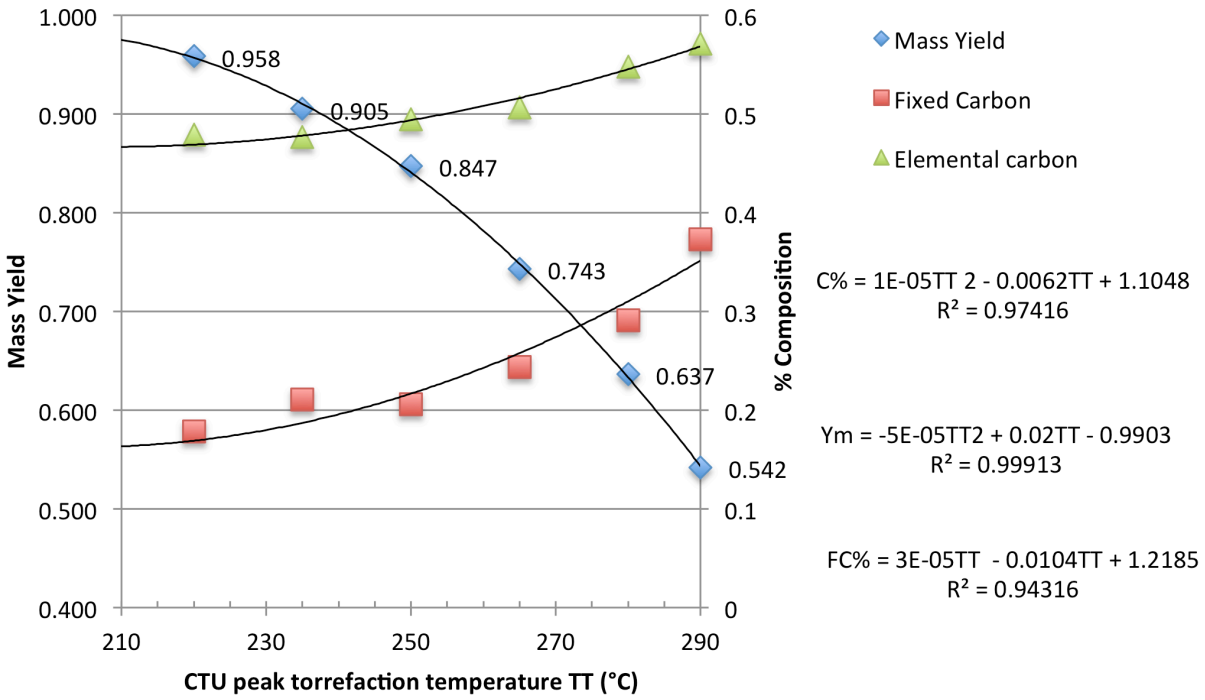

Figure A.4.2: CTU experimental mass yields, elemental and fixed carbon concentrations for torrefaction of wheat straw granules

Figure A.4.3: Photograph comparing five biomass, before and after torrefaction in CTU pilot plant. From left 1. *Moringa* leaf, 2. Cattail (*typha spp.*) 3. Wheat Straw 4. Coppice willow. 5. Spruce pellets

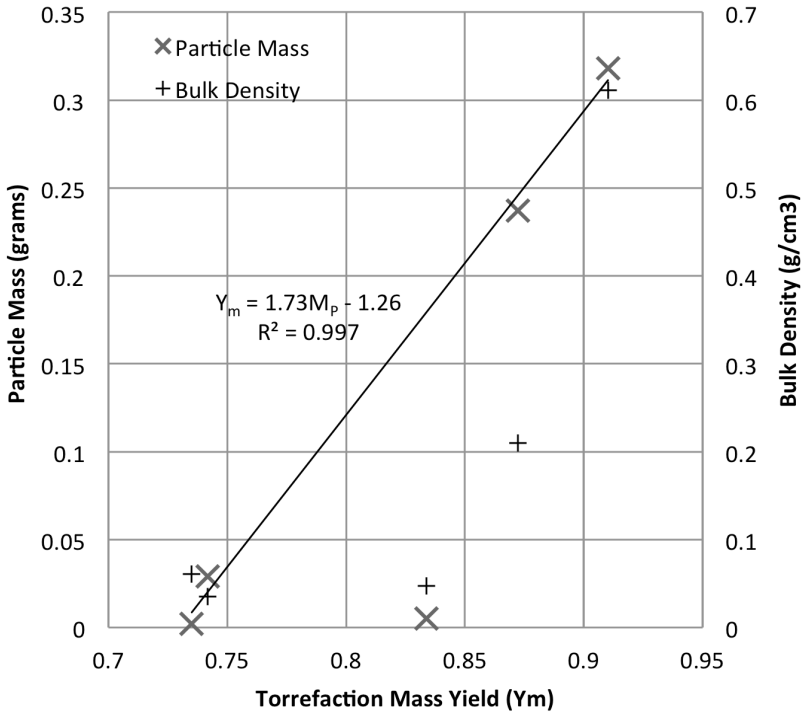

Figure A.4.4: Comparison of particle mass and bulk density relative to mass yield for five biomass types

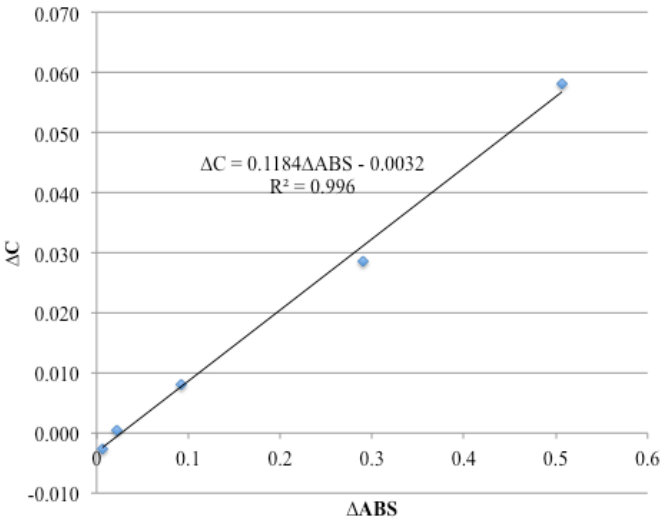

Figure A.6.1: Change in Carbon composition relative to change in diffuse absorbance - Willow

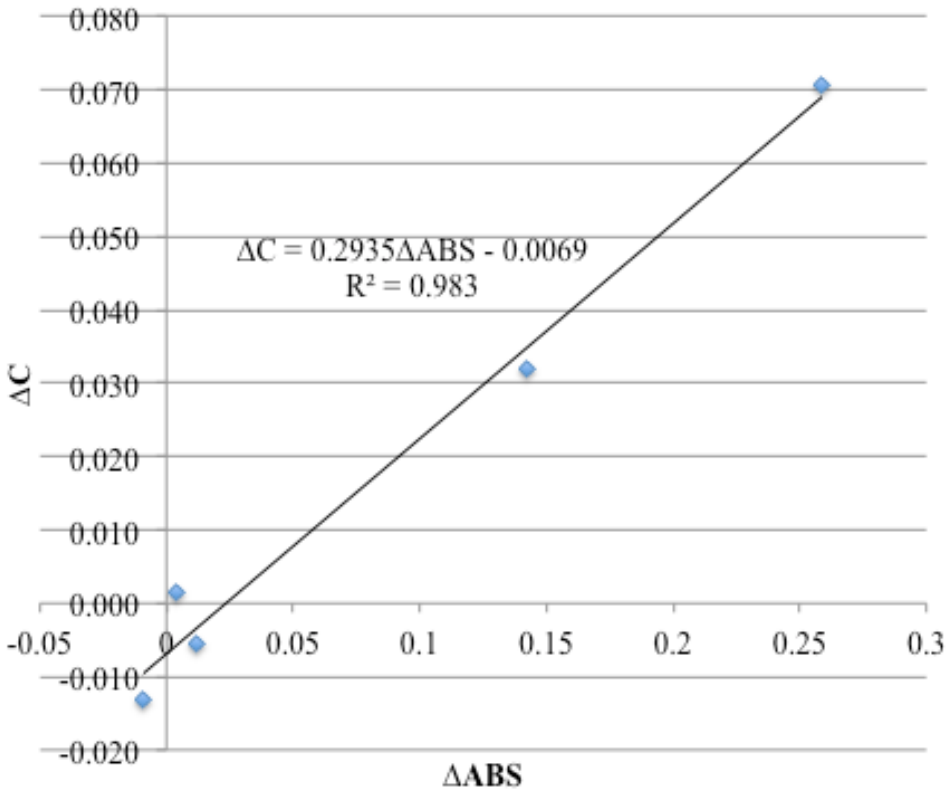

Figure A.6.2: Change in Carbon composition relative to change in diffuse absorbance – Flax straw

Temp. (°C)	220	235	250	265	280	290

Figure A.6.3: Raw and continuous torrefied wheat straw samples, peak temperature indicated.
8.6 minutes residence time.

Appendix B: Supplemental Tables

Table B.3.1: Continuous Torrefaction Unit Conveyor Range, Rate and Throughput

CTU CONVEYOR 1 DATA						
Motor Frequency (Hz)	6	10	13.5	30	60	100
Motor RPM	1.725	2.875		8.625	17.25	28.75
Linear velocity mm/min	55	92	124	276	552	916
Residence time total (mins)		17.39	12.83	5.80	2.90	1.75
Residence time heat (mins)		9.783	7.218	3.261	1.630	0.982
Vol. throughput (m^3/min)	0.00006	0.00010	0.00013	0.00029	0.00058	0.00096
Vol throughput (Litres/hour)	3.464	5.773	7.762	17.319	34.637	57.498
Mass Input (kg/min) Willow	0.011	0.018	0.025	0.055	0.110	0.182
Mass input (kg/hour) Willow	0.658	1.096	1.474	3.289	6.578	10.919
Mass Input (kg/min) Wh. Straw	0.001	0.002	0.003	0.007	0.014	0.022
Mass Input (kg/hr) Wh. Straw	0.081	0.135	0.182	0.405	0.811	1.345
CTU CONVEYOR 2 DATA						
Motor Frequency (Hz)	6	10	13.5	30	60	100
Motor RPM	0.43	0.72		2.16	4.31	7.19
Linear velocity mm/min	26.74	44.56	59.92	133.69	267.38	443.84
Residence time heat (mins)		50.27	38.33	16.76	8.38	5.05
Motor Frequency (Hz)		21.54	15.96	7.18	3.59	2.16
Vol. throughput (m^3/min)	0.0001	0.00016	0.00022	0.00049	0.00099	0.0016
Vol throughput (Litres/hour)	6.0	10.0	13.4	30.0	60.0	99.5
Mass Input (kg/min) Willow	0.015	0.025	0.033	0.074	0.148	0.245
Mass input (kg/hour) Willow	0.89	1.48	1.98	4.43	8.86	14.70
Mass Input (kg/min) Wh. Straw	0.0026	0.0043	0.0058	0.0130	0.0260	0.0431
Mass Input (kg/hr) Wh. Straw	0.16	0.26	0.35	0.78	1.56	2.59

Table B.4.1: Biomass and Chars Analysis For Continuous Torrefaction Experiments

RUN Code	Feedstock	Experiment Date	T_{tor}	t_{tor}	Initial Mass	Moisture Content	Initial (Dry) Mass	Final Mass	DRY Mass Yield	Energy Yield (db)	Moisture Content (TGA)	C (dry)	H (dry)	N (dry)	S (dry)	O (dry)	ash (dry)	HHV (db) (Channiwala)	HHV (dry) (Sheng)
			°C	min	g	%	g	g	%	%	%								kJ/g
0-W	WILLOW								100.0%	100.0%	3.72	49.41	6.30	0.37	0.01	42.55	1.36	20.2	19.9
000-W	WILLOW								100.0%	100.0%	5.07	50.29	6.27	0.36	0.10	41.12	1.86	20.7	20.1
1-W	WILLOW	15-04-21	250.0	16.0	3201	6.8	2983	2339.3	78.42%										
2-W	WILLOW	15-06-08	250.0	16.0	3650	17.8	3000	2396.6	79.88%										
03-W	WILLOW	15-06-15	250.0	16.0	4395	9.15	3993	3109.2	77.87%	84.89%	2.95	54.92	5.75	0.53	0.11	37.30	1.40	22.1	21.1
04-W	WILLOW	15-06-22	250.0	8.0	6643	9.69	5999	5250.2	87.51%	91.29%	2.60	52.51	5.79	0.53	0.11	38.67	2.39	21.1	20.4
05-W	WILLOW	15-07-07	250.0	24.0	3347	10.39	2999	2273.3	75.79%	82.99%	2.54	55.04	5.70	0.68	0.05	35.85	2.69	22.2	21.0
06-W	WILLOW	15-07-16	220.0	16.0	3964	11.96	3490	3136.3	89.87%	92.17%	1.60	51.48	5.93	0.61	0.06	40.34	1.58	20.8	20.2
07-W	WILLOW	15-07-21	250.0	16.0	3991	11.79	3521	2797.5	79.46%	85.95%	2.37	54.37	5.76	0.55	0.06	36.99	2.27	21.9	20.9
08-W	WILLOW	15-08-10	280.0	16.0	4548	12.05	4000	2586.2	64.66%	74.41%	1.84	58.37	5.46	0.65	0.05	33.69	1.77	23.3	21.9
09-W	WILLOW	15-08-17	271.0	10.3	4479	10.7	4000	2998.9	74.97%	83.05%	2.32	55.11	5.97	0.49	0.02	36.85	1.56	22.4	21.3
10-W	WILLOW	15-10-14	250.0	16.0	3769	7.13	3500	2740	78.29%	87.15%	2.10	55.02	6.05	0.48	0.02	36.37	2.05	22.5	21.3
11-W	WILLOW	15-11-25	229.0	10.3	3681	5.237	3488	3196.2	91.62%	94.38%	2.87	51.20	6.15	0.25	0.01	40.99	1.40	20.8	20.3
12-W	WILLOW	15-12-08	229.0	21.7	2116	5.82	1993	1703.6	85.49%	91.18%	2.40	53.05	6.06	0.34	0.01	39.14	1.39	21.6	20.8
13-W	WILLOW	15-12-21	271.0	21.7	2090	4.64	1993	1373.6	68.93%	79.81%	2.65	57.28	5.99	0.41	0.01	34.71	1.59	23.4	21.9
14-W	WILLOW	16-02-08	250.0	16.0	3108	4.59	2966	2328.2	78.51%	87.68%	2.05	54.70	6.20	0.42	0.03	36.30	2.35	22.6	21.3
15-W	WILLOW	16-06-10	250.0	16.0	2219	8.6	2029	1592.8	78.50%	88.08%	1.9	55.1	6.1	0.5	0.0	35.9	2.4	22.7	21.4
16-W	WILLOW	16-06-24	250.0	16.0	1520	9.5	1377	1096.2	79.62%	89.99%	1.8	55.0	6.3	0.5	0.0	35.7	2.5	22.9	21.4
17-W	WILLOW	17-06-20	265	16.0	2214	9.0	2014	1474.7	73.24%	80.36%	3.2	56.5	5.2	0.6	0.3	35.7	1.7	22.2	21.2
18-W	WILLOW	17-06-22	265	16.0	2683	8.5	2455	1821.5	74.21%	84.00%	3.5	58.0	5.2	0.7	0.5	33.8	1.7	22.9	21.6
19-W	WILLOW	17-06-28	265	16.0	2292	9.0	2087	1528.1	73.24%	83.89%	3.7	58.3	5.4	0.6	0.1	33.8	1.8	23.2	21.8
20-W	WILLOW	17-06-29	265	16.0	2089	8.9	1903	1392.4	73.15%	84.47%	4.0	58.8	5.4	0.6	0.1	33.5	1.6	23.4	21.9
21-W	WILLOW	17-07-04	265	16.0	2726	10.9	2430	1782.5	73.37%	84.00%	3.9	58.2	5.4	0.6	0.0	33.8	2.0	23.2	21.8
22-W	WILLOW	17-07-10	255	10.0	3850	11.3	3413	2817.7	82.55%	91.34%	3.3	56.0	5.6	0.6	0.0	36.1	1.7	22.4	21.3
23-W	WILLOW	17-08-01	235	20.0	2259	11.1	2008	1664.2	82.86%	90.61%	3.3	55.5	5.6	0.5	0.0	36.9	1.4	22.1	21.2
00-WS	WHEAT STR.								100.00%	100.00%	8.3	46.2	6.0	0.5	0.2	39.6	7.6	18.9	18.6
01-WS	WHEAT STR.	16-08-03	250	8.6	583	9.7	526.7	446.2	84.72%	88.88%	3.6	49.5	6.1	0.5	0.1	34.5	9.3	20.6	19.5
02-WS	WHEAT STR.	16-08-03	220	8.6	583	9.7	526.7	504.7	95.83%	99.49%	4.5	47.9	6.3	0.6	0.1	37.1	8.0	20.2	19.3
03-WS	WHEAT STR.	16-08-04	280	8.6	582.8	9.9	525.4	334.5	63.67%	70.98%	3.8	54.7	5.7	0.7	0.1	27.6	11.1	22.8	20.7
04-WS	WHEAT STR.	17-08-24	235	8.6	599.9	8.8	547.3	495.3	90.50%	89.72%	2.3	47.7	5.2	0.6	0.3	38.2	8.1	18.6	18.4
05-WS	WHEAT STR.	17-08-29	265	8.6	600	8.4	549.5	408.36	74.31%	76.95%	2.3	50.6	5.2	0.6	0.0	34.4	9.2	20.0	19.2
06-WS	WHEAT STR.	17-12-19	290	8.6	606.2	4.6	578.5	313.54	54.20%										
0-CT	CATTAIL								100.00%	100.00%	6.7	46.1	5.3	0.3	0.1	45.5	2.8	17.5	
01-CT	CATTAIL	17-10-17	250	6.8	533.1	7.5	493.3	371.53	75.31%	83.88%	2.9	50.8	5.0	0.5	0.1	38.0	5.8	19.5	
0-MO	MORINGA																		
01-MO	MORINGA	17-11-14	250	8.6	2586	8.4	2370	1747	73.71%										
0-SP	SPRUCE PEL.																		
01-SP	SPRUCE PEL.	18-02-15	210	8.6	4230	5.5	3995	3921.1	98.14%										
02-SP	SPRUCE PEL.	18-04-26	245	10.0	5007	6.4	4688	4382.7	93.49%										
03-SP	SPRUCE PEL.	18-04-30	250	10.0	4219	6.4	3951	3628.8	91.8%										

Table B.4.2: CTU pilot plant validation results: measured and predicted mass yield values.

Experiment	Meas. Ym	Predicted. Ym	Error
235/20	82.9%	83.5%	-0.6%
255/10	82.6%	83.0%	-0.4%
265/16 (1)	73.2%	73.8%	-0.6%
265/16 (2)	74.2%	73.8%	0.2%
265/16 (3)	73.2%	73.8%	-0.6%
265/16 (4)	73.2%	73.8%	-0.6%
265/16 (5)	73.4%	73.8%	-0.4%
265/16 (AVG)	73.4%	73.8%	-0.4%

Table B.4.3: Comparison of five biomass types torrefied in CTU pilot plant

	Torrefaction Conditions								Composition (db)					(db)	
	Bulk Dens.	Avg Part. mass	Sphericity	T_{tor}	t_{tor}	Q	F_{S2}	Y_m	C	H	N	O	Ash	HHV	Y_e
	kg/m^3	g	ϕ	°C	min.	kg/s	M^3/s	%						MJ/ kg	%
Moringa (leaf)	61	0.002	0.66						45.8	5.6	5.1	34.4	8.3	17.8	
Moringa char				250	8.6	0.00034	0.0004	73.5	52.4	4.8	6.0	24.5	11.4	19.5	80.8
Cattail	35	0.029	0.85						46.1	5.3	0.3	45.5	2.8	19.0	
Cattail char				250	6.8	0.00024	0.0004	74.2	50.8	5.0	0.5	38.0	5.8	20.4	80.5
Wheat straw	47	0.003	0.55						46.2	6.0	0.5	39.6	7.6	19.0	
Wheat straw char				250	8.6	0.0025	0.0004	83.4	49.5	6.1	0.5	34.5	9.3	20.1	89.7
Willow	210	0.237	0.80						49.4	6.3	0.4	42.6	1.4	20.2	
Willow char				250	8.0	0.00122	0.0015	87.2	52.5	5.8	0.5	38.7	2.4	21.2	91.9
Spruce pellets	611	0.318	0.86						50.3	5.4	-	44.0	0.3	20.3	
Spruce char				250	10	0.00169	0.0023	91.2	52.4	5.5	-	41.6	0.3	21.2	95.6

Appendix C: Permissions to Reproduce

This section includes permissions to reproduce from the Journal of publication for papers reproduced in whole or in part within this dissertation.

JOHN WILEY AND SONS LICENSE TERMS AND CONDITIONS

Aug 09, 2018

This Agreement between Dept of Chemical & Biological Engineering -- William Campbell ("You") and John Wiley and Sons ("John Wiley and Sons") consists of your license details and the terms and conditions provided by John Wiley and Sons and Copyright Clearance Center.

License Number	4404871365509
License date	Aug 09, 2018
Licensed Content Publisher	John Wiley and Sons
Licensed Content Publication	Canadian Journal of Chemical Engineering
Licensed Content Title	Char quality response surfaces from torrefaction of coppiced willow in a horizontal moving bed pilot plant
Licensed Content Author	William A. Campbell, Kurt Woytiuk, Regan Gerspacher, et al
Licensed Content Date	May 28, 2018
Licensed Content Volume	0
Licensed Content Issue	0
Licensed Content Pages	9
Type of use	Dissertation/Thesis
Requestor type	Author of this Wiley article
Format	Print and electronic
Portion	Full article
Will you be translating?	No
Title of your thesis / dissertation	Adaptive torrefaction of stem biomass in a horizontal moving bed with normalized direct measurement of quality characteristics
Expected completion date	Oct 2018
Expected size (number of pages)	145
Requestor Location	Dept of Chemical & Biological Engineering - Univer 57 Campus Drive Saskatoon, SK s7n 5a9 Canada Attn: William Campbell
Publisher Tax ID	EU826007151
Total	0.00 CAD
Terms and Conditions	

TERMS AND CONDITIONS

This copyrighted material is owned by or exclusively licensed to John Wiley & Sons, Inc. or one of its group companies (each a"Wiley Company") or handled on behalf of a society with which a Wiley Company has exclusive publishing rights in relation to a particular work (collectively "WILEY"). By clicking "accept" in connection with completing this licensing transaction, you agree that the following terms and conditions apply to this transaction

(along with the billing and payment terms and conditions established by the Copyright Clearance Center Inc., ("CCC's Billing and Payment terms and conditions"), at the time that you opened your RightsLink account (these are available at any time at http://myaccount.copyright.com).

Terms and Conditions

- The materials you have requested permission to reproduce or reuse (the "Wiley Materials") are protected by copyright.

- You are hereby granted a personal, non-exclusive, non-sub licensable (on a stand-alone basis), non-transferable, worldwide, limited license to reproduce the Wiley Materials for the purpose specified in the licensing process. This license, **and any CONTENT (PDF or image file) purchased as part of your order,** is for a one-time use only and limited to any maximum distribution number specified in the license. The first instance of republication or reuse granted by this license must be completed within two years of the date of the grant of this license (although copies prepared before the end date may be distributed thereafter). The Wiley Materials shall not be used in any other manner or for any other purpose, beyond what is granted in the license. Permission is granted subject to an appropriate acknowledgement given to the author, title of the material/book/journal and the publisher. You shall also duplicate the copyright notice that appears in the Wiley publication in your use of the Wiley Material. Permission is also granted on the understanding that nowhere in the text is a previously published source acknowledged for all or part of this Wiley Material. Any third party content is expressly excluded from this permission.

- With respect to the Wiley Materials, all rights are reserved. Except as expressly granted by the terms of the license, no part of the Wiley Materials may be copied, modified, adapted (except for minor reformatting required by the new Publication), translated, reproduced, transferred or distributed, in any form or by any means, and no derivative works may be made based on the Wiley Materials without the prior permission of the respective copyright owner.**For STM Signatory Publishers clearing permission under the terms of the STM Permissions Guidelines only, the terms of the license are extended to include subsequent editions and for editions in other languages, provided such editions are for the work as a whole in situ and does not involve the separate exploitation of the permitted figures or extracts,** You may not alter, remove or suppress in any manner any copyright, trademark or other notices displayed by the Wiley Materials. You may not license, rent, sell, loan, lease, pledge, offer as security, transfer or assign the Wiley Materials on a stand-alone basis, or any of the rights granted to you hereunder to any other person.

- The Wiley Materials and all of the intellectual property rights therein shall at all times remain the exclusive property of John Wiley & Sons Inc, the Wiley Companies, or their respective licensors, and your interest therein is only that of having possession of and the right to reproduce the Wiley Materials pursuant to Section 2 herein during the continuance of this Agreement. You agree that you own no right, title or interest in or to the Wiley Materials or any of the intellectual property rights therein. You shall have no rights hereunder other than the license as provided for above in Section 2. No right, license or interest to any trademark, trade name, service mark or other branding ("Marks") of WILEY or its licensors is granted hereunder, and you agree that you shall not assert any such right, license or interest with respect thereto

- NEITHER WILEY NOR ITS LICENSORS MAKES ANY WARRANTY OR REPRESENTATION OF ANY KIND TO YOU OR ANY THIRD PARTY,

EXPRESS, IMPLIED OR STATUTORY, WITH RESPECT TO THE MATERIALS OR THE ACCURACY OF ANY INFORMATION CONTAINED IN THE MATERIALS, INCLUDING, WITHOUT LIMITATION, ANY IMPLIED WARRANTY OF MERCHANTABILITY, ACCURACY, SATISFACTORY QUALITY, FITNESS FOR A PARTICULAR PURPOSE, USABILITY, INTEGRATION OR NON-INFRINGEMENT AND ALL SUCH WARRANTIES ARE HEREBY EXCLUDED BY WILEY AND ITS LICENSORS AND WAIVED BY YOU.

- WILEY shall have the right to terminate this Agreement immediately upon breach of this Agreement by you.

- You shall indemnify, defend and hold harmless WILEY, its Licensors and their respective directors, officers, agents and employees, from and against any actual or threatened claims, demands, causes of action or proceedings arising from any breach of this Agreement by you.

- IN NO EVENT SHALL WILEY OR ITS LICENSORS BE LIABLE TO YOU OR ANY OTHER PARTY OR ANY OTHER PERSON OR ENTITY FOR ANY SPECIAL, CONSEQUENTIAL, INCIDENTAL, INDIRECT, EXEMPLARY OR PUNITIVE DAMAGES, HOWEVER CAUSED, ARISING OUT OF OR IN CONNECTION WITH THE DOWNLOADING, PROVISIONING, VIEWING OR USE OF THE MATERIALS REGARDLESS OF THE FORM OF ACTION, WHETHER FOR BREACH OF CONTRACT, BREACH OF WARRANTY, TORT, NEGLIGENCE, INFRINGEMENT OR OTHERWISE (INCLUDING, WITHOUT LIMITATION, DAMAGES BASED ON LOSS OF PROFITS, DATA, FILES, USE, BUSINESS OPPORTUNITY OR CLAIMS OF THIRD PARTIES), AND WHETHER OR NOT THE PARTY HAS BEEN ADVISED OF THE POSSIBILITY OF SUCH DAMAGES. THIS LIMITATION SHALL APPLY NOTWITHSTANDING ANY FAILURE OF ESSENTIAL PURPOSE OF ANY LIMITED REMEDY PROVIDED HEREIN.

- Should any provision of this Agreement be held by a court of competent jurisdiction to be illegal, invalid, or unenforceable, that provision shall be deemed amended to achieve as nearly as possible the same economic effect as the original provision, and the legality, validity and enforceability of the remaining provisions of this Agreement shall not be affected or impaired thereby.

- The failure of either party to enforce any term or condition of this Agreement shall not constitute a waiver of either party's right to enforce each and every term and condition of this Agreement. No breach under this agreement shall be deemed waived or excused by either party unless such waiver or consent is in writing signed by the party granting such waiver or consent. The waiver by or consent of a party to a breach of any provision of this Agreement shall not operate or be construed as a waiver of or consent to any other or subsequent breach by such other party.

- This Agreement may not be assigned (including by operation of law or otherwise) by you without WILEY's prior written consent.

- Any fee required for this permission shall be non-refundable after thirty (30) days from receipt by the CCC.

- These terms and conditions together with CCC's Billing and Payment terms and conditions (which are incorporated herein) form the entire agreement between you and

WILEY concerning this licensing transaction and (in the absence of fraud) supersedes all prior agreements and representations of the parties, oral or written. This Agreement may not be amended except in writing signed by both parties. This Agreement shall be binding upon and inure to the benefit of the parties' successors, legal representatives, and authorized assigns.

- In the event of any conflict between your obligations established by these terms and conditions and those established by CCC's Billing and Payment terms and conditions, these terms and conditions shall prevail.

- WILEY expressly reserves all rights not specifically granted in the combination of (i) the license details provided by you and accepted in the course of this licensing transaction, (ii) these terms and conditions and (iii) CCC's Billing and Payment terms and conditions.

- This Agreement will be void if the Type of Use, Format, Circulation, or Requestor Type was misrepresented during the licensing process.

- This Agreement shall be governed by and construed in accordance with the laws of the State of New York, USA, without regards to such state's conflict of law rules. Any legal action, suit or proceeding arising out of or relating to these Terms and Conditions or the breach thereof shall be instituted in a court of competent jurisdiction in New York County in the State of New York in the United States of America and each party hereby consents and submits to the personal jurisdiction of such court, waives any objection to venue in such court and consents to service of process by registered or certified mail, return receipt requested, at the last known address of such party.

WILEY OPEN ACCESS TERMS AND CONDITIONS

Wiley Publishes Open Access Articles in fully Open Access Journals and in Subscription journals offering Online Open. Although most of the fully Open Access journals publish open access articles under the terms of the Creative Commons Attribution (CC BY) License only, the subscription journals and a few of the Open Access Journals offer a choice of Creative Commons Licenses. The license type is clearly identified on the article.

The Creative Commons Attribution License

The Creative Commons Attribution License (CC-BY) allows users to copy, distribute and transmit an article, adapt the article and make commercial use of the article. The CC-BY license permits commercial and non-

Creative Commons Attribution Non-Commercial License

The Creative Commons Attribution Non-Commercial (CC-BY-NC)License permits use, distribution and reproduction in any medium, provided the original work is properly cited and is not used for commercial purposes.(see below)

Creative Commons Attribution-Non-Commercial-NoDerivs License

The Creative Commons Attribution Non-Commercial-NoDerivs License (CC-BY-NC-ND) permits use, distribution and reproduction in any medium, provided the original work is properly cited, is not used for commercial purposes and no modifications or adaptations are made. (see below)

Use by commercial "for-profit" organizations

Use of Wiley Open Access articles for commercial, promotional, or marketing purposes requires further explicit permission from Wiley and will be subject to a fee.

Further details can be found on Wiley Online Library

http://olabout.wiley.com/WileyCDA/Section/id-410895.html

RightsLink®

Home | Create Account | Help

Title: Determining the Severity of Torrefaction for Multiple Biomass Types Using Carbon Content

Author: William A. Campbell, Richard W. Evitts

Publication: Energy & Fuels

Publisher: American Chemical Society

Date: Sep 1, 2018

PERMISSION/LICENSE IS GRANTED FOR YOUR ORDER AT NO CHARGE

This type of permission/license, instead of the standard Terms & Conditions, is sent to you because no fee is being charged for your order. Please note the following:

- Permission is granted for your request in both print and electronic formats, and translations.
- If figures and/or tables were requested, they may be adapted or used in part.
- Please print this page for your records and send a copy of it to your publisher/graduate school.
- Appropriate credit for the requested material should be given as follows: "Reprinted (adapted) with permission from (COMPLETE REFERENCE CITATION). Copyright (YEAR) American Chemical Society." Insert appropriate information in place of the capitalized words.
- One-time permission is granted only for the use specified in your request. No additional uses are granted (such as derivative works or other editions). For any other uses, please submit a new request.

BACK | CLOSE WINDOW